PERFORMANCE IMPROVEMENT OF BLIND CLASSIFICATION OF DIGITAL MODULATIONS

A

Thesis submitted

for the award of the degree of

DOCTOR OF PHILOSOPHY

By

Gaurav Jyoti Phukan

DEPARTMENT OF ELECTRONICS AND ELECTRICAL ENGINEERING
INDIAN INSTITUTE OF TECHNOLOGY GUWAHATI
GUWAHATI - 781039, ASSAM, INDIA

May 2017

Dedicated
to my beloved Mother and Late Father who showed me the lights of this universe . . .

Certificate

This is to certify that the thesis entitled "**Performance Improvement of Blind Classification of Digital Modulations**", submitted by Gaurav Jyoti Phukan (Roll No 09610212), a research scholar in the *Department of Electronics and Electrical Engineering*, *Indian Institute of Technology Guwahati*, for the award of the degree of Doctor of Philosophy, is a record of an original research work carried out by him under my supervision and guidance. The thesis has fulfilled all requirements as per the regulations of the institute and in my opinion has reached the standard needed for submission. The results embodied in this thesis have not been submitted to any other University or Institute for the award of any degree or diploma.

Signed: _____

Supervisor: Prof. Prabin Kumar Bora
Department of Electronics and Electrical Engineering,
Indian Institute of Technology Guwahati,
Guwahati-781039, Assam, India.

Date: _____

Acknowledgements

I owe my sincere gratitude to my parent organization Bharat Electronics Ltd for providing me the opportunity to carry out the research work. My sincere gratitude goes with my family members and close friends, who constantly supported me during the entire period of the research. I am indebted to my principal thesis supervisor Prof. Prabin Kumar Bora, who's precious guidance has made it possible to reach the goals of the research. I am equally grateful to my local supervisor Dr. Chaveli Ramesh for providing timely guidance and feedback on the progress of the research work.

I would like to extend my sincere gratitude to the members of my doctoral committee Dr. A Rajesh, Dr. Kannan Karthik, Prof. Rohit Sinha and Prof. P. R. Sahu for providing valuable guidance and continuous feedback for improving the work. I would like to thank all the faculty, staff members and research scholars of the EEE department, IIT Guwahati for providing an interactive and co-operative atmosphere all throughout.

Last but not the least, my special thanks goes to fellow researchers Mridupawan Sonowal, Ramesh Chandra Mishra and Dr. Kuntal Deka for their all round help and support during the entire duration of the research.

Sincerely
Gaurav Jyoti Phukan

Abstract

Non-data aided (NDA) modulation classification (MC) is widely used in several military and civilian applications. Certain military applications like communication intelligence (COMINT) demands the automatic MC in a completely blind scenario with challenging channel conditions. The need for improvement of the existing MC methods in such adverse channel conditions is the principal motivation behind this research work. A detailed analysis of the existing modulation classification methods shows that, the likelihood based (LB) method is the best due to the availability of the optimum solution. From the practical point of view, a complete blind scenario without any information about the received signal parameters is considered. In such a scenario, blind parameter estimation becomes the essential pre-processing stage for the MC. In this research, the performance of the LB MC is explored with the symbol rate, the signal gain, the noise power, the phase offset and the channel impulse response as the unknown parameters with primary focus on developing new parameter estimation algorithms in deteriorated signal conditions. To ensure an accurate timing recovery during the IQ demodulation process in the receiver, a robust estimator of the symbol rate using the second order cyclostationarity of the modulated signals is proposed . Due to the robustness of the estimator at low signal to noise ratio (SNR) and fading scenarios, there is a significant improvement in performance as compared to the existing estimators. After ensuring an accurate timing recovery, the MC is performed on the complex base-band signal. However, the signal needs to be preprocessed to mitigate the distortions imparted by the channel to make it suitable for the LB MC. A new gain estimator is proposed using the fuzzy-c means clustering algorithm with a pre-defined number of clusters. Upon comparison with the existing methods, the new proposal showed certain improvement of performance in low SNR conditions. To improve the performance of the gain estimator further and for addressing the blind scenario in a comprehensive manner, an approach using the Gaussianity of the received base-band signal is proposed. Using this approach, the robust estimation of the signal gain, the phase offset and the noise power can be achieved under slow fading scenarios. The main step in the new method is to estimate the cluster centers of the received signal using the expectation maximization (EM) algorithm. The cluster centers and the noise power of the clusters are estimated using the EM algorithm. The number of clusters of the received signal is estimated using an additional pre-processing

step in the EM algorithm, thereby improving the estimation performance of the cluster centers. Once the cluster centers are estimated, the signal gain and the phase-offset are derived using geometric transformations. The performance bounds of the proposed estimators are established by the Cramer-Rao Lower Bound (CRLB). With the proposed estimates, a significant improvement in the performance of the *quasi-hybrid likelihood ratio test* (QHLRT) classifier is achieved with reference to the existing LB and the feature based (FB) methods. Also, using the new method, the classification performance has reached close to the theoretical QHLRT upper bound. Further, the issue of the signal distortion in a residual fading scenario with the case of inter symbol interference (ISI) is taken up. Without a training sequence, the blind equalization is a challenging problem and the faithful recovery of the base-band signal is limited by the severity of the ISI. A new method is proposed for the blind channel equalization in an NDA MC scenario and the effectiveness for use in the MC under frequency selective fading is illustrated. The main focus area of this research for the improvement of classification performance under adverse channel impairments has shown bright prospects. Finally, certain field results obtained from the case of a practical implementation is brought out to highlight the operational effectiveness of the proposed MC algorithms in this research work. Among the major scope for future research includes the development of a generic signal classifier to address diverse types of signals including single carrier, multi-carrier, multiple input multiple output (MIMO) and Radar signals.

Contents

List of Figures

List of Tables

List of Symbols

$H^{(i)}$ i^{th} hypothesis

$\mathcal{C}$ Total number of modulation schemes in the pool of candidates

$\hat{}$ Notation for estimation

$r_c(t)$ Received modulated carrier signal

f_c Carrier frequency

Δf Carrier frequency offset

ϕ Carrier phase offset

s_k k^{th} complex base-band symbol

h Channel impulse response

$n_g(t)$ Additive white Gaussian noise

$\mathbf{n}$ Complex AWGN noise vector n_{ng} Complex Non-Gaussian noise

T_s Symbol period

f_s Symbol rate

t_0 Timing offset

x_k k^{th} sample of the complex base-band received signal

$x_{I,k}$ In-phase component of x_k

$x_{Q,k}$ Quadrature-phase component of x_k

$\tilde{}$ Notation for normalization

N Power spectral density of AWGN

α Channel gain

ψ Base-band phase offset

P_{cc} Probability of correct classification

P_{fc} Probability of false classification

N_b Base-band sample size

$M^{(i)}$ Number of symbols of the i^{th} modulation

Θ Vector of the unknown parameters

L Likelihood function

l Log-likelihood function

$\mathbf{h}$ Channel impulse response vector

σ^2 Variance of AWGN

σ_n^2 Variance of the n^{th} noise component

λ_n probability that n^{th} noise component of noise is present

$C_{p,q}$ p^{th} order, q conjugate cumulant

ω Cyclic frequency

τ Time delay

$R_r^{\omega}(\tau)$ Cyclic autocorrelation function

$S_r^{\omega}(f)$ Spectral correlation function

$C_r^{\omega}(f)$ Spectral correlation coefficient

$I(\omega)$ Cyclic domain profile

$C_x(\omega;\tau)_{p,q}$ p^{th} order q conjugate cyclic cumulant

$\mathbf{F}_r$ Feature vector

G^{ω} Cyclic domain power profile

J Cost function

μ_k Center of the k^{th} cluster

e Error

$\mathbf{\Sigma}_k$ Covariance matrix

$p_k(\mathbf{x}_n)$ PDF of the k^{th} Gaussian cluster

$P(\omega_k)$ Prior probability of the k^{th} cluster

$\omega_{k,n}^{(t)}$ Probability that the n^{th} sample belongs to the k^{th} cluster

$Kurt$ Kurtosis

N_k Number of samples in the k^{th} cluster

S_I In-phase component of the unit magnitude library symbol

S_Q Quadrature-phase component of the unit magnitude library symbol

μ_{max} Center of the outermost cluster

M_{outer} Number of symbols in the outermost constellation ring

$\boldsymbol{\theta}$ Parameter vector

$\mathbf{w}_k$ k^{th} weight vector of the equalizer

$Q(.)$ Decision function

List of Abbreviations

ALRT: Average likelihood ratio test

AWGN: Additive white Gaussian noise

BW: Baum Welch

CDP: Cyclic domain profile

CDMA: Code division multiple access

CDPP: Cyclic domain power profile

COMINT: Communication intelligence

CMA: Constant modulus algorithm

CRLB: Crammer Rao lower bound

DA: Data aided

DDLMS: Decision directed least mean square

ECM: Expectation conditional maximization

EM: Expectation maximization

FAM: FFT accumulation method

FB: Feature based

FH: Frequency hopping

FIR: Finite impulse response

FKM: Fuzzy k-means

GLRT: General likelihood ratio test

GMM: Gaussian mixture model

HLRT: Hybrid likelihood ratio test

HOS: Higher order statistics

HWT: Haar wavelet transform

ICA: Independent component analysis

IIR: Infinite impulse respopnse

ISI: Inter symbol interference

KM: k-means

LB: Likelihood based

LLF: Log-likelihood function

LRT: Likelihood ratio test

MC: Modulation classification

MCMC: Markov chain Monte Carlo

M-CMA: Modified constant modulus algorithm

MDCE: Minimum distance centroid estimation

MIMO: Multiple input multiple output

ML: Maximum likelihood

MoM: Method of moments

MSE: Mean square error

MUMC: Multiuser modulation classification

NDA: Non-data aided

NPLF: Non-parametric likelihood function

OFDM: Orthogonal frequency division multiplexed

PDF: Probability density function

PSD: Power spectral density

QHLRT: Quasi-hybrid likelihood ratio test

SCC: Spectral correlation coefficient

SC-FDE: Single channel frequency domain equalization SCF: Spectral correlation function

SCLD: Single channel linear digital

SDR: Software defined radios

SGD: Stochastic gradient descent

SNR: Signal to noise ratio

SS: Spread spectrum

SSCA: Strip spectral correlation algorithm

1

Introduction

1.1 Blind Classification of Digital Modulations

The electromagnetic spectrum has been highly populated in the recent time. In several applications, it is necessary to ascertain the characteristics of the communication signals without any knowledge of the signal and channel parameters. The two major steps involved in this process are the blind detection and estimation of the signal characteristics. In the current scenario, communication signals are digitally modulated primarily, with a large possibility of the modulation types and variations in the parameters like the bandwidth, the symbol rate, etc. Once a signal is detected, the subsequent process of estimation is blind, since the signal and the propagation channel parameters are either completely unknown, or only partially known. The blind classification of digital

modulations, known as the automatic modulation classification (MC) in the literature starts with certain preprocessing stages to condition the signal for the final stage of MC. The preprocessing is carried out to mitigate the distortion imparted by the propagating channel. The process involves the blind estimation of the channel and signal parameters. The blind approach primarily needs to pay the penalty for the computational complexity while estimating the parameters. Moreover, the practical parameter estimators are not perfect. They suffer from the estimation error, while the severity of the error is dependent on the algorithms as well as the channel conditions. The price for the gross effect of the estimation errors is finally paid by the MC performance. Once the signal is conditioned, the MC can be carried out by using several available methods [1, 2]. Broadly, the MC methods are categorized into the *likelihood based* (LB) [3–7] and the *feature based* (FB) [8–10]. In the LB method, MC is carried out using multiple hypotheses testing, while the likelihood of the received signal is maximized with respect to the hypotheses to decide about the modulation type. The LB provides an optimum solution, since it is carried out by minimizing the decision error. The FB classification involves feature extraction and pattern recognition to perform the MC. Although FB is sub-optimal, it is simple to implement [1]. The selection of the appropriate method is governed by the application and the usual propagation conditions for that scenario.

1.2 Motivation

The MC technology has been evolving during the last two decades. The primary focus for the improvement was to shift from the semi-blind classification scenario towards complete blind or non-data-aided (NDA) scenarios. Another important area of focus has been the need for a robust classifier for weak signals received under adverse channel conditions. The automatic MC has a widespread use in military and civilian applications.

1.2.1 Military applications

Among the military applications, automatic MC finds extensive use in communication intelligence (COMINT) [1, 11]. The COMINT systems are used for gathering intelligence

from the adversary's communication signals. In a typical COMINT monitoring system, signal activities are detected, the direction of arrival is estimated and signals originating from adversary's territory are further analyzed to find the carrier parameters like the symbol rate and the modulation type. After successful classification, the signal is demodulated and processed to extract the information within the signal. Since these signals are often intercepted from a long distance, the quality of the received signal is poor in terms of the signal to noise ratio (SNR). In many cases, the signals also suffer from severe multi-path fading due to the successive reflections in the mountainous terrains.

1.2.2 Civilian applications

Cognitive radio and spectrum monitoring are the main applications of automatic MC in the civilian domain [1]. As the available spectrum is reducing rapidly, the cognitive radio attempts to re-use the occupied bandwidth during the silent periods of the allotted communication systems. Most significantly, this requires efficient and faster ways to sense the spectrum activity and estimate the channel conditions. The cognitive radio estimates the best spectrum slot for transmitting the data and depending on the channel condition, uses a particular modulation technique for transmission [12]. On the other hand, the receiver senses the channel condition and receives the signal. However in a scarce bandwidth arena, without a preamble in the signal to inform about the modulation, the receiver has to classify the modulation and automatically configure itself to receive the signal. Although in the cognitive radio application, the list of possible modulation schemes is known, the MC algorithm has to be efficient in terms of computational performance to achieve the required response time. Further challenges are introduced if the signal suffers from fading in the urban and mobile scenarios. Hence, the mitigation of fading impairment remains a mandatory feature in the MC for civilian applications. Spectrum monitoring applications [13] are generally used by telecommunication regulatory authorities to ensure the authorized use of the allocated spectrum. Each allocated slot in the spectrum is monitored by the system to detect if there is any violation in the usage. To characterize the signal sources, automatic MC is used as one of the important analysis tools.

The widespread applications of the MC provide the following major motivations for further research:

1. For the military applications of MC, the performance benchmarks of the available classifiers under the adverse channel conditions needs improvements for effective practical implementations. This stands the main motivation behind this research work. Considering the typical received signal quality in a target deployment scenario, a significant improvement is envisaged in the classification performance. The work is aimed at achieving a complete blind classifier with robust classification performance in adverse channel conditions.

2. In the civilian domain, the classification has to be carried out for a large pool of candidate modulation schemes with reasonably good classification accuracy and speed. This has to be achieved along with a robust performance under difficult channel conditions. The need for formulating robust parameter estimators that can be used for a generic pool of modulations is also one of the major motivating factors for this research.

1.3 Problem Definition

1.3.1 Signal Model

The signal model is defined in a scenario containing $\mathcal{C}$ candidate modulations. In MC, the i^{th} candidate modulation is denoted as the hypothesis $H^{(i)}$. The received modulated carrier signal model for the i^{th} hypothesis is given by [14]

$$r_c(t) = e^{j2\pi(f_c+\Delta f)t}e^{j\phi}\sum_{k=-\infty}^{\infty} s_k^{(i)}h(t-kT_s-t_0)+n_g(t), \tag{1.1}$$

where, f_c and Δf are the carrier frequency and carrier frequency offset respectively, ϕ is the carrier phase offset, $h(\cdot)$ is the combined effect of fading and pulse shaping, T_s is the symbol period, t_0 is the timing offset, $s_k^{(i)}$ is the k^{th} symbol and $n_g(t)$ is the additive white Gaussian noise (AWGN). The unknown parameters f_c, Δf, T_s, t_0, ϕ and h need to be estimated for performing the baseband recovery for use in the MC. Denoting $\mathbf{x}$

as the vector of the complex base-band signal, $\mathbf{s}^{(i)}$ as the vector of transmitted symbols for $H^{(i)}$ and $\mathbf{n}$ as the vector of the complex AWGN, the matched filtered output of the signal is given by [15]

$$\mathbf{x} = \alpha^{(i)} e^{j\psi^{(i)}} \mathbf{s}^{(i)} + \mathbf{n} \tag{1.2}$$

where, $\alpha^{(i)}$ is the resultant channel gain and $\psi^{(i)}$ is the resultant phase offset due to all the impairments. With the practical difficulty of signal imperfections due to the receiver implementations added with the adverse channel impairments, the unknown parameters $\alpha^{(i)}$, $\psi^{(i)}$ and the power spectral density of AWGN $N^{(i)}$ need to estimated in the baseband for using in MC. The blind MC problem can be defined as the problem of achieving high accuracy of classification, given a wide range of unknown and uncertain parameters. The major issues of the MC problem are listed below:

1.3.2 Robustness to Wide Range of SNRs

In general, the signal of interest is received under a wide range of SNRs. In many applications, the received SNR is so low that the signal is buried in the noise. For example, the performance of the LB MC is effected by the modulation order. The higher order modulations have more densely packed decision boundaries for the received symbols. This deteriorates the decision performance at adverse channel conditions. However, the blind MC algorithm needs to be robust enough to handle such adverse SNR conditions.

1.3.3 Robustness to Channel Impairments

Multipath fading is unavoidable in modern wireless communication systems. Blind MC has to perform with adequate level of accuracy in such circumstances. Depending on the scenario of implementation, the blind MC has to be robust against slow and flat fading channels as well as fast and frequency selective ones. Apart from the propagating channel, imperfections in the receiver characterized by Δf, ϕ and t_0 contribute to the performance degradation of blind MC. The blind classifier needs to be robust against the overall effects of the channel impairments.

1.3.4 Suitability for a Large Pool of Modulations

In certain civilian applications like cognitive radios and software defined radios (SDRs), the candidate pool may be limited to only the assigned group of modulations as per the design of the communication system. However in military applications and certain civilian applications like spectrum monitoring, the blind MC has to be robust enough to identify the correct modulation among a large pool of possible candidates. There is a reasonable uncertainty and challenge to design a blind classifier to provide accurate classification in such scenarios.

1.3.5 Simplicity of Implementation

In applications like cognitive radios and SDRs, the blind MC has to be fast enough to be suitable for real time applications. Hence, the MC algorithms need to be computationally simple, such that the processing time is very short. However, the classification accuracy remains a demand anyway. In practical scenarios, various factors effects the computation complexity in MC. For example, the complexity of the QHLRT MC is given by $\mathcal{O}(\sum_{i=1}^{\mathcal{C}} N_b M^{(i)})$, where N_b and $M^{(i)}$ are the sample size and order of the i^{th} modulation respectively. As evident in this example, the computational complexity increases if the pool of candidates contain modulations of higher order. Further, bigger the size of the candidate pool, the higher is the computational complexity of the MC. In modern implementations, the availability of high-speed processing resources has enabled possibility of implementing more sophisticated algorithms to process the signal within a short duration. The trade off between the classification accuracy and the real time processing demand has to be addressed in the design of the blind classifiers.

In this thesis, the following problems are addressed:

1. Blind estimation of the symbol rate for accurate recovery of the base-band under fading and pulse-shape uncertainties.

2. Estimation of the channel gain for a generic pool of PSK and QAM modulations.

3. Blind estimation of the phase-offset for slow and flat fading channels.

4. Estimation of the noise power for constant and multi-amplitude modulation schemes.

5. Mitigation of the frequency selective fading as a pre-processing step for blind LB MC.

1.4 Outline of the Thesis and Contributions

The thesis comprises of 8 chapters including the present one. The rest of the thesis is organized as follows:

In Chapter 2, a thorough literature survey on the blind MC algorithms is presented and a performance benchmark is established. Using the performance benchmark, the shortfalls of the existing blind classifiers have been analyzed and the direction for improvement of the performance has been formulated. Due to the availability of the near optimal solutions, the likelihood based (LB) classification is primarily adopted for the subsequent work in this dessertation.

In Chapter 3, the issue of the signal timing accuracy is addressed by proposing a blind estimation method for the symbol rate using cyclostationarity property of the modulated signals. Using the new method, better estimation accuracy has been achieved in multipath fading scenarios at low SNR region. The symbol rate estimation is a necessary pre-processing stage for all the MC algorithms involving demodulated base-band signals. Due to robust performance of the new symbol rate estimation approach, timing uncertainty has been ignored in the subsequent chapters for achieving robust blind MC performance.

In Chapter 4, the problem of signal gain uncertainty is addressed to achieve better classification performance in low SNR conditions. Although, the approach is semi-blind, it provides a basis for addressing other parameters towards a blind MC in the subsequent work in this thesis.

Chapter 5 presents a comprehensive approach for the MC using blind parameter estimation and signal pre-processing. The final classification in the LB framework is illustrated. The proposed LB classifier employs the demodulated base-band signal in the I-Q plane.

The effect of channel impairment is mitigated by using the new methods proposed for estimating the channel gain, the phase offset and the noise power. The performance of the parameter estimators has been examined in a fading scenario. It is observed that, the proposed estimator outperform the existing algorithms in similar deployment conditions. At the same time, the LB classifier attains a near ideal performance while being robust for a range of fading severities, even in the low SNR region.

In Chapter 6, the problem of residual fading effect in the base-band signal is addressed, considering a frequency selective fading scenario. The inter-symbol interference (ISI) is the primary effect of the frequency selective fading. In consequence, the received baseband becomes un-recognizable in the I-Q plane. To mitigate this issue, a new blind equalization approach is proposed to suit the blind MC scenario. Applicability of the proposed method for the LB MC is verified under various fading severities.

In Chapter 7, an illustration of practical implementation of the proposed MC algorithms is brought out. MC performance recorded in the trial deployment is presented to correlate the theoretical and the practical scenarios.

Chapter 8 concludes the thesis with a summary of the contributions made and an outline on future research directions.

2

A Survey of Blind Classification of Digital Modulations

2.1 Introduction

Digital MC is a widely investigated topic for the last two decades as discussed in the earlier chapter. The utility of digital MC has spanned from military applications in COMINT to civilian applications like software defined radios, cognitive radios and spectrum monitoring for regulatory purposes. Although a vast literature on this topic is available with a variety of approaches, the main focus of this survey will be on the work carried out to address the problems involving adverse channel conditions and practical implementation aspects. A detailed literature survey was conducted in [1], which

provided a comprehensive overview of various approaches to MC. Subsequently several work have been carried out towards the design of more robust classifiers. Dobre in [2] provides an updated perspective of the progress of MC in cognitive radio applications, with a special focus on the generic problem of signal classification with diverse candidates like single channel linear digital (SCLD) modulations, single channel frequency domain equalization (SC-FDE) signals, orthogonal frequency division multiplexed (OFDM) signals, multiple input multiple output (MIMO) signals. The method also addresses the classification of AM and FSK signals. Although the author provides a broader view of signal classification problem in general, a focused study towards MC performance improvements for specific applications like COMINT, spectrum monitoring etc. needs to be taken up.

Recall that, the MC is broadly categorized into the LB and the FB approaches. The LB approach formulates the MC as a multiple hypothesis testing problem with $\mathcal{C}$ composite hypotheses $H^{(0)}, H^{(1)}, ..., H^{(\mathcal{C}-1)}$ corresponding to $\mathcal{C}$ modulation types. This principle is based on the *likelihood ratio test* (LRT), derived from the Bayesian a-posteriori probability decision rule [16]. For the multiple hypothesis testing, the likelihood of the received signal is maximized with respect to the hypotheses to decide about the modulation type. Early LB methods [3, 4, 17] were primarily focused on the problem of MC in AWGN with certain imperfections like the phase offset, the timing offset etc. in the receiver. In these scenarios, with no or only a few unknown parameters, the *average likelihood ratio test* (ALRT) [3, 4] was used due to the availability of the optimal solution. However, since the complexity of the ALRT classifier increases with the increasing number of the unknown parameters, the sub-optimal and modified LB classifiers like the *general likelihood ratio test* (GLRT) [5], the *hybrid likelihood ratio test* (HLRT)[6, 7] were proposed. Although these early classifiers provided a good theoretical basis for the MC problem, their practical utilities were limited, since the assumed scenario was either ideal with the knowledge of the signal parameters or semi-ideal with the partial knowledge of certain parameters. A practical modulation classifier must be blind, without any prior knowledge of the signal parameters and channel conditions. The desirable features of a robust classifier include

1. high overall accuracy of classification,

2. efficiency in a short observation interval,

3. operability in large range of signal to noise ratios (SNRs),

4. accuracy in a large pool of modulations,

5. robustness to model mismatch under diverse propagation conditions and

6. low computational complexity during implementation.

With these challenging requirements, the MC from ideal to semi-blind to blind LB classification approaches [15, 18–27] has been evolving over a period of time, until non-data aided (NDA) blind MC has become the state of the art in recent time. The *quasi-hybrid likelihood ratio test* (QHLRT) [15, 21–24] classifier has been used in recent time for practical implementation.

Although suboptimal, the FB approaches have been proposed widely due to the simplicity of implementation. The FB framework has the feature extraction followed by the pattern recognition as two stages in the classification process. In the first stage, certain signal features specific to the modulated signals are extracted. The selected features vary depending on the method. Among the wide variety of features used, instantaneous carrier parameters [8], carrier DFT [28], the PDF of the carrier phase [29], the variance of the Haar wavelet transform (HWT) [30], statistical moments [31], statistical higher order cumulants [9, 32–34], cyclic cumulants [10] etc. are prominent. In the pattern recognition stage, the set of features is used to identify the modulation scheme. The early FB algorithms were proposed in ideal conditions of AWGN only. The issue of unknown receiver parameters was first addressed in [35], followed by more practical approaches involving non-ideal channel conditions [9, 10, 32–34, 36–47].

In this chapter, the focus is centered around the performance of the specific MC algorithms, proposed to mitigate various channel impairments in a blind scenario. In Section 2.2, the common signal model under the propagation channel effects is illustrated. The commonly used performance measures for MC is described in 2.3. In Section 2.4, the achievements of the LB approach to mitigate the impairments are examined. Illustration of the performance of the blind FB classifier in mitigating the same set of effects

is covered in Section 2.5. Section 2.6 summarizes the MC methods towards practical applications in the blind scenario. In section 2.7 we take up the performance comparison of the major classification aspects of the LB and the FB methods and thereby establish a generalized performance benchmark. Concluding remarks are presented with a specific mention on the scope of the present research in Section 2.8.

2.2 Signal Model and the Effects of the Channel on the Received Signal

Consider the modulated carrier and the matched filtered output as described in Chapter 1.

$$r_c(t) = e^{j2\pi(f_c+\Delta f)t} e^{j\phi} \sum_{k=-\infty}^{\infty} s_k^{(i)} h(t - kT_s - t_0) + n_g(t), \tag{2.1}$$

and

$$\mathbf{x} = \alpha^{(i)} e^{j\psi^{(i)}} \mathbf{s}^{(i)} + \mathbf{n} \tag{2.2}$$

where the symbols have their usual meanings as explained earlier. In a blind scenario, the unknown parameters for the MC are f_c, Δf, T_s, t_0, ϕ, h, $\alpha^{(i)}$, $\psi^{(i)}$ and the power spectral density of the AWGN component $\mathbf{n}$. Depending on the application scenario, the severities of these unknown parameters vary. For example, for a high performance receiver, Δf, t_0 and ϕ terms may be considered insignificant. The multipath fading effect can be modeled as a finite impulse response (FIR) filter. The impulse response of the fading channel has been most commonly modeled as a three-tap FIR filter represented by the vector $\mathbf{h} = [h_1\ h_2\ h_3]^T$ [15, 21]. The coefficient h_1 represents the line of sight component, whereas h_2 and h_3 represent the variance of the gain of the multipath components respectively. Consider a slow-fading Rician channel, which is time invariant within the sample duration. The effect of the channel parameters on the received signal is illustrated in Figure 2.1. We consider a 16QAM signal at 10 dB SNR. Figure 2.1a shows the received signal in the AWGN scenario. This is the ideal reception scenario, where the receiver imperfections and the channel effects are not significant. The effect of signal gain due to the channel propagation effect is illustrated in Figure 2.1b. The channel gain introduces a model mismatch in LB classification. A model mismatch occurs when the

magnitude and phase orientation of the received signal differs from those of the library symbols stored in the receiver. In a more practical scenario, the received signal suffers from the multipath fading as well as receiver imperfections. In case of the flat and slow fading environment, the model mismatch will result from a combined effect of the channel gain and the phase offset, as illustrated in Figure 2.1c. The model mismatch takes a severe form in a fast fading channel, as shown in Figure 2.1d. In such cases, the received signal is affected by ISI, apart from the gain mismatch and the phase-offset. The ISI is also predominant in a frequency selective channel as shown in Figure 2.1e. The issue of the man-made impulse noise in the dense urban electromagnetic environment, was studied recently in the context of MC [22, 25, 27]. In such cases, due to the presence of impulses in an AWGN scenario, the received signal will take a non-Gaussian form with scattered symbols (2.1f) in the I-Q plane. Depending on the severity of such impulse noise, the performance of the MC algorithms is affected.

2.3 Performance Measures

The performance measure of the modulation classifier is based on the success count in classifying the modulation in a predefined candidate pool. The pool of candidates is often decided based of the application. A performance measure is very useful during the formulation and design stages of the classifier. It is also used as the benchmark measure among the various classifiers available.

Probability of Correct Classification

For the i^{th} modulation, the performance of the MC algorithm is measured by the probability of correct classification $P_{cc}^{(i)} = P\left(\hat{H} = H^{(i)}/H^{(i)}\right)$, where $\hat{H}$ is the hypothesis decided at the receiver [1, 3, 4, 17]. It is the probability that the received signal is declared as $H^{(i)}$, when the actual modulation is $H^{(i)}$. For experimental evaluation, P_{cc} is estimated as

$$\widehat{P}_{cc}^{(i)} = \frac{N_C^{(i)}}{N_T}, \tag{2.3}$$

where, $N_C^{(i)}$ and N_T are the number of correct decisions and total number of experiments respectively.

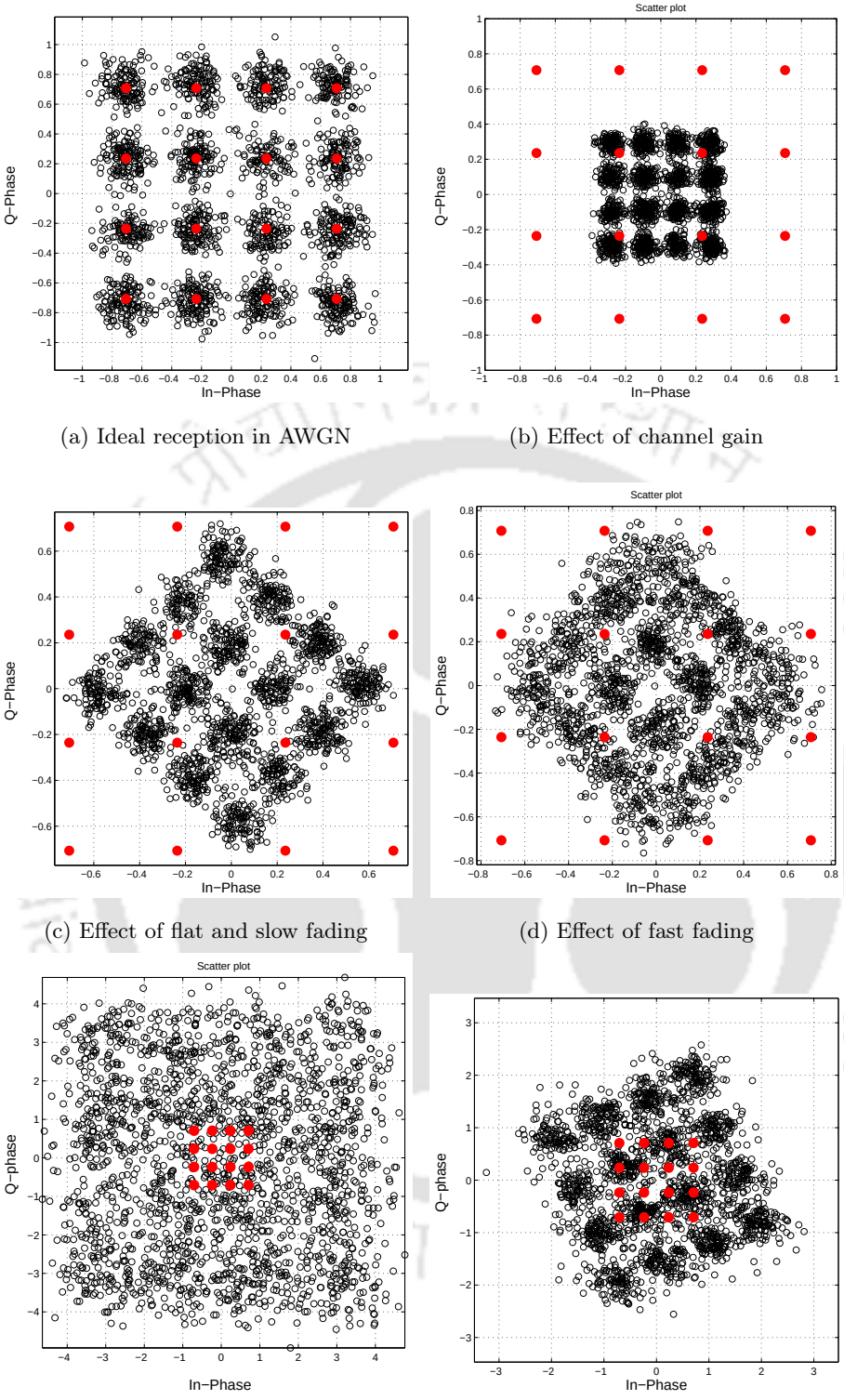

(a) Ideal reception in AWGN

(b) Effect of channel gain

(c) Effect of flat and slow fading

(d) Effect of fast fading

(e) Effect of frequency selective fading

(f) Effect of non-Gaussian noise

FIGURE 2.1: Effect of channel parameters for 16QAM signal at 10 dB SNR

Probability of False Classification

This is another way of measuring the performance of the modulation classifier and defined as

$$P_{fc}^{(i)} = P\left(\hat{H} \neq H^{(i)}/H^{(i)}\right) \tag{2.4}$$

The corresponding estimate of $P_{fc}^{(i)}$ is $\widehat{P}_{fc}^{(i)} = \frac{N_F^{(i)}}{N_T}$, where $N_F^{(i)}$ is the number of false decisions made by the classifier for the i^{th} hypothesis.

2.4 LB Techniques Towards Blind Scenario

The LB classification of digital modulations is based on the estimation of the maximum likelihood (ML) among the hypotheses representing $\mathcal{C}$ modulations. The Bayesian maximum a-posteriori probability decision rule is given by

$$\frac{P\left(H^{(i)}|\mathbf{x}\right)}{P\left(H^{(j)}|\mathbf{x}\right)} \underset{H^{(j)}}{\overset{H^{(i)}}{\gtrless}} 1, \tag{2.5}$$

where, $P\left(H^{(i)}|\mathbf{x}\right)$ and $P\left(H^{(j)}|\mathbf{x}\right)$ denote the posterior probabilities for the hypotheses $H^{(i)}$ and $H^{(j)}$ respectively for the given received signal $\mathbf{x}$. In the MC scenario, all modulations are considered to have equal prior probabilities, so that $P\left(H^{(i)}\right) = P\left(H^{(j)}\right)$. Using the Bayes rule [16], Equation (2.5) is converted into the likelihood ratio $\Lambda(\mathbf{x})$ and given by

$$\Lambda(\mathbf{x}) = \frac{P\left(H^{(i)}|\mathbf{x}\right)}{P\left(H^{(j)}|\mathbf{x}\right)} = \frac{L\left(\mathbf{x}|H^{(i)}\right)}{L\left(\mathbf{x}|H^{(j)}\right)} \underset{H^{(j)}}{\overset{H^{(i)}}{\gtrless}} 1, \tag{2.6}$$

where, $L\left(\mathbf{x}|H^{(i)}\right)$ is the likelihood function of $\mathbf{x}$ given the hypotheses $H^{(i)}$. In the context of blind MC, the likelihood ratio test method is extended to the multiple hypothesis testing [16]. Depending on the method of implementation, various likelihood functions are defined for the ML method. Suppose $\mathbf{x}_1, \mathbf{x}_2, \cdots, \mathbf{x}_{N_b}$ are N_b samples of the received signal. Based on the simplification of the models for the modulation parameters, different LRT schemes are proposed. These methods are briefly described below.

2.4.1 ALRT

The optimal ALRT [3, 4] likelihood function for the i^{th} hypothesis is defined as

$$\begin{aligned} L_{ALRT}(\mathbf{x}|H^{(i)}) &= \int_{\Theta^{(i)}} L(x_k|\Theta^{(i)}) f(\Theta^{(i)}) d\Theta^{(i)} \\ &= \int_{\Theta^{(i)}} \prod_{k=1}^{N_b} \sum_{m=1}^{M^{(i)}} \frac{1}{M^{(i)}\pi N^{(i)}} \times exp\left\{ -\frac{1}{N^{(i)}} \left| x_k - \alpha^{(i)} e^{j\psi^{(i)}} s_m^{(i)} \right|^2 \right\} \\ &\quad f(\Theta^{(i)}) d\Theta^{(i)} \end{aligned} \tag{2.7}$$

where, $L(x_k|\Theta^{(i)})$ is the likelihood given the unknown parameter vector $\Theta^{(i)}$, $f(\theta|H^{(i)})$ is the probability density function of the parameter set $\Theta^{(i)}$ under hypotheis $H^{(i)}$, $M^{(i)}$ is the number of ideal symbols for the i^{th} hypothesis, $N^{(i)}$ is the noise power and $s_m^{(i)}$ is the m^{th} ideal symbol. The MC is carried out by the decision rule

$$\hat{H} = \arg\max_i L_{ALRT}(\mathbf{x}|H^{(i)}) \tag{2.8}$$

The computational complexity of the ALRT is very high due to the involvement of multiple levels of integration as the number of unknown parameters increase in a blind scenario [15].

2.4.2 GLRT

The GLRT [5] offered a simplified likelihood function given by

$$L_{GLRT}(\mathbf{x}|H^{(i)}) = \arg\max_{\Theta^{(i)}} \prod_{k=1}^{N_b} \arg \max_{s_m^{(i)} \in S^{(i)}} \frac{1}{M^{(i)}\pi N^{(i)}} \times exp\left\{ -\frac{1}{N^{(i)}} \left| x_k - \alpha^{(i)} e^{j\psi^{(i)}} s_m^{(i)} \right|^2 \right\} \tag{2.9}$$

where, $S^{(i)}$ is the symbol space for $H^{(i)}$. However, the GLRT failed to distinguish between the nested modulation schemes like the QPSK and the 16QAM. This has led to the proposal of the HLRT [5].

2.4.3 HLRT

The likelihood function of the HLRT is calculated by averaging the likelihood function over the transmitted symbols and then maximizing the resulting likelihood function with respect to the unknown parameters. The HLRT likelihood function is given by

$$L_{HLRT}(\mathbf{x}|H^{(i)}) = \arg\max_{\Theta^{(i)}} \prod_{k=1}^{N_b} \sum_{m=1}^{M^{(i)}} \frac{1}{M^{(i)}\pi N^{(i)}} \times exp\left\{ -\frac{1}{N^{(i)}} \left| x_k - \alpha^{(i)} e^{j\psi^{(i)}} s_m^{(i)} \right|^2 \right\} \tag{2.10}$$

Although the HLRT is constituted with the advantages of both the ALRT and the GLRT, the maximization process requires exhaustive search within the range of $\Theta^{(i)}$. As the number of unknown parameters increases, the HLRT classification becomes impractical.

2.4.4 QHLRT

The QHLRT is a simplified LB method, where the estimates of the unknown parameters are used in the likelihood function. Under the framework of the QHLRT, the log likelihood function for the hypothesis $H^{(i)}$ is defined as

$$l(\mathbf{x}|H^{(i)})_{QHLRT} = \sum_{k=1}^{N_b} \ln \left[\sum_{m=1}^{M^{(i)}} \frac{1}{M^{(i)}\pi N^{(i)}} \times exp\left\{ -\frac{1}{N^{(i)}} \left| x_k - \alpha^{(i)} e^{j\psi^{(i)}} s_m^{(i)} \right|^2 \right\} \right] \tag{2.11}$$

The proposed work in the subsequent chapters use the QHLRT LB classifier for MC. We review the existing literature on the QHLRT based LB MC. Fahed et al [15] adopted the QHLRT based approach while considering a blind scenario in a flat fading channel, due to the advantage of the computational simplicity. In this case, the unknown parameters are estimated for using in the likelihood function. The authors establish a benchmark performance among the optimum ALRT and the QHLRT classifiers. The independent parameter estimation approach considered in this work is primarily due to the marginal performance gain in the joint estimates at the higher cost of computational complexity. The joint parameter estimate is an ML based approach [15], theoretically involving the original baseband signal sequence. The computational complexity for this method in a

MC problem is $\mathcal{O}\Big(\mathcal{C}M^{(i)^{N_b}}\Big)$. Evidently, the computational complexity significantly increases for any practical candidate pool consisting of simple binary modulation to higher order PSK and QAM modulations. Hence, in a blind MC scenario, this approach is not feasible for practical implementation. For simplicity of implementation, the method of moments (MoM) based blind parameter estimation is used for estimating the unknown parameters like the signal gain, the phase offset and the noise power. The QHLRT−MoM classification performance of the BPSK and the QPSK signals is compared with the classical ALRT and the ideal QHLRT. Further, a residual fading channel model is considered to compare the performance of the QHLRT−MoM classifier with the ideal QHLRT. The paper establishes a clear performance benchmark for practical LB classification technique using parameter estimation.

We further examine the other latest works [21–24, 26] on the QHLRT based classification method in a blind scenario. In [21], iterative methods for parameter estimation is adopted using the Baum Welch (BW) algorithm and Markov chain Monte Carlo (MCMC) methods. In this proposal, the frequency offset, the phase offset and the residual channel parameters are estimated iteratively to finally use the QHLRT framework for MC. Although the MCMC method provides a better accuracy by approximating the numerical integration process used for the mean square error (MSE) based parameter estimator, it has been achieved at the cost of significant computational resources.

The scenario of non-Gaussian channel (Figure 2.1f) has been considered in [22, 25, 27], with the man-made impulse noise contributing to the natural AWGN. In [22, 25], the non-Gaussian noise has been modeled as a mixture of several Gaussians with different variances and probability of occurances. The corresponding likelihood function has been adapted to the scenario of the impulse noise added to the AWGN. The additive non-Gaussian noise model is defined in terms of the noise probability density function (PDF).

$$p(n_{ng}) = \sum_{n=1}^{N_a} \frac{\lambda_n}{2\pi\sigma_n^2} exp\Big(- \frac{|n_g|^2}{2\sigma_n^2}\Big), \tag{2.12}$$

where, $\{n_{ng}[k]\}_{k=1}^{N_b}$ is the k^{th} sample of the noise, λ_n is the probability that n_g contributes to the n^{th} term in the PDF, N_a is the number of individual Gaussian noise components contributing to the additive noise and σ_n^2 is the variance of the n^{th} component. The

likelihood function is derived by considering the noise parameter as a Gaussian mixture model (GMM). The corresponding MC decision rule is given by

$$\hat{H} = \arg\max_{i} \sum_{k=1}^{K} log\Big\{ \frac{1}{M^{(i)}} \sum_{m=1}^{M^{(i)}} \sum_{n=1}^{N_a} \Big\{ \frac{\hat{\lambda}_n^{(i)}}{2\pi(\hat{\sigma}_n^{(i)})^2} \times \exp\Big(- \frac{|x_k - \hat{\alpha_f}^{(i)} s_m^{(i)}|^2}{2(\hat{\sigma}_n^{(i)})^2} \Big) \Big\} \Big\}, \quad (2.13)$$

where, the unknown parameter vector is defined as $\Theta = \{\alpha, \lambda_1, \lambda_2, ..., \lambda_{N_a}, \sigma_1, \sigma_2, ..., \sigma_{N_a}\}$. The complex fading parameter α_f represents the channel gain and the phase offset caused by the channel. The estimation of the unknown parameters has been carried out using the expectation maximization (EM) algorithm, while the likelihood function of (2.13) is employed to derive the ML estimates for the iterative process. The parameters for each hypothesis are calculated and the MC decision is finally arrived at. The method addresses the blind LB classification in a non-Gaussian scenario. However, due to high complexity, the authors used a modified version of the EM algorithm known as expectation conditional maximization (ECM). The ECM estimation method is built-on the assumption that the number of Gaussian noise components are known a-priori. In [27], the issue is addressed by removing the impulse noise components by using sparse signal decomposition. However, the method assumes the knowledge of the symbol timing, the signal gain and the phase offset in a coherent environment.

With an ML based parameter estimation approach, [23] uses the blind QHLRT classifier in a slow flat fading environment with the signal gain, the noise power and the transmitted symbols as unknown parameters. Although this approach provided a near ideal performance with respect to the HLRT approach, the ML parameter estimation is exhaustive in terms of mathematical resources.

In [24], the blind MC problem is addressed in an asynchronous scenario, where a significant timing offset is introduced in the receiver. The unknown parameters like the timing offset, the signal gain and the noise power are estimated using the MoM in a flat fading channel. The proposal provides a satisfactory performance benchmark for non-ideal scenario, but the phase offset is not considered as an unknown parameter for the QHLRT MC.

2.4.5 NPLF

A detailed work carried out in [26] addresses the blind MC problem from a different angle. For the first time, instead of using a conventional likelihood function, the authors employ a *non-parametric likelihood function* (NPLF), defined as

$$L_{NPLF}(\mathbf{x}|H^{(i)}) = \sum_{k=1}^{N_b} \sum_{m=1}^{M^{(i)}} \mathbb{I}\Big\{ \Big|\Big| x_k - \hat{A}_m^{(i)}, \Big|\Big| < R_i \Big\} \tag{2.14}$$

where, $\hat{A}_m^{(i)}$ is the estimated centroid of the m^{th} symbol for $H^{(i)}$ and R_i is the threshold value determined from the estimated channel gain $\hat{\alpha}^{(i)}$. The indicator operator $\mathbb{I}(.)$ returns 1 for true and 0 for false input condition. The estimation of the centroid is done using an iterative process based on minimization of the Euclidian distance of the assumed centroid and the actual centroid. This method is named as the minimum distance centroid estimation (MDCE). The NPLF is calculated for each hypothesis and the MC decision is arrived at by

$$\hat{H} = \arg\max_i L_{NPLF}(\mathbf{x}|H^{(i)}) \tag{2.15}$$

The method provides a low complexity approach to LB classification without taking the noise parameter into consideration. However, the classification performance deteriorates significantly in low SNR conditions.

2.5 FB Techniques Towards Blind Scenario

As stated earlier, the FB classification approach has been addressed widely due to the advantage of simplicity. We focus on three classes of algorithms: the cumulant based, the cyclostationarity based and the clustering based methods.

2.5.1 Cumulant Based Methods

The cumulant based methods [32–35] have been widely used for FB classification. The moment generating function (MFG) for a random variable X is defined in continuous

time as

$$M_X(s) = E(e^{sX}), \tag{2.16}$$

where s is a real variable. The cumulant generating function (CGF) of a random variable is defined as

$$C_X(s) = \ln(M_X(s)) = \ln(Ee^{sX}) \tag{2.17}$$

If $M_X(s)$ exists and is non-zero, then $C_X(s)$ also exists. Also since $M_X(0) = 1$, $C_X(0) = 0$. The Taylor series expansion of $C_X(s)$ about the origin gives

$$C_X(s) = \sum_{n=1}^{\infty} C(n)\frac{s^n}{n!}, \tag{2.18}$$

where the n^{th} coefficient $C(n)$ is termed as the n^{th} cumulant of the random variable X. In the discrete I-Q domain, the cumulant features are extracted from the statistical moments of the received constellation. We use the generic notation for the p^{th} order q conjugate cumulant as $C_{p,q}$, while $\hat{C}_{p,q}$ is the corresponding estimate. The second order cumulants and their corresponding estimates are given by [35]

$$C_{2,0} = E[\mathbf{x}_n^2] \quad and \quad \hat{C}_{2,0} = \frac{1}{N_b}\sum_{n=1}^{N_b}\mathbf{x}_n^2, \tag{2.19}$$

$$C_{2,1} = E[|\mathbf{x}_n^2|] \quad and \quad \hat{C}_{2,1} = \frac{1}{N_b}\sum_{n=1}^{N_b}|\mathbf{x}_n|^2 \tag{2.20}$$

Similarly, the fourth order cumulants are estimated as

$$\hat{C}_{4,0} = \frac{1}{N_b}\sum_{n=1}^{N_b}\mathbf{x}_n^4 - 3\hat{C}_{2,0}^2,$$

$$\hat{C}_{4,1} = \frac{1}{N_b}\sum_{n=1}^{N_b}\mathbf{x}_n^3\mathbf{x}_n^* - 3\hat{C}_{2,0}\hat{C}_{2,1},$$

and

$$\hat{C}_{4,2} = \frac{1}{N_b}\sum_{n=1}^{N_b}|\mathbf{x}_n|^4 - |\hat{C}_{2,0}^2| - 2\hat{C}_{2,1}^2 \tag{2.21}$$

where, $*$ represents the conjugate operation. In a similar manner, higher order cumulants are derived. Generally a decision tree is employed to classify the modulation using

threshold parameters pre-fixed for taking decision at each branch. In some cases, a set of cumulant features forms a feature vector. In the next stage, the system is trained for various signal scenarios using specific training algorithms and thereby the system is configured for the actual phase of deployment for MC. The majority of cumulant based MC algorithms are limited to the AWGN scenario only. The practical aspects of model mismatch due to fading related effects are not addressed. By using the normalized cumulants, the approach overcomes the problem of signal gain uncertainty [9]. Further, while extracting the cumulant features, the prior knowledge of the timing information is assumed. In [40] and [44], cumulant based channel estimation was applied for MC. However, the performance at low SNR region requires significant improvement for practical implementation.

The problem of MC for interfering transmitters was addressed in [33] using multiuser MC (MUMC). The scenario is typically suitable for the cognitive radios and the spectrum monitoring applications. In this method, the feature vector is formed using the received signals from the interfering transmitters. The FB classification is carried out assuming that the number of interfering transmitters are known and a perfect timing recovery has been achieved by the receiver. However, the classification performance is not adequate to be considered for the scenarios of low SNR.

Unlike the conventional cumulant based approach, [45] employed a pre-processing stage for channel estimation using the independent component analysis (ICA) algorithm in a MIMO scenario. In the MIMO transmission, N_t independent streams of symbols are transmitted via N_t transmit antennas. In the receiver, N_r antennas are used for receiving N_r signal streams. The multipath fading channel coefficients are represented by the $N_t \times N_r$ matrix $\mathbf{h}_{MIMO}$. In data-aided scenarios, $\mathbf{h}_{MIMO}$ is estimated by using the pilot symbols, with the knowledge of the number of transmitted streams. For blind MC, the MIMO channel estimation is an added challenge, since the pilot symbols and the number of transmitted components are not known. In this method N_t is assumed to be known. The channel phase offset is estimated using the ICA algorithm, which in turn is used to estimate $\mathbf{h}_{MIMO}$. The feature vector is constituted by using the fourth order cumulants. The MC decision is based on the ML principle, applied on the asymptotic likelihood function of the feature vector. This is a novel FB classifier with promising

performance in a flat fading environment. In a similar implementation [47], the channel estimation was carried out using the ICA and the MC was performed by the cumulant features in a MIMO scenario. However, the performance comes at the cost of system complexity for the multiple receiving resources and a larger sample length.

A mitigation to signal distortion due to multipath fading channel was proposed in [42]. The proposed adaptive channel estimation uses the combined inputs from the minimization of a cost function extracted from the normalized n^{th} order cumulants and the performance of the MC itself. The method provides a mitigation for the fading channel effect, using the conventional cumulant based MC.

2.5.2 Cyclostationarity Based Methods

Signal cyclostationarity features are explored by several authors for the blind MC problem due to the robustness of these features against the fading channel and the receiver imperfections. The second order cyclostationary features are commonly used for MC. For the second order cyclostationary received signal, the Fourier transform of the delay products $r_c(t-\tau_1)r_c(t-\tau_2)$ should produce spectral lines at some nonzero frequencies ω [48]. The expression of the delay product can be generalized by introducing symmetric delay products and conjugation for complex signals. Thus the delay product $y_\tau(t)$ is given by

$$y_\tau(t) = r_c(t+\tau/2)r_c^*(t-\tau/2) \tag{2.22}$$

The corresponding *cyclic autocorrelation function* (CAF) can be expressed by the Fourier coefficients.

$$R_r^\omega(\tau) = \lim_{T\to\infty}\frac{1}{T}\int_T r_c(t+\frac{\tau}{2})r_c^*(t-\frac{\tau}{2})e^{-j2\pi\omega t}dt \tag{2.23}$$

For a cyclostationary signal with period T, the cyclic autocorrelation function will have a component at cycle frequency $\omega = \frac{1}{T}$. The Fourier transform of the CAF is given by

$$S_r^\omega(f) = F\{R_r^\omega(\tau)\} = \int_{-\infty}^{\infty} R_r^\omega(\tau)e^{-j2\pi f\tau}d\tau. \tag{2.24}$$

S_r^ω is termed as the *spectral correlation function* (SCF). The SCF of a cyclostationary signal provides insight into various characteristic features, which are not detectable in

time domain. In practice, the SCF is determined by using the correlation between the frequency shifted versions $u(t) = r_c(t)e^{-j\pi\omega t}$ and $v(t) = r_c(t)e^{j\pi\omega t}$ of the received signal [42]. A normalized version of the SCF is available for convenience of signal processing. This is measured at frequency f by using the correlation between the PSD of the frequency shifted signals. The resulting normalized function is termed as *spectral correlation coefficient* (SCC) and given by

$$C_r^{\omega}(f) = \frac{S_r^{\omega}(f)}{[S_r^{\omega}(f+\omega/2)S_r^{\omega}(f-\omega/2)^*]^{1/2}} \tag{2.25}$$

The function $C_r^{\omega}(f)$ is a measure of spectral redundancy as a result of spectral correlation [48]. The *cyclic domain profile* (CDP) has been used in MC [38, 42] and is derived from the SCC as follows.

$$I(\omega) = \max_f |C_r^{\omega}(f)| \tag{2.26}$$

The CDP has been used in MC under low SNR conditions. However, these approaches do not address the fading related issues. The cyclic autocorrelation function, the SCF, the SCC and the CDP are used to extract the feature vectors for the FB MC.

CDP has been used in the recent work on FB MC. In [10], cyclic cumulants up to eighth order were used to form the feature vector for a candidate pool containing ASK, PSK and QAM class of signals. The p^{th} order q conjugate cyclic cumulant at cyclic frequency ω for a delay vector $\tau = [\tau_1\ \tau_2\ ...\ \tau_{p-1}]^T$ is given by [2]

$$C_x(\omega;\tau)_{p,q} = \lim_{T\to\infty} T^{-1} \int_{-T/2}^{T/2} C_{p,q}(t;\tau)e^{-j2\omega t}dt, \tag{2.27}$$

where $C_{p,q}(t;\tau)$ is the p^{th} order q-conjugate time varying cumulant expressed by the Fourier series

$$C_{p,q}(t;\tau) = \sum_{l/T_0} C_x(\omega;\tau)_{p,q}e^{j2\pi\omega t} \tag{2.28}$$

for a set of cyclic frequencies given by $\omega = lT_0^{-1}$ with fundamental period T_0 and l as an integer, T is the observation interval. The feature vector $\mathbf{F}^{(i)}$ is formed using the magnitude of the cyclic cumulant of various orders. MC is carried out by the decision

rule

$$\hat{H} = \arg\min_{i} ||\mathbf{F}_r - \mathbf{F}^{(i)}||, \tag{2.29}$$

where, $\mathbf{F}_r$ is the feature vector extracted from the received signal. The application was extended for multi-antenna diversity reception to mitigate fading [10]. In this approach, spatially apart multiple receiving systems are used. Instead of channel estimation, the method uses selection combiners for selecting the receiver branch with highest SNR. MC is performed by FB approach employing 8^{th} order cyclic cumulants as feature vector. However, the method requires multiple number of receiver branches to achieve marginal advantage in the MC performance with the computational complexity increasing significantly with each additional receiver branch. Diversity reception may be considered as a scope of further study in LB framework. On the performance, a marked improvement over the stationary cumulant based classifiers was achieved by using the cyclic cumulants.

In [43], features derived from the SCF have been used to classify PSK and QAM modulations. The CDP was used in [38] for MC in low SNR conditions. The extracted CDP features were used in a training phase using artificial neural network. However, these approaches do not address the fading related distortion.

In [46], the correlation function of the received signal for specific values of time lag is employed as the discriminating features for certain modulation schemes. The approach has been applied for discriminating basic modulation pools like BPSK, QPSK and 8PSK, 16QAM in a MIMO scenario. This MC approach is based on the peaks of the correlation function against the specific lag values. The features are observed to be robust against the frequency selective fading. However, though the discrimination has been successful for the small pool of modulations, the application for a larger pool needs to be explored.

2.5.3 Clustering Based Methods

The constellation pattern of the modulated base-band signal can be used as a distinguishing feature for MC. In [39], MC is considered as a problem of shape recognition based on the constellation pattern of the received signal. By using the fuzzy K-means clustering

algorithm, the cluster centers are first determined and mapped onto the first quadrant of the I-Q plane. In the next step, using the hierarchical clustering, the clusters estimated in the previous step are merged to get estimated number of clusters for each hypothesis. The number of clusters are estimated by minimizing an objective function of the Euclidian distances of the estimated merged clusters from the ideal symbols. Although this approach performs well in an AWGN scenario with ideal reception conditions, the utility of the same in a fading and a blind scenario is limited. In [49] and [50], the number of clusters was used as a distinguishing feature for the MC, considering AWGN scenario. These approaches are not able to distinguish between PSK and QAM signals, when there is an ambiguity due to the same number of symbols in both the groups (e.g. 8PSK and 8QAM). Also, the performance in fading scenarios is not investigated.

2.6 Summary of MC methods

The major proposals for the LB and the FB MC in a blind scenario have been summarized in Table 2.1 and 2.2 respectively.

2.7 Performance Benchmarks

The usefulness and the possibility for practical implementations of the MC algorithms can be examined by their performances under the likely deployment conditions. Further, using these performance benchmarks, the necessary areas of further improvements can be identified. In this section, the performances of the practical MC algorithms previously discussed are consolidated. The performance parameters are considered under the same experimental conditions to set up a benchmark. For simulations, we consider a basic candidate pool containing BPSK and QPSK modulations in a slow flat fading channel $\mathbf{h} = [1\ 0.3\ 0.2]^T$. The performance comparison for the LB and the FB classifiers is given in Table 2.3 and 2.4 respectively. The probability of correct classification P_{cc} is evaluated at a low SNR level of 0 dB to bring out the suitability of the algorithms in adverse conditions.

Author	**Classifier**	**Modulations**	**Unknowns**	**Channel**
Hameed and Dobre [15]	QHLRT-MoM	BPSK, QPSK	$\alpha^{(i)}$, $\psi^{(i)}$, $N^{(i)}$	Residual fading in AWGN
Puengnim et al. [21]	QHLRT-MCMC	GMSK, BPSK, QPSK, 8PSK	Δf, $\psi^{(i)}$, h	Residual base-band fading in AWGN
Derakhtian et al. [23]	QHLRT-ML	BPSK, QPSK, 8QAM, 16QAM	$\alpha^{(i)}$, $N^{(i)}$, $s_m^{(i)}$	AWGN
Headley and da Silva [24]	QHLRT-MoM	BPSK, QPSK, 8PSK, 16QAM, 64QAM	$\alpha^{(i)}$, $N^{(i)}$, t_0	Flat fading in AWGN
Chavali and da Silva [22]	QHLRT-ECM	BPSK, QPSK, 8PSK, 16QAM	$\alpha_f^{(i)}$, $\lambda_n^{(i)}$, σ_n	Flat fading in non-Gaussian
Zhu and Nandi [26]	NPLF-MDCE	BPSK, QPSK, 8PSK, 16QAM, 64QAM	$\alpha^{(i)}$, $\psi^{(i)}$	Flat and fast fading in AWGN and non-AWGN

TABLE 2.1: Summary of the factors considered in the blind LB algorithms

Figure 2.2 shows the comparative performances of some of the significant LB and the FB algorithms under various levels of fading severity. The Rician fading severity is defined in terms of the Rician factor, which is the ratio between the power of the line of sight component and the resultant power of the reflected components. The performance is evaluated under 0 dB SNR to simulate the practical scenarios of COMINT. The LB classifiers with parameter estimation for $\alpha^{(i)}$, $\psi^{(i)}$, $N^{(i)}$ are more robust in a fading scenario. Among the FB classifiers, the performance of the cumulant based classifier without channel estimation degrades as the severity of the fading increases. However, with blind equalization as the pre-processing stage, the cumulant based classifier becomes more robust in fading scenarios. For MIMO processing, the FB classifiers of [45–47] have become comparable to the recent blind LB classifiers. However, the MIMO processing introduces additional complexity, and the performance is achieved with higher sample

Author	**Classifier**	**Modulations**	**Unknowns**	**Channel**
Zaerin and Seyfe [33]	6th order cumulants	BPSK, QPSK, 4PAM, 16QAM	Δf, ϕ_n, t_0	AWGN
Orlic and Dukic [40]	6th order cumulants	QPSK, 16QAM, 64QAM	h	Residual fading in AWGN
Markovic and Dukic [44]	4th order cumulants	BPSK, QPSK, 16QAM, 64QAM	h	Residual fading in AWGN
Muhlhaus et al. [45]	ICA and cumulant features	BPSK, QPSK, 8PSK, 16QAM	h	Flat fading in AWGN
Bahloul et al. [47]	ICA and Cumulants,	BPSK, QPSK, 8PSK, 16PSK, 16QAM, 64QAM	h	Frequency selective fading
Dobre et al. [10]	8th order cyclic cumulants	4ASK, 8ASK, BPSK, QPSK, 8PSK, 16PSK, 16QAM, 32QAM, 64QAM	h	Flat fading in AWGN
Fehske et al. [38]	Cyclic frequency domain profile	BPSK, QPSK, FSK, MSK	h	Flat fading in AWGN
Marey and Dobre [46]	Lag correlation peaks	BPSK, QPSK and 8PSK, 16QAM	h	Frequency selective fading
Ramkumar [42]	6th order cumulants and blind equalization	BPSK, QPSK, 8PSK, 16QAM	h	Flat fading in AWGN

TABLE 2.2: Summary of the factors considered in the blind FB algorithms

sizes.

Classifier	**Sample length**	**Unknowns**	**Pcc**
QHLRT-MoM [15]	100	$\alpha^{(i)}$, $\psi^{(i)}$, $N^{(i)}$	0.93
QHLRT-MCMC [21]	1000	Δf, $\psi^{(i)}$, h	0.96
QHLRT-ML [23]	100	$\alpha^{(i)}$, $N^{(i)}$, $s_m^{(i)}$	0.91
QHLRT-MoM [24]	1000	$\alpha^{(i)}$, $N^{(i)}$, t_0	0.55
QHLRT-ECM [22]	100	$\alpha_f^{(i)}$, $\lambda_n^{(i)}$, σ_n	0.55
NPLF-MDCE [26]	100	$\alpha^{(i)}$, $\psi^{(i)}$	0.94

TABLE 2.3: Performance of blind LB classifiers

Classifier	**Sample length**	**Unknowns**	**Pcc**
6th order cumulants [33]	100	Δf, ϕ_n, t_0	0.71
6th order cumulants [40]	2000	h	0.55
4th order cumulants [44]	2000	h	0.75
ICA and cumulant features [45]	1000	h	0.92
ICA and cumulant features [47]	4096	h	0.82
8th order cyclic cumulants [10]	100	h	0.74
8th order cyclic cumulants [10]	100	-	1.0
Cyclic frequency domain profile [38]	100	h	0.82
Lag signal correlation [46]	1000	h	0.97
6th order cumulants and blind equalization [42]	100	h	0.80

TABLE 2.4: Performance of blind FB classifiers

2.8 Summary

In this Chapter, the blind classification algorithms in LB and the FB frameworks have been examined to highlight the suitability for their use in a practical scenario. Among the blind LB classifiers, the QHLRT has been established as the practical approach due to the simplicity and the closeness of the performance with the optimum classifier. The MC performance is also governed by the quality of the parameter estimators. Although ML parameter estimators are optimum, they are time consuming. On the other hand,

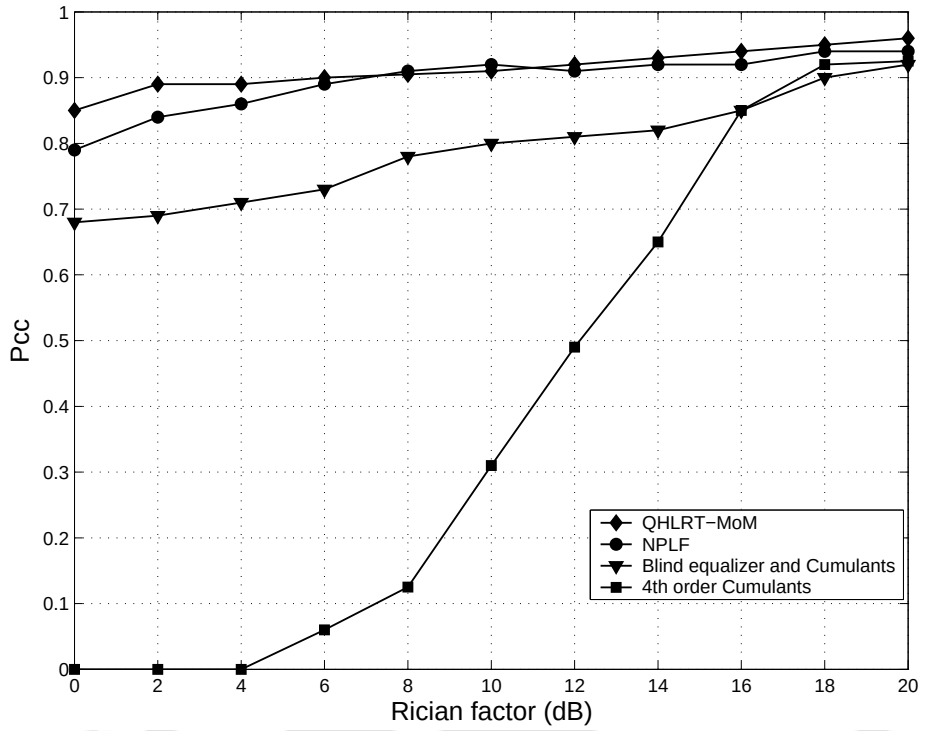

FIGURE 2.2: Comparative classification performance of BPSK and QPSK modulations with $N_b = 1000$, $SNR = 0$ dB in a Rician fading channel

the performance of the MoM based parameter are generic for all modulation types. The NPLF classifier employs relatively simple iterations to estimate the unknown parameters. However, since the algorithm does not use noise as an unknown parameter, there is a scope for further improvement by the exploitation of the noise parameters. Among the blind LB classifiers, the parameter estimators using the iterative approach have provided superior classification performance.

The performance of the blind FB classifiers using cumulants derived from the received constellations are found to be robust in gain mismatch, but susceptible to phase offset due to the channel imperfections. The cyclic cumulant based classifier performs very well in an AWGN scenario, but the algorithm performance degrades significantly in model mismatch scenarios in a fading channel. Blind equalization along with the MC using cumulants is observed to be feasible for the practical implementation. In terms of classification performance, the approach has introduced promising perspective.

In general, the blind LB classifier outperforms the FB classifiers in practical situations. There is a scope for future work to improve the low SNR performance of the LB classifier

by employing efficient parameter estimators. A classifier with unknown parameters at the carrier and the baseband level may be more useful for implementation. At the same time, the trade-off between classification performance and computational complexity need to be considered for optimizing the classifier for practical implementations.

3

Symbol Rate Estimation For Robust Recovery of Base-Band Signal

3.1 Introduction

In Chapter 2, the blind classification of digital modulations has been analyzed from the angle of practical implementations involving weak signal reception and fading. The subsequent chapters in this thesis will focus on improving the performance of MC under such challenging conditions. Based on the interpretation from the performance benchmarks, and the availability of an optimum solution, the LB approach is adopted with emphasis on formulating improved parameter estimators to finally boost the MC performance. The performance of the LB classification is governed by the pre-processing stages, where

the received modulated signal needs to be conditioned to mitigate various uncertainties in the channel. Referring to the signal models of (2.1), the knowledge of the carrier frequency f_c and the symbol rate T_s is necessary to demodulate the signal. Due to the imperfections of receiver implementations, other parameters like the carrier frequency offset Δf, the carrier phase offset ϕ and the timing offset t_0 also can contribute to the model mismatch in the LB classification. However, in modern receiver implementations, the carrier frequency detection has been addressed extensively. In certain sophisticated applications like COMINT, the uncertainty due to the carrier frequency offset can be neglected in the context of MC.

In this chapter, the pre-processing requirement of the I-Q demodulation process is addressed. The estimates of the carrier signal parameters like the center frequency and the symbol rate are used for the LB MC [3–5, 51], in the demodulation process to recover the base-band signal. The extracted I-Q values are used as the test samples to generate the likelihood function. In several FB classifiers [35, 52–54], symbol rate estimation is a prerequisite to extract the feature vectors from the demodulated I-Q stream. Since the estimation of f_c and carrier recovery at low SNR are covered extensively under data aided (DA) and NDA signal reception scenarios [55–58], the focus is extended towards the parameters after the receiver has locked on to a signal of interest. In this context, the symbol rate of the received modulated signal is the first important parameter to be estimated before proceeding towards I-Q demodulation. The accurate estimation of the symbol rate ensures faithful timing recovery. Some of the existing methods for symbol rate estimation used the wavelet transform of the received signal [59], the ML principle [60, 61], the cyclostationarity based principles [14, 62–64] and the estimation using filter banks [65]. The performance of the sympobl rate estimator using the wavelet transform scheme significantly deteriorates at low SNR conditions. Similarly, the method based on the filter banks [65] relies on the assumption that the received signal is at comfortable level of SNR. The fading related distortion is also not considered in these two methods. The ML and the cyclic autocorrelation based methods are designed to handle signals in deteriorated conditions. These methods are briefly described below.

3.1.1 ML estimator

The envelop of the received signal, obtained after mixing with the recovered carrier and low pass filtering is employed for estimation of the symbol rate. The signal model is given by

$$r(t) = e^{j2\pi\Delta f t} e^{j\phi} \sum_{k=0}^{K-1} s_k^{(i)} h(t - kT_s - t_0 - \tau) + n_g(t) \tag{3.1}$$

where, τ is the propagation delay. On over-sampling the signal with a sampling period T_n, we get

$$r(nT_n) = e^{j2\pi\Delta f n T_n} e^{j\phi} \sum_{k=-\infty}^{\infty} s_k^{(i)} h(nT_n - kT_s - t_0 - \tau) + n_g(nT_n) \tag{3.2}$$

For the estimation of the symbol rate, the sample vector $\mathbf{r} = [r(0)\ r(T_n)\ ...r((N_c-1)T_n)]^T$ of size N_c is used. The ML method employs the likelihood function to obtain the symbol period as

$$\hat{T}_{s,ML} = \arg\max_{T_s \in S} p(\mathbf{r}|T_s), \tag{3.3}$$

with

$$p(\mathbf{r}|T_s) = E_{\mathbf{s}^{(i)},\tau,h}[p(\mathbf{r}|\mathbf{s}^{(i)}, \tau, h, T_s)] \tag{3.4}$$

where, $E_{\mathbf{s}_{(i)},\tau,h}[.]$ is the averaging operator over the possible symbols of $\mathbf{s}^{(i)}$, the propagation delay τ and the channel response h. The search space is defined as $S = \{T_{min}, \ldots, T_{max}\}$, where T_{min} and T_{max} are the lower and the upper search limits respectively. In practice, the ML estimation is performed using the EM algorithm, which also involves the estimation of τ and h. The performance of the ML estimator is susceptible to the pulse shape of the received signal [60, 61]. The ambiguity of the ML peak increases for lower values of roll off factors of the baseband pulse shaping filters. Moreover, the estimation performance depends on the estimation of τ and h, at the same time making the overall process computationally complex.

3.1.2 Cyclic correlation based estimator

Existing symbol rate estimators [14, 62–64] using cyclostationarity use the maximization of the cyclic autocorrelation function over the cyclic frequencies. The signal model of

(3.1) is used once again. The cyclic frequency value corresponding to the peak value of the cyclic autocorrelation function $R_r^{\omega}(f)$ is estimated as the symbol rate [14]. Thus the symbol rate is given by

$$\hat{f}_s = \arg \max_{\omega \in [\omega_1, \omega_2]} R_r^{\omega}(\frac{1}{2\omega}), \tag{3.5}$$

where $|R_r^{\omega}(\tau)|$ attains maximum for time delay $\tau = \frac{T}{2} = \frac{1}{2\omega}$, and ω_1 and ω_2 define the search interval. The search is carried out in two stages, a coarse search to shrink the search range, followed by finer search to locate the autocorrelation peak. Unlike the ML method, the additional estimation of the time delay and the channel response is not necessary in the cyclic correlation based estimator. However, due to the sensitivity to the pulse shape uncertainties, the estimator performance deteriorates for signals having low values of roll off factor in the baseband pulse shape [64].

In this Chapter, the cyclostationary of linearly modulated signals is used to formulate a simplified estimator of the symbol rate. The approach is especially suitable for the blind scenario at low SNR conditions. The proposed blind estimator of the symbol rate employs the second order cyclostationarity. A new cyclostationary feature named as the *cyclic domain power profile* (CDPP) has been introduced as the key feature for estimation. Since the CDPP is defined as the accumulated power over the spectral frequency components at each cyclic frequency, it is robust against pulse shape uncertainty and multi-path fading. The scheme is extended to the scenario of co-channel interference with multiple carriers. The experimental analysis of the proposed scheme is presented for a pool of digital modulation schemes, with reference to the performance of earlier methods. Concluding remarks are provided with the emphasis on the scope for further work.

3.2 Cyclostationary Features for Blind Symbol Rate Estimation

3.2.1 Formulation of the Cyclostationary Features

Modulated signals exhibit hidden periodicities due to the carrier frequency, the symbol rate, coding etc. Such periodicity is visible when the received signal is modeled as cyclostationary. Consider a scenario with the AWGN, the unknown channel impulse response and the unknown baseband pulse shape. Under such conditions, the i^{th} modulation signal is modeled as (2.1). The same is reproduced here for easy reference.

$$r_c(t) = e^{j2\pi(f_c+\Delta f)t}e^{j\phi}\sum_{k=-\infty}^{\infty} s_k^{(i)}h(t-kT_s-t_0)+n_g(t)$$

As described in Chapter 2, the fundamental cyclostationary feature is the cyclic autocorrelation function $R_r^{\omega}(\tau)$. The SCF $S_r^{\omega}(f)$ and the SCC $C_r^{\omega}(f)$ are derived from $R_r^{\omega}(\tau)$. In practice, these features are required to be estimated from a finite sample of the received signal.

3.2.2 Estimation of the Cyclostationary Features

The estimate of this fundamental parameter of the second order cyclostationarity for a continuous time process $r_c(t)$ can be expressed as [48]

$$R_r{}^{\omega}(\tau) \triangleq \langle r_c(t+\tau/2)r_c^*(t-\tau/2)e^{-j2\pi\omega t}\rangle, \tag{3.6}$$

where the operator $\langle\cdot\rangle$ is used for the time averaging operation and is defined as

$$\langle\cdot\rangle \triangleq \lim_{T\to\infty}\frac{1}{T}\int_{-T/2}^{T/2}(\cdot) \tag{3.7}$$

On over-sampling the continuous signal of (2.1), the discrete version is obtained as [60].

$$r_c[n] = e^{j2\pi(f_c+\Delta f)nT_n}e^{j\phi}\sum_{k=-\infty}^{\infty} s_k^{(i)}h(nT_n-kT_s-t_0)+n_g(nT_s) \tag{3.8}$$

where, T_n is the sampling period. The corresponding cyclic autocorrelation function for the discrete signal $r_c[n]$ is [48]

$$R_r^{\omega}[k] \triangleq \langle r_c[n] r_c^*[n-k] e^{-j2\pi\omega n} \rangle e^{j\pi\omega k}, \tag{3.9}$$

where the time averaging operator for the discrete domain is given by

$$\langle \cdot \rangle \triangleq \lim_{N_c \to \infty} \frac{1}{2N_c + 1} \sum_{t=-N_c}^{N_c} (\cdot) \tag{3.10}$$

In practice, the cyclostationary features are estimated from a sample of finite length discrete data. The estimation of the SCF can be carried out broadly by the temporal smoothing and the frequency smoothing methods. Since the temporal smoothing method is computationally more efficient, we briefly discuss the same. The estimation scheme [48, 66] is shown in Figure 3.1. There are two approaches [66] under this method, namely the

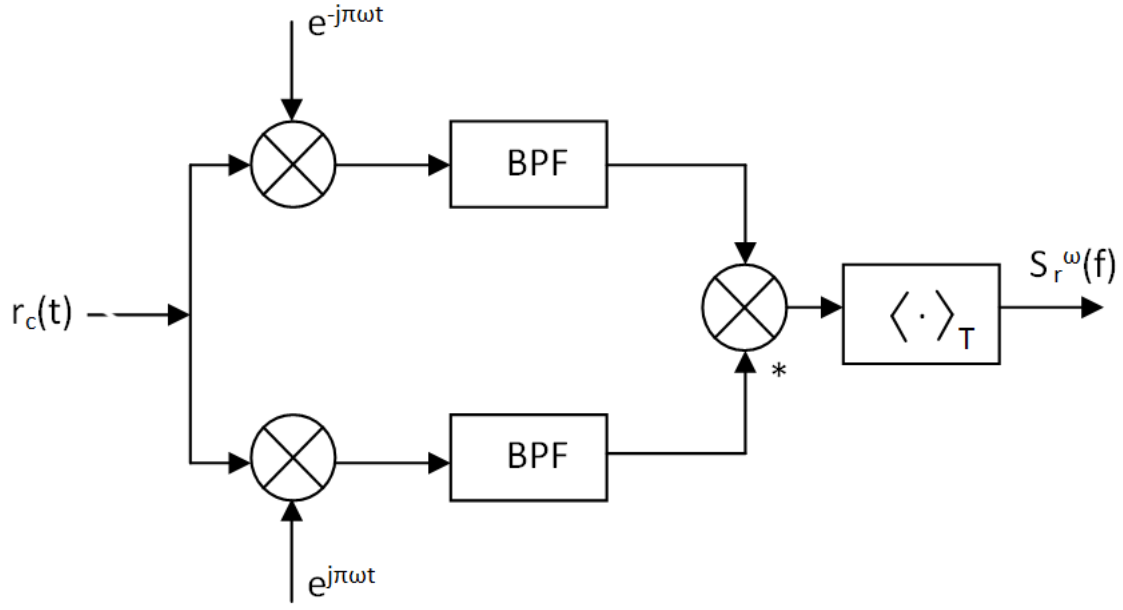

FIGURE 3.1: General scheme for the estimation of the SCF

FFT accumulation method (FAM) and the strip spectral correlation algorithm (SSCA). The discrete time expression for the SCF is given by [66]

$$S_r^{\omega}[f] = \sum_{k=-\infty}^{\infty} R_r^{\omega}[l] e^{-j2\pi f k T_n}, \tag{3.11}$$

The spectral correlation in spectral domain is determined by passing the frequency translated versions of the received signal $u(t) = r_c(t)e^{-j\pi\omega t}$ and $v(t) = r_c(t)e^{j\pi\omega t}$ through the same set of band pass filters and then measuring the temporal correlation of the filtered signals [66].

$$S_r^{\omega}[f]_{\Delta t} = \frac{1}{T}\Big\langle V_n\Big[f + \frac{\omega}{2}\Big]U_n{}^*\Big[f - \frac{\omega}{2}\Big]\Big\rangle_{\Delta t}, \tag{3.12}$$

where Δt represents the time span, $V_n\Big[f+\frac{\omega}{2}\Big]$ and $U_n{}^*\Big[f-\frac{\omega}{2}\Big]$ are the complex envelopes of narrow-band, bandpass components of the received signal. The complex envelopes are computed as [66]

$$U_n[f] = \sum_{k=N/2}^{N/2} a[k]u[n-k]e^{-j2\pi f(n-k)T_n}, \tag{3.13}$$

and

$$V_n[f] = \sum_{k=N/2}^{N/2} a[k]v[n-k]e^{-j2\pi f(n-k)T_n}, \tag{3.14}$$

where $a[k]$ is a data tapering window of length NT_n.

We estimate the SCF from the discrete sample $r_c[n]$ using the FAM approach [66]. The main steps employed for the FAM estimation are listed below.

1. Over-sample the received signal $r_c[n]$ to ensure that $T_n < T_s/4$, where T_n is the sampling period of the received signal and T_s is the symbol period [63].

2. Constitute L frames of the incoming signal. For a signal of N samples, number of samples in each frame is $\frac{N}{L}$. The sample length is given by $N = \frac{1}{T_s\Delta f}$, where Δf is the desired resolution of the spectral frequency.

3. Compute the Fast Fourier Transform (FFT) of each frame after passing them through the tapering window.

4. Frequency shift the FFT of each frame by $+\frac{\omega}{2}$ and $-\frac{\omega}{2}$ and multiply them to obtain $\frac{1}{T}V_n[f+\frac{\omega}{2}]U_n^*[f-\frac{\omega}{2}]$.

5. Time smoothen the product using a P-point FFT, where $P = \frac{1}{T_sL\Delta\omega}$ and $\Delta\omega$ is the resolution of the cyclic frequency.

6. Repeat the above steps for each value of cyclic frequency ω.

The SCC can be estimated by normalizing the SCF. The resulting estimate SCC can be plotted in a 3-D space over the spectral and the cyclic frequency axes. Figure 3.2 shows the SCC plot for BPSK and QPSK signals received at 10 dB SNR. Figures 3.2a and 3.2c visualize the 3-D pattern along the spectral, the cyclic and the normalized magnitude axes, while the 2-D plots in Figures 3.2b and 3.2d illustrate the locations of the spectral artifacts due to the second order cyclostationarity.

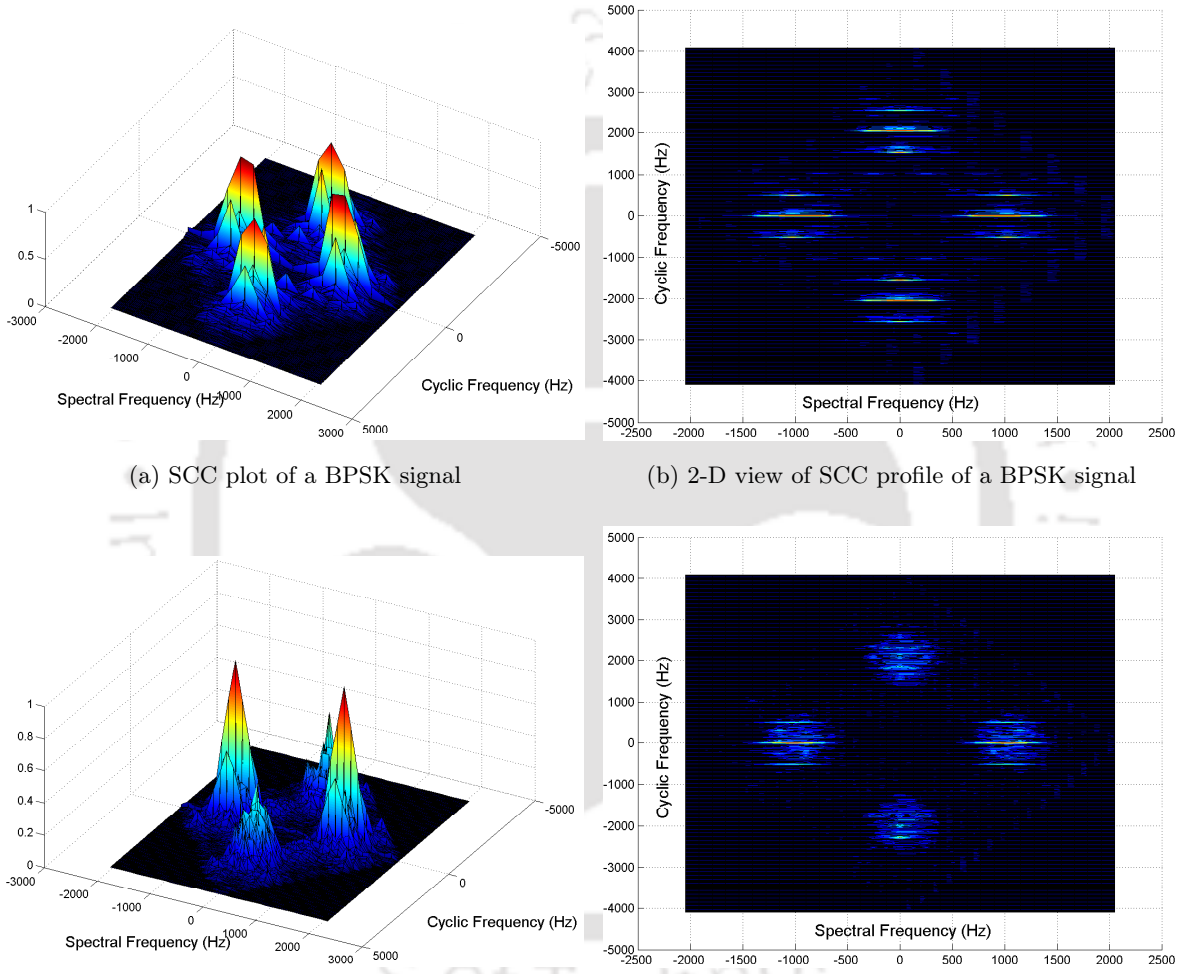

(a) SCC plot of a BPSK signal

(b) 2-D view of SCC profile of a BPSK signal

(c) SCC plot of a QPSK signal

(d) 2-D view of SCC profile of a QPSK signal

FIGURE 3.2: Spectral Correlation Coefficient plots at 10 dB SNR

3.3 Proposed Method for Symbol Rate Estimation

3.3.1 Formulation of a Robust Feature

Taking reference at the carrier frequency located at the spectral frequency axis, the cyclostationary spectral artifacts are generated corresponding to cyclic frequency $\omega = \frac{1}{T_s}$. These artifacts at a particular cyclic frequency corresponding to the cyclostationary frequencies like the symbol rate, appear along the spectral frequency axis. We observe two particular cases:

1. The SCC plot in Figure 3.3 illustrates the appearance of the cyclic frequency components corresponding to the BPSK symbol rate for a channel at a reasonably good SNR of 10 dB and without fading. From the cross-sectional view of the SCC along the cyclic frequency axis as shown in Figure 3.3b, it is evident that the symbol rate can be detected using the CDP within a valid search range.

2. The SCC profile under multipath fading with channel impulse response $\mathbf{h} = [1\ 0.5\ 0.3]^T$ is shown in Figure 3.4a. In this case, the cyclic frequency component corresponding to the symbol rate spreads out along the spectral frequency axis due to the ISI. Our experimental observations show that the position and magnitude of these cyclic components vary with the severity of the fading and the pulse shape uncertainty. In such a scenario, the detection of the symbol rate using the CDP becomes ambiguous, as shown in Figure 3.4b. Under such adverse channel conditions, a robust feature is required for the unambiguous estimation of the symbol rate.

The variations in the frequency response under the channel impairments need to be considered while selecting a feature for the estimation process. We propose the CDPP feature which considers these variations. The CDPP G^{ω} at a cyclic frequency ω is defined as

$$G^{\omega} = \int_{-\infty}^{\infty} |C_r^{\omega}(f)| df \tag{3.15}$$

The symbol rate estimate $\hat{f}_s$ is now given by

$$\hat{f}_s = \arg\max_{\omega} G^{\omega}, \quad \omega \in [\omega_1, \omega_2] \tag{3.16}$$

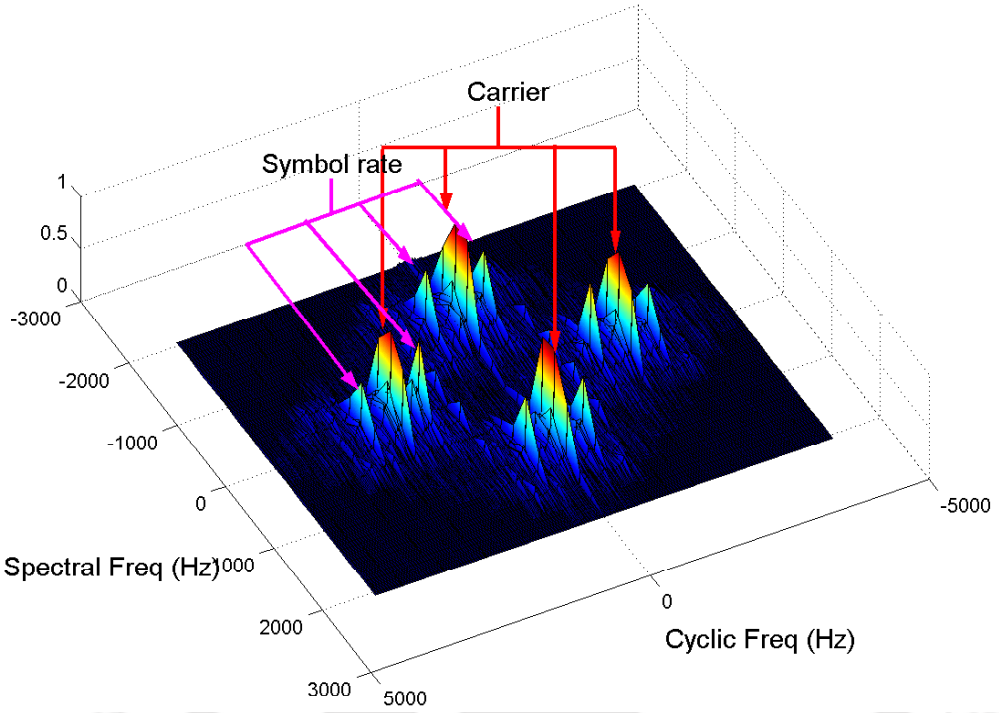

(a) SCC

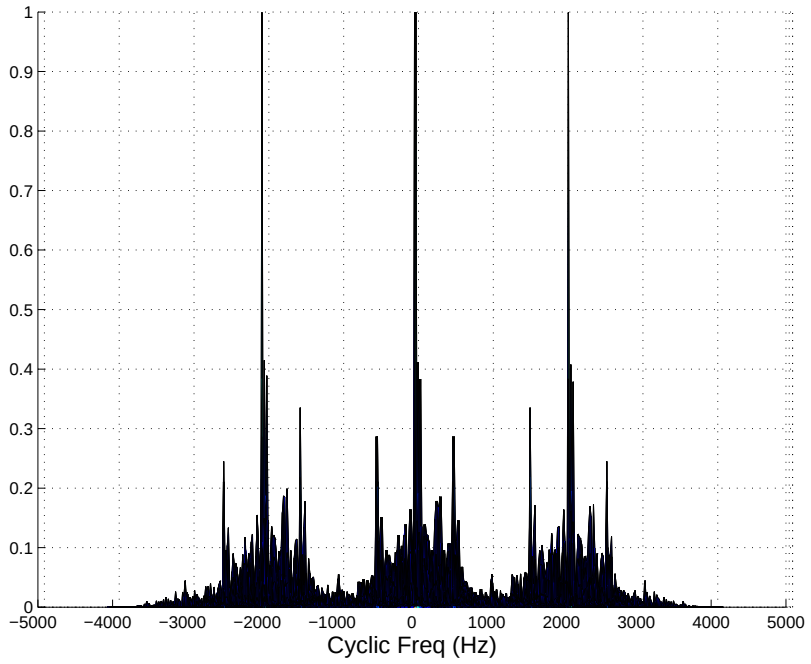

(b) Clear CDP

FIGURE 3.3: Cyclic components in the absence of fading

where ω_1 and ω_2 are cyclic frequencies corresponding to start and stop of the search range. The search interval $[\omega_1, \omega_2]$ is to be chosen appropriately in the cyclic frequency axis. The symbol rate of a bandpass signal cannot exceed the carrier frequency. This is

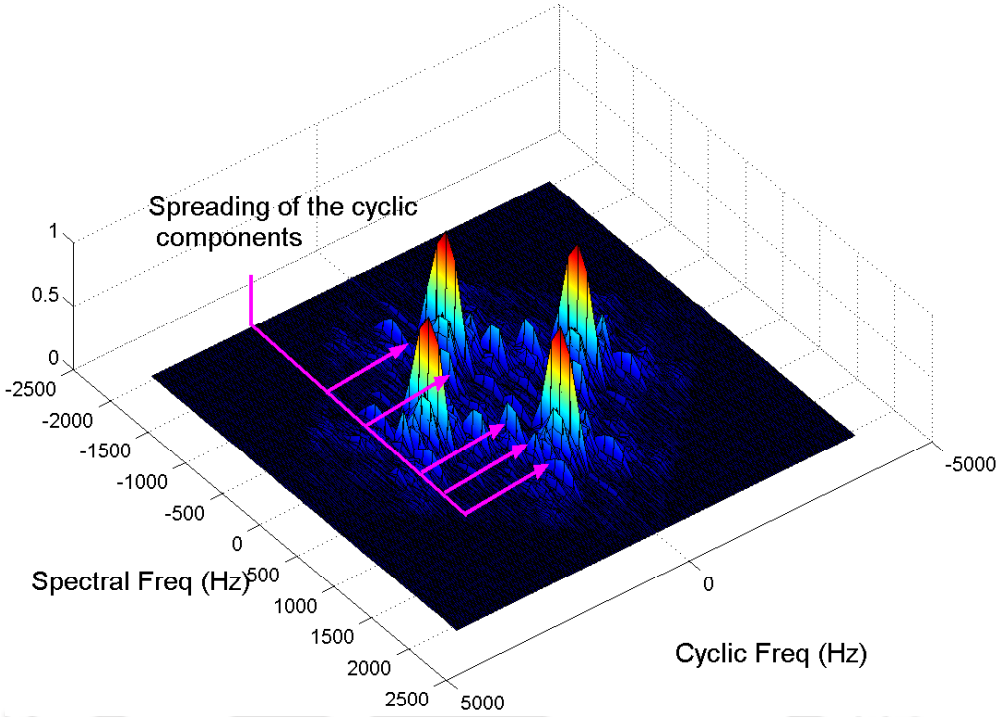

(a) SCC

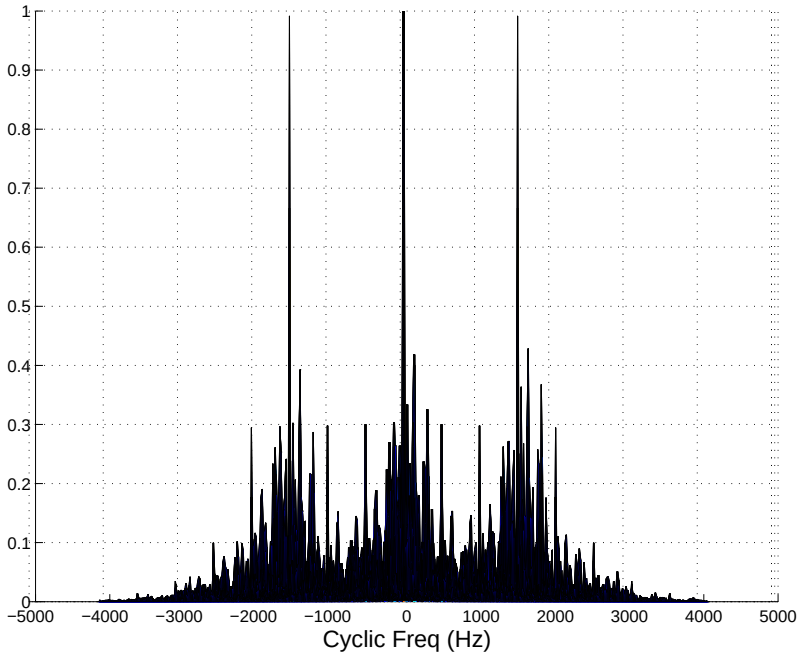

(b) Ambiguity in finding CDP

FIGURE 3.4: Cyclic components under fading

the basis for defining the valid search range for estimation of the symbol rate.

3.3.2 Practical Implementation

The practical estimation of the symbol rate is carried out from a finite discrete data. The steps adopted for the estimation are given below.

1. **Generation of $C_r^{\omega}(f)$**: N samples of the received modulated signal $r_c[n]$ are used as the input data for generating the SCC matrix. Since only the coarse estimate of the carrier frequency is necessary, $\Delta f \geq 4\Delta\omega$ is used, where Δf and $\Delta\omega$ are spectral and cyclic frequency resolutions respectively. The estimation assumes coarse knowledge of the signal band. The resulting SCC matrix $\mathbf{C}_{P,Q}$ is defined as

$$\mathbf{C}_{P,Q} = \begin{pmatrix} C_{1,1} & C_{1,2} & \cdots & C_{1,Q} \\ C_{2,1} & C_{2,2} & \cdots & C_{2,Q} \\ \vdots & \vdots & \ddots & \vdots \\ C_{P,1} & C_{P,2} & \cdots & C_{P,Q} \end{pmatrix} \tag{3.17}$$

   where the row and column indices correspond to the index of the spectral and cyclic frequency axes respectively. The matrix is constituted such that, P and Q are odd numbers and the mid points of a row and a column of $\mathbf{C}_{P,Q}$ represents the zero frequency values for the spectral and the cyclic frequency components, with $\mathbf{f}(\frac{P+1}{2}) = 0$ and $\omega(\frac{Q+1}{2}) = 0$. The feature matrix $\mathbb{F}_{P,Q}$ is derived by taking the absolute value of each element of $\mathbf{C}_{P,Q}(p,q)$.

$$\mathbb{F}_{P,Q}(p,q) = |\mathbf{C}_{P,Q}(p,q)| \tag{3.18}$$

2. **Coarse estimation of the carrier frequency**: The carrier frequency is considered as the reference for defining an optimum search interval to detect the CDPP peak corresponding to the symbol rate. In practice, the symbol rate is typically confined to a maximum of half the carrier frequency. Experimentally it is observed that, a coarse estimate of the carrier frequency within 10% tolerance is achievable even in severe cases of fading. With a more conservative approach, the tolerance can be added to the estimated frequency as a margin of safety. The coarse estimate of the carrier frequency is carried out within the same framework of the SCC and

can be considered adequate for the present requirement, although accurate estimate of the frequency can be referred from the carrier detection stage. The carrier frequency $\hat{f}_c$ is estimated by detecting the spectral frequency corresponding to the peak value of $\mathbb{F}_{P,Q}$ along the zero cyclic frequency axis. The spectral frequency index corresponding to the maximum spectral frequency component is first evaluated as

$$p_{\hat{f}_c} = \arg\max_{p} \mathbb{F}_{P,Q}(p,q), \quad p \in [(\frac{P+1}{2}+1), P]; \tag{3.19}$$
$$q = \frac{Q+1}{2}$$

where, p and q are the spectral and the cyclic frequency indices. The search range is formed along the positive frequency axis starting from the spectral frequency index $(\frac{P+1}{2}+1)$, which is the lower limit of the search range excluding the zero spectral frequency. The upper limit of the search range P corresponds to the maximum spectral frequency in the overall analysis bandwidth. Now using the mapping operator $I_s(\cdot)$ between spectral frequency index and spectral frequency, the estimate of the carrier frequency is obtained.

$$\hat{f}_c = I_s^{-1}(p_{\hat{f}_c}) \tag{3.20}$$

3. **Calculation of the CDPP**:We derive the Q element vector $\mathbf{G_Q}$, of the CDPP with the values from $\mathbb{F}_{P,Q}$ taken across the spectral frequencies for each cyclic frequency index q.

$$\mathbf{G}_Q(q) = \sum_{i=1}^{P} \mathbb{F}_{P,Q}(i)^q, \quad q = 1, 2, \cdots, Q \tag{3.21}$$

4. **Estimation of the symbol rate:** Within the search interval $[(\frac{Q+1}{2}+1), I_c(\hat{f}_c)]$ the cyclic frequency corresponding to the maximum value of $\mathbf{G}_Q$ is measured, where $I_c(\cdot)$ is the mapping operator between the cyclic frequency index and the actual cyclic frequency. The search interval is defined based on the assumption $\frac{1}{T_s} < f_c$. The index of the symbol rate $f_s = \frac{1}{T_s}$ is estimated as

$$q_{\hat{f}_s} = \arg\max_{q} \mathbf{G}_Q(q), \quad q \in [(\frac{Q+1}{2}+1), I(\hat{f}_c)] \tag{3.22}$$

The estimate of the symbol rate is obtained by taking inverse of the mapping operator $I_c(\cdot)$ at the estimated cyclic frequency index. Thus,

$$\hat{f}_s = I_c^{-1}(q_{\hat{f}_s}) \tag{3.23}$$

3.3.3 Detection of symbol rate for interfering carriers

Under co-channel interference, the symbol rates can be measured for the individual carriers by extending the above routine. Here, the search is carried out above a defined threshold value of $\mathbf{G}_Q$. The threshold can be defined based on the average of spurious peaks of $\mathbf{G}_Q$ within the search range in a training process, where each training sample is taken for known symbol rates. The search interval remains same as depicted.

Figure 3.5 shows the cross section view of the $C_x^{\omega}(f)$ plot for a QPSK signal with carrier frequency and symbol rates 1024 Hz and 512 Hz respectively. The ambiguity arising due to artifacts of non-symbol rate frequencies is visible. The plot of $\mathbf{G}_Q$ in Figure 3.6

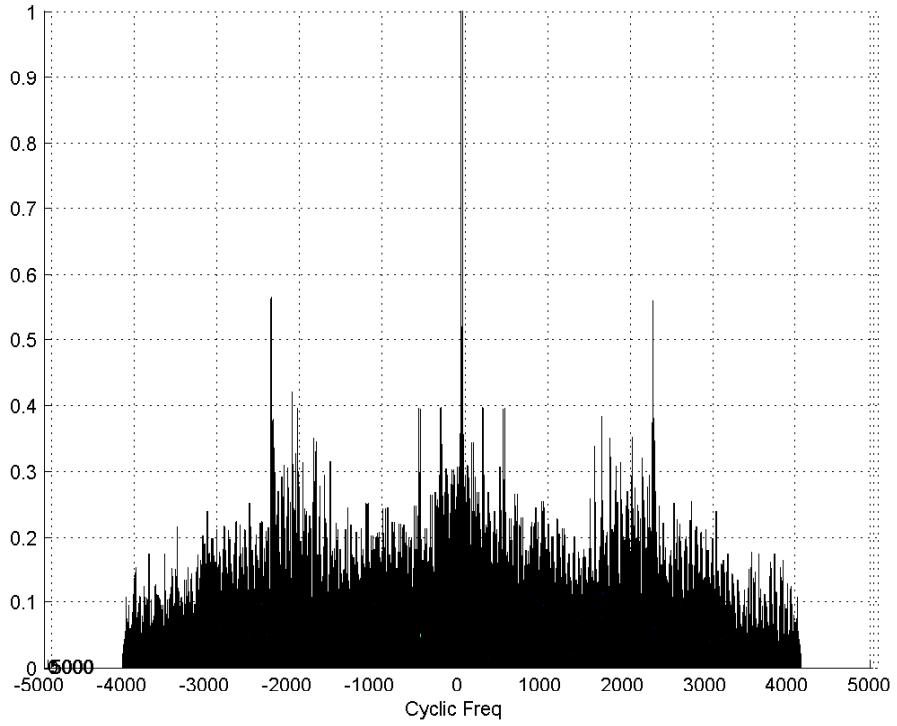

FIGURE 3.5: Cross section view of the Spectral Correlation Coefficient of QPSK signal at -2 dB.

shows the prominent peak of the symbol rate even at a low SNR of -2 dB. Figure 3.7

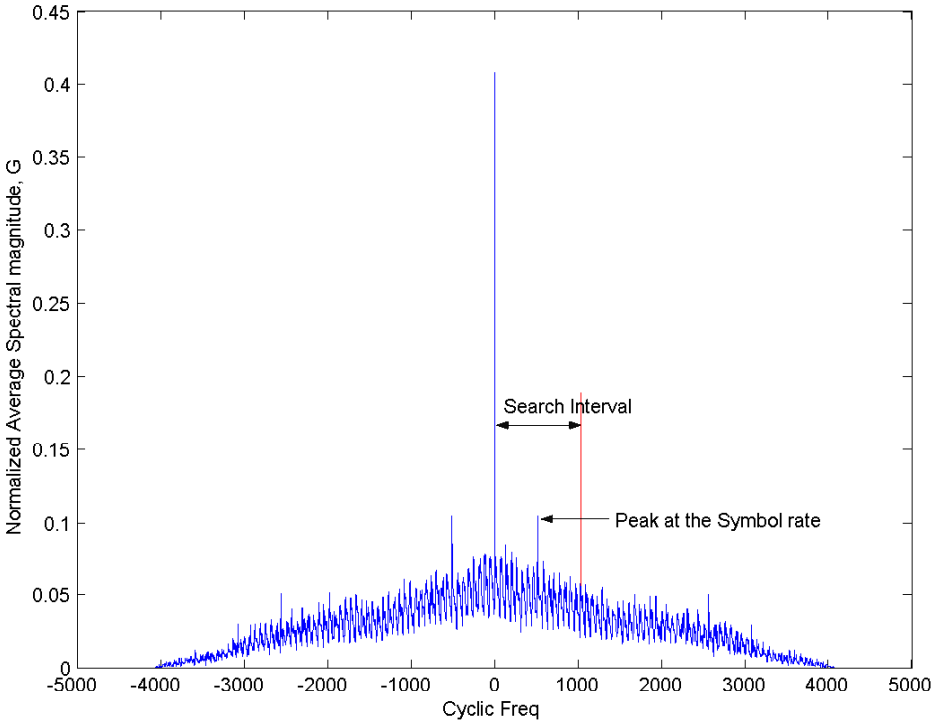

FIGURE 3.6: Normalized average spectral magnitude profile for QPSK signal at -2 dB.

illustrates the symbol rate detection scenario for two interfering carriers having the same carrier frequency.

3.4 Experimental Results and Discussion

We consider a pool of modulated signals containing BPSK, QPSK, 8PSK, 8QAM, 16QAM and 32QAM. The multipath fading is simulated with a real valued three-tap FIR filter with impulse response $\mathbf{h} = [h_0\ h_1\ h_2]^T$. The base-band pulse shaping filter (root raised cosine) with roll-off varying from 0.1 to 1 is considered. The performance of the estimator is analyzed using the

1. probability of correct estimation (P_{cc}) against a range of SNRs,
2. P_{cc} against a range of fading severities and
3. mean square error (MSE) of the estimator.

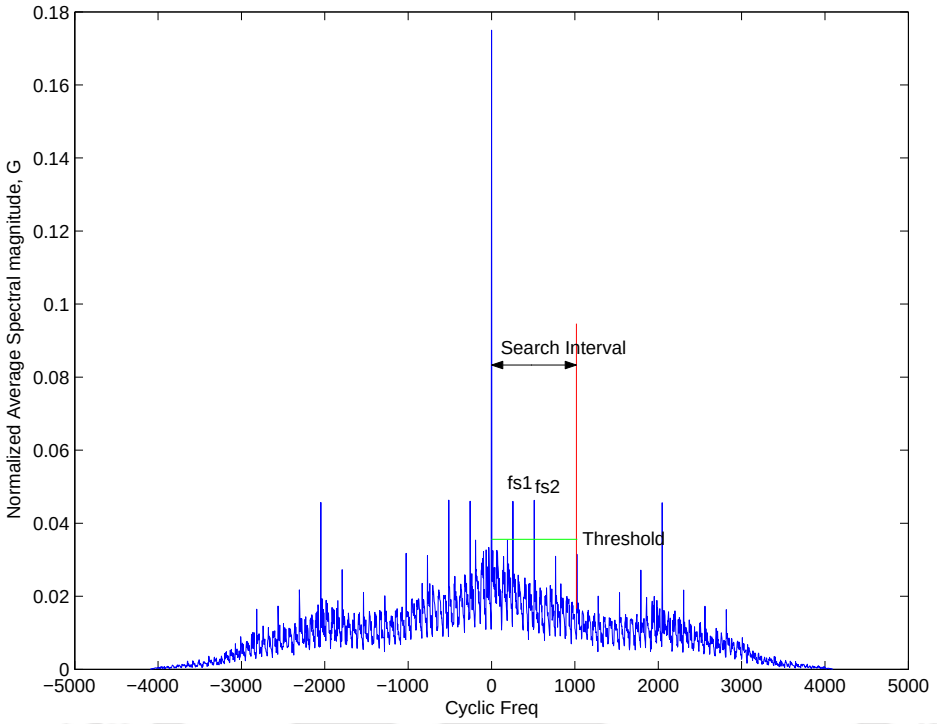

FIGURE 3.7: Interfering QPSK (symbol rate 512 Hz) and BPSK (symbol rate 256 Hz) carriers at frequency 1024 Hz each at 0 dB SNR.

3.4.1 P_{cc} against SNR

The P_{cc} against a range of SNRs is simulated using the Monte Carlo method with 4096 samples of received signal for every modulation. The average probability of correct estimation is calculated by considering the correctness of the estimation within a tolerance of $\pm 1\%$. The average P_{cc} for the candidate modulation schemes at various channel conditions and pulse shaping filters are plotted.

The performance of the symbol rate estimator in a multipath environment is shown in Figure 3.8. Due to the generation of multiple spectral components in a multipath scenario, $\mathbf{G}_Q$ at the cyclic frequency is more prominent in a lower SNR region. However, the plot indicates identical performance for SNR values greater than -1 dB. The effect of the pulse shaping filter on the performance of the estimator for a range of roll off factors is shown in Figure 3.9. Due to accumulation of the spectral components during the averaging operation, the cyclic frequency component at the symbol rate is detectable irrespective of the roll off factors of the base-band pulse shape.

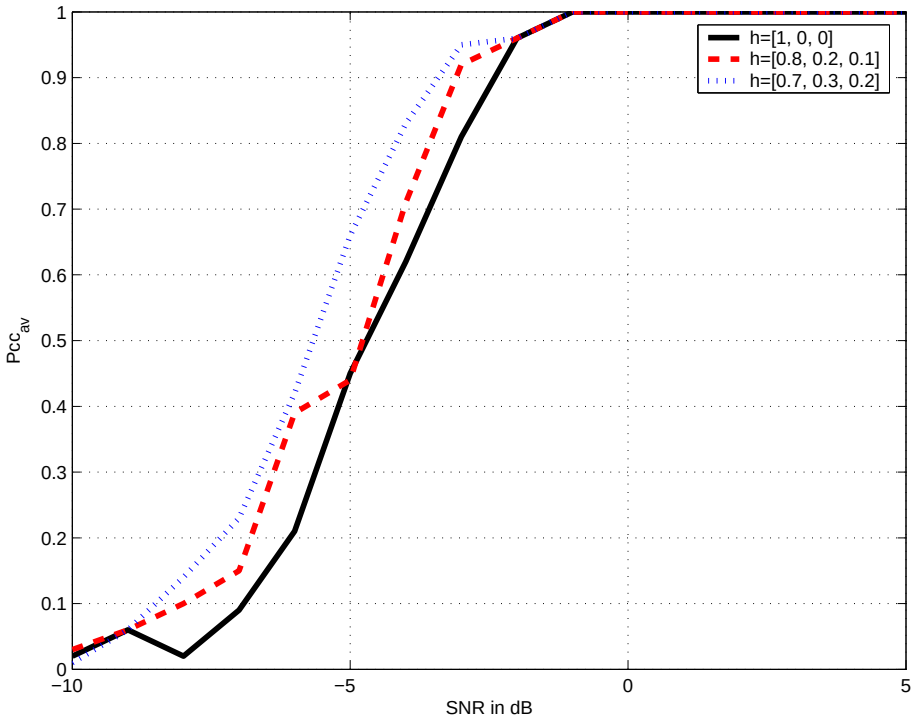

FIGURE 3.8: Average probability of correct estimation in multipath fading

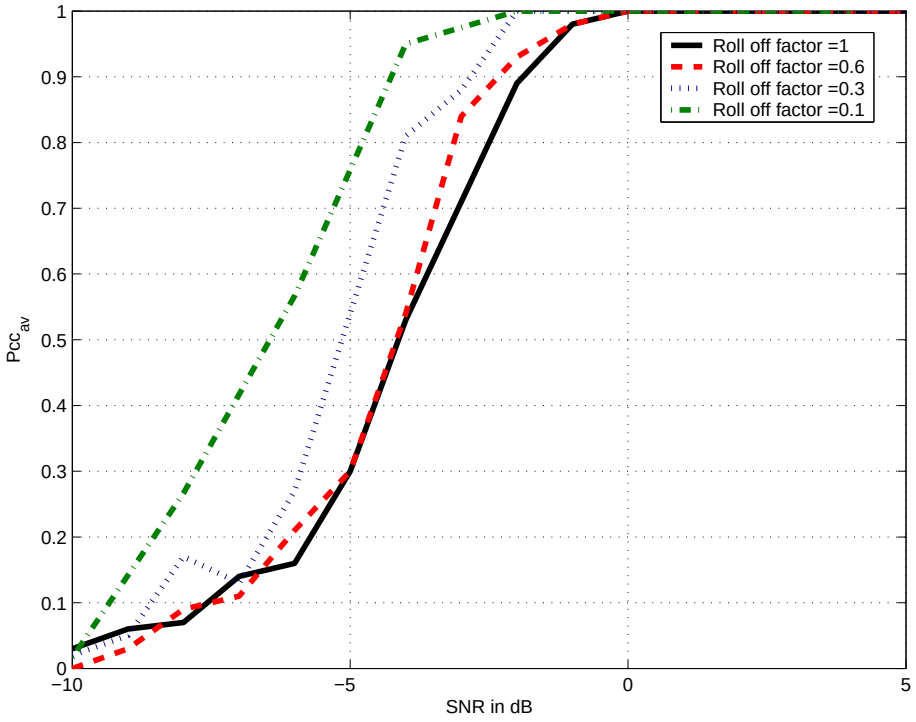

FIGURE 3.9: Average probability of correct estimation in the presence of base-band pulse shaping uncertainty

3.4.2 P_{cc} against a Range of Fading Severities

We consider a Rician fading scenario. The Rician factor signifies the severity of the fading scenario. The Rician factor is defined as the ratio of the received power level of the line of sight component to the resultant received power of the reflected components. We consider a range of Rician factors at the low SNR region and evaluate the average probability of correct estimation. Figure 3.10 shows the plot of the average P_{cc} for three different SNR levels. From the figure it is observed that the severity of the fading channel

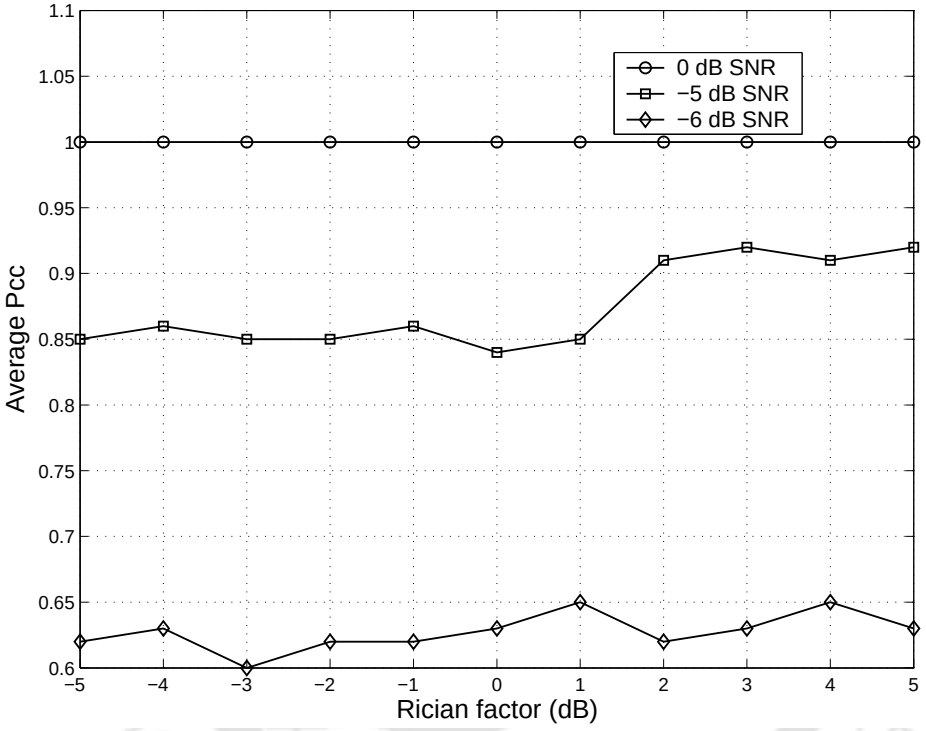

FIGURE 3.10: Average probability of correct estimation under Rician fading

does not have any significant effect on the performance of the symbol rate estimator does. Hence, the estimator is robust against fading impairments. However, the performance degrades with further decrease in the SNR.

3.4.3 MSE Performance

Figure 3.11 shows the plot of the mean square error (MSE) $E|\hat{f}_s - f_s|^2$ against the SNR for the ML estimator, the CAF based estimator and the proposed estimator. The MSE for the proposed method is much better in a low SNR region. The new estimator is

non-linear, with a threshold SNR for detection of the CDPP peak corresponding to the symbol rate. Hence, the MSE drastically drops beyond the threshold SNR. The ML method is based on the time domain signal envelop. As a result, the accuracy is effected by the AWGN at low SNRs. The proposed second order cyclostationary feature based method exploits the accumulated power profile of cyclic frequency corresponding to the symbol rate. The derived cyclostationary feature CDPP is prominent at very low SNRs. The second order cyclic features for the AWGN is zero. Hence for the same channel conditions, the proposed method has shown better estimation performance as compared to the ML based method. The stable MSE as seen in the figure is due to resolution of the cyclic frequency axis. The stabilized MSE can be reduced by increasing the resolution of the cyclic frequency axis. The complexity of the proposed algorithm is derived to be $\mathcal{O}\left(\frac{1}{\Delta\omega^2 T_s}\log\frac{1}{4\Delta\omega T_s L}\right)$. The complexity increases considerably with the decrease in the resolution of the cyclic frequency. However, for most of the practical applications, the detection of symbol rate within 5% accuracy provides acceptable recovery of the signal. Depending on the frequency, typical workable resolution of the cyclic frequency may be ranging from 1 Hz for audio frequency range to several KHz for microwave frequencies. The exact trad-off between the resolution and the computation time may be fixed based on the application. Figure 3.12 shows the performance of the symbol rate estimator in a fading channel with various sample sizes. The low SNR performance improves with the increase in the number of carrier samples.

3.5 Summary

In this Chapter, an alternative approach for estimation of the symbol rate in a blind scenario using the CDPP has been proposed. Due to the multipath fading and pulse shaping filter, the signal power spreads out in the spectral frequency axis. Since the CDPP is the accumulated power of the spectral components at any cyclic frequency, the symbol rate can be estimated using the prominent peak at the cyclic frequency within the valid search interval. As a result, a robust estimator is obtained even at deteriorated channel conditions and pulse shape uncertainties. Due to the improved performance, the proposed estimator may serve as a reliable pre-processing stage for the blind MC.

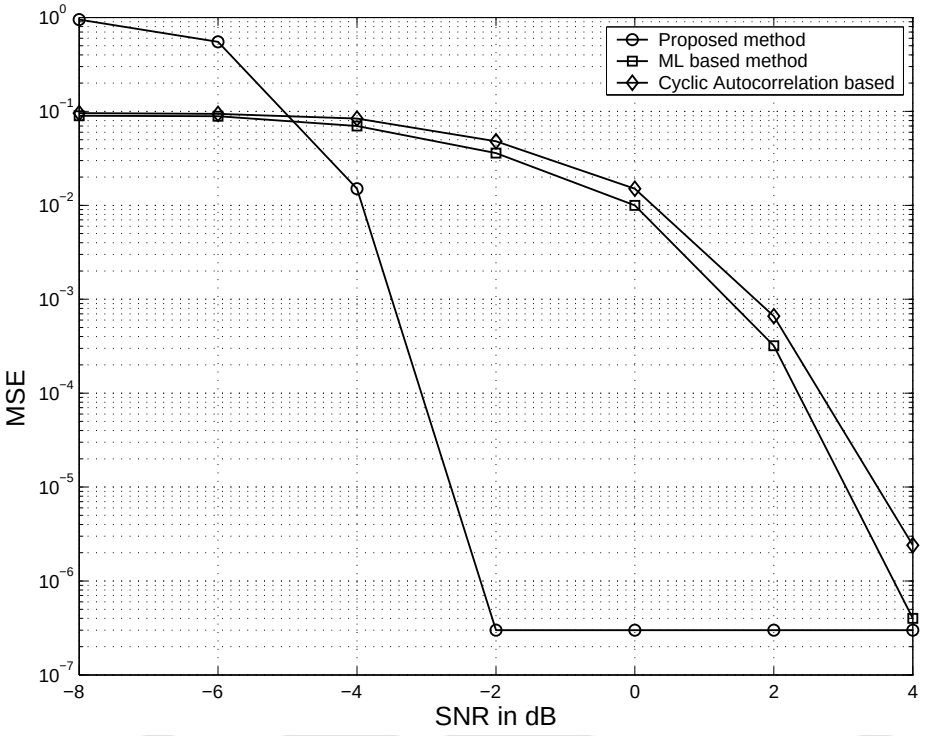

FIGURE 3.11: Comparative MSE for base band pulse roll off factor 0.35

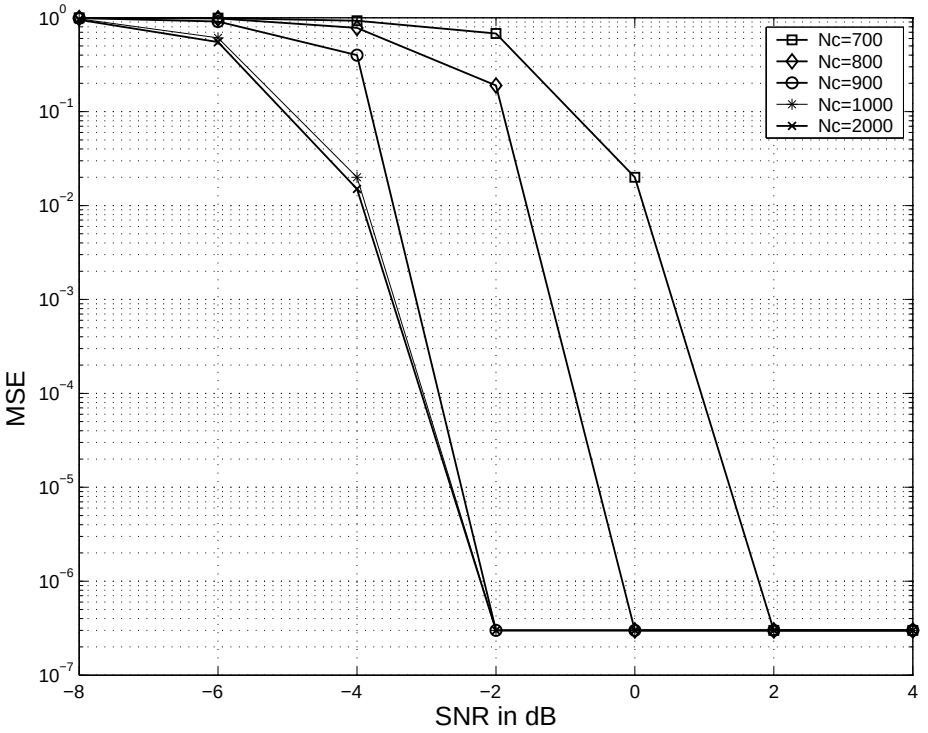

FIGURE 3.12: MSE at a fading channel $[1\ 0.3\ 0.2]^T$

The impact of observation interval on the processing complexity is a significant factor while maintaining the estimation accuracy. Future work may be taken up to reduce the

processing complexity.

4

Gain Normalization for Blind Modulation Classification

4.1 Introduction

As discussed in Chapter 2, the LB methods are best suited for blind MC, where high performance is a demand under challenging channel conditions. However, the classification performance is also governed by the LB method chosen and the algorithms used for estimation of the unknown parameters. This approach also suffers from the vulnerability to the model mismatch due the uncertain channel parameters [24, 67]. In this Chapter, the LB MC problem has been taken up under an unknown channel gain. The channel gain is the primary cause of model mismatch in LB MC.

Here, a new approach to mitigate the effect of the gain uncertainty due to the channel gain and the receiver implementation has been proposed. For the proposed LB classification, we consider the normalized constellations of all the candidate modulation schemes. To maintain the same scaling, the received signal constellation is required to be normalized before the MC stage, so that the model mismatch due to the unknown channel gain in evaluating the likelihood function is taken care.

4.2 Signal Gain Uncertainty in Maximum Likelihood Framework

4.2.1 QHLRT likelihood function

Recall that the LB classification is the most popular and widely discussed classifier. It is based on the Bayes rule and also termed as the optimal modulation classifier [68]. The initial work in this area was proposed in [3–5]. Rewriting the baseband signal model of Chapter 2, we get

$$\mathbf{x} = \alpha^{(i)} e^{j\psi^{(i)}} \mathbf{s}^{(i)} + \mathbf{n}$$

The approach to digital MC based on the maximum likelihood principle is to first derive the log-likelihood function (LLF) of the received signal according to the assumed signal model. Next, the value of the likelihood function is determined for all the candidate modulation schemes, using their constellation characteristics.

Suppose there are $\mathcal{C}$ modulation schemes in an M-ary system. The library symbols for the i^{th} modulation are expressed as

$$S^{(i)} = \left[s_1^{(i)} \; s_2^{(i)} \; ... s_M^{(i)} \right], \quad i = 1, 2, ..., \mathcal{C} \tag{4.1}$$

The MC is a problem of testing $\mathcal{C}$ hypotheses. $H^{(i)}$ is the hypothesis that the constellation is $S^{(i)}$. Assume N_b data samples are received. The received symbols are given by

$$x_k = \sqrt{x_{I,k}^2 + x_{Q,k}^2}, \quad k = 1, 2, ..., N_b \tag{4.2}$$

where $x_{I,k}$ is the in-phase component and $x_{Q,k}$ is the quadrature phase component of k^{th} sample. We consider that the candidate modulation schemes are equi-probable. Hence, maximizing the *a posteriori* probability is equivalent to maximizing the likelihood function. Therefore, the optimal hypothesis $\hat{H}$ is given by

$$\begin{aligned}\hat{H} &= \arg\max_i \mathbf{P}(H^{(i)}|x_1, x_2, ..., x_{N_b}) \\ &= \arg\max_i L(x_1, x_2, ..., x_{N_b}|H^{(i)})\end{aligned} \tag{4.3}$$

For the AWGN channel, the QHLRT likelihood function can be expressed as [20]

$$\prod_{k=1}^{N_b} \mathbf{p}(x_k|H^{(i)}) = \prod_{k=1}^{N_b} \sum_{m=1}^{M^{(i)}} \frac{1}{M^{(i)} 2\pi\sigma^2} \exp\left(-\frac{1}{2\sigma^2} ||x_k - \alpha^{(i)} s_m^{(i)}||^2 \right) \tag{4.4}$$

where $s_m^{(i)}$ is the m^{th} constellation point of hypothesis $H^{(i)}$ and σ^2 is the variance of the AWGN. Denoting $2\sigma^2$ by $N^{(i)}$, the following QHLRT [15, 21–24] likelihood function is obtained:

$$L(x_1, x_2, ..., x_{N_b}|H^{(i)}) = \prod_{k=1}^{N_b} \sum_{m=1}^{M^{(i)}} \frac{1}{M^{(i)} \pi N^{(i)}} \exp\left(-\frac{1}{N^{(i)}} ||x_k - \alpha^{(i)} s_m^{(i)}||^2 \right) \tag{4.5}$$

Now, the LLF is given by

$$\begin{aligned}\ln\left\{ L(x_1, x_2, ..., x_{N_b}|H^{(i)}) \right\} &= \ln\left\{ \prod_{k=1}^{N_b} \sum_{m=1}^{M^{(i)}} \frac{1}{M^{(i)} \pi N^{(i)}} \exp\left(-\frac{1}{N^{(i)}} ||x_k - \alpha^{(i)} s_m^{(i)}||^2 \right) \right\} \\ &= \sum_{k=1}^{N_b} \ln\left\{ \sum_{m=1}^{M^{(i)}} \frac{1}{M^{(i)} \pi N^{(i)}} \exp\left(-\frac{1}{N^{(i)}} ||x_k - \alpha^{(i)} s_m^{(i)}||^2 \right) \right\}\end{aligned} \tag{4.6}$$

4.2.2 Parameter estimation and MC performance

The performance of the LB classification depends on the accuracy of estimating the critical signal parameters. In practice, the blind classifier has to operate within a certain degree of parameter estimation error. As an example, the phase synchronization error results in a constant rotation of the recovered constellation. Similarly, the timing error in symbol recovery produces a smearing effect in the constellation. All these inaccuracies

cause model mismatches in the LB classification. As a result, classification accuracy also deteriorates. The issues of symbol timing, carrier frequency offset and phase synchronization are addressed in [21, 69–71]. The LB classification requires a good pre-processing stage to ascertain the channel gain, the carrier phase offset, the symbol timing, the center frequency offset and in some cases measures to mitigate the baseband residual channel effects. In this Chapter, the scenario is simplified by considering that the signal is received in a coherent condition, so that $\psi^{(i)} \simeq 0$. In such a scenario, the received signal vector can be expressed as

$$\mathbf{x} = \alpha^{(i)}\mathbf{s}^{(i)} + \mathbf{n} \tag{4.7}$$

However, in the LLF of (4.6), the noise power $N^{(i)}$ and the channel gain $\alpha^{(i)}$ are the still unknown parameters. Here, focus is centered around the mitigation of the unknown parameter $\alpha^{(i)}$, while the MoM principle of [15] is employed for the estimation of the noise power. A novel approach to the estimation of the noise power is deferred till Chapter 5. In the classical literature on LB approach [3–5, 20, 51, 72], the channel gain factor is considered as unity and the model mismatch due to the gain uncertainty is ignored. However, towards a blind MC application, the mitigation of the channel gain uncertainty is mandatory. A typical case of model mismatch for blind reception of the 16QAM signal is shown in Figure 4.1. The uncertainty of the channel gain results in a situation, where the actual gain of the modulated signal becomes unknown.

4.2.3 Background of the gain estimation

Estimation of $\alpha^{(i)}$ has been formulated in several QHLRT based classifications along with the estimation of $\psi^{(i)}$ and $N^{(i)}$. The method of moments (MoM) based estimators for $\alpha^{(i)}$, $\psi^{(i)}$ and $N^{(i)}$ were proposed in [18, 73, 74], and the results were used in [15] and [24] for the QHLRT based MC. The MoM estimates of the unknown parameters under the i^{th} hypothesis are given by

$$\widehat{\alpha}^{(i)} = \left(2\widehat{M}_{r,21}^2 - \widehat{M}_{r,42}\right)^{1/4}, \tag{4.8}$$

$$\widehat{\psi}^{(i)} = {M_i}^{-1} \arg\Big(\sum_{k=1}^{K} {x_k}^{M_i}\Big), \tag{4.9}$$

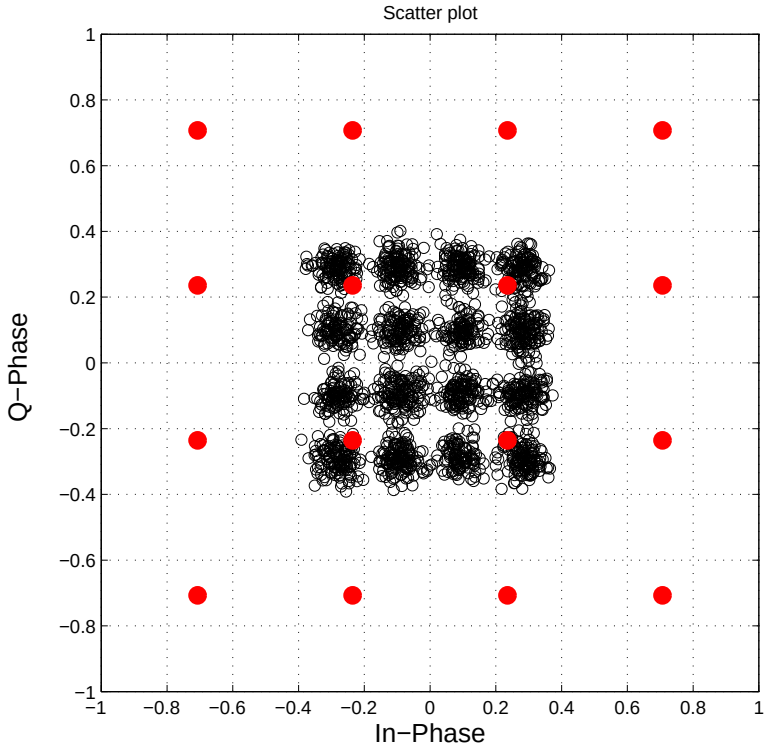

FIGURE 4.1: Model mismatch in AWGN scenario due to the unknown channel gain

and

$$\widehat{N}^{(i)} = \widehat{M}_{r,21} - \left(2\widehat{M}_{r,21}^2 - \widehat{M}_{r,42}\right)^{1/2}, \tag{4.10}$$

where $\widehat{M}_{r,21}$ and $\widehat{M}_{r,42}$ are the estimates of the second-order one-conjugate and fourth-order two-conjugate moments of the received linearly modulated signal. Lower complexity is the major strength of the MoM based estimators. A recent work in [26] (described in Chapter 2) uses the centroid estimation of received constellation using the MDCE method (see Subsection 2.4.5). The channel gain is derived from the estimated centroids. Although, the method provides a fairly reliable estimate of $\alpha^{(i)}$, the need for improvement of the estimation performance at a low SNR is still a strong motivation for investigating alternate estimators. The work carried out in this chapter focuses on formulating an improved method to mitigate the uncertainty caused by the channel gain in the QHLRT MC framework across a wide range of SNR. A comparative study of the estimation performance is presented in the experimental section.

4.3 Proposed Approach to the Mitigation of the Gain Uncertainty

4.3.1 Formulation of a generic gain estimator

Consider signal model of Equation (4.7) and the LLF for the received signal in Equation (4.6). The unknown parameters $N^{(i)}$ and $\alpha^{(i)}$ need to be estimated using blind estimation algorithms. As the mitigation to the problem of the unknown gain, the incoming signal is to be normalized after I-Q demodulation. It is proposed to use the normalized versions of the constellation model and the received signal in the likelihood function. In [8], the gain is normalized by performing simple averaging on a pool of candidate modulation schemes. This is a feature-based decision tree approach to distinguish between constant gain digital modulation signals like FSK2 and FSK4 as one class and ASK2, ASK4, BPSK and QPSK as the other. The average value A_{av} of the sampled signal sequence is calculated by

$$A_{av} = \frac{1}{N_b} \sum_{k=1}^{N_b} A_k \tag{4.11}$$

where A_k is the magnitude of the k^{th} sample in the received constellation and given by $A_k = \sqrt{x_{I,k}^2 + x_{Q,k}^2}$. The instantaneous value of the received signal is normalized by

$$A_{k,norm} = \frac{A_k}{A_{av}} \tag{4.12}$$

The above method of gain normalization is suitable only for the constat-amplitude modulation schemes. Hence, to address modulation schemes with multi-amplitude signals like 16QAM, there is a need for a generic approach. The normalization of the received constellation is carried out in conventional communication systems with the knowledge of the transmitted constellation [75]. This approach is based on normalization of constellation power using a known normalizing factor for a specific modulation. However, this approach is not suitable for blind MC, as there is no prior information of the incoming signal. In [76], signal power normalization was proposed as pre-processing requisite for the FB classifier to distinguish between QPSK, 16QAM and 64QAM of the WiMax standard. Here, normalization is proposed by using an automatic gain control mechanism.

This is a common mechanism employed in radio receivers, where normalization is carried out by simple averaging over a section of received data. The problem of multi-level signal constellation is still not addressed by this mechanism. The performance of the LB classifier showing degradation due to gain mismatch is included in the experimental section.

Therefore, a better and generalized method is necessary for mitigating the uncertainty of the signal gain in the recovered constellations. Referring to (4.6), the model mismatch due to the gain uncertainty can be mitigated either by estimating the gain $\alpha^{(i)}$ in (4.6) or by normalizing x_k. However, both the approaches offer the same results. Here, it is proposed to normalize the received samples, so that the method is applicable for each hypothesis. Now the LLF of (4.6) is modified as

$$l\left(\tilde{x}_1, \tilde{x}_2, ..., \tilde{x}_k | H^{(i)}\right) = \sum_{k=1}^{N_b} \ln\left\{\sum_{m=1}^{M^{(i)}} \frac{1}{M^{(i)}\pi\hat{N}^{(i)}} \exp\left(\frac{-1}{\hat{N}^{(i)}}||\tilde{x}_k - s_m^{(i)}||^2\right)\right\} \tag{4.13}$$

where $\tilde{x}_k$ is the k^{th} normalized sample and the MoM estimate of the noise variance is $\hat{N}^{(i)} = \left\{\widehat{M}_{r,21} - \left(2\widehat{M}_{r,21}^2 - \widehat{M}_{r,42}\right)^{1/2}\right\}$. The normalization of a noisy constellation is challenging due to the random distribution of the sample points around the actual constellation points. In noise free environment, the normalization of the received I-Q sample can be carried out as

$$\tilde{x}_k = \frac{x_k}{x_{max}}, \tag{4.14}$$

where x_k is the k^{th} sample point and x_{max} is the magnitude of the outermost sample point in the I-Q space. However, in a noisy scenario, accurately finding x_{max} is not possible due to the variance of the AWGN. In this case the demodulated symbol points are scattered widely around original constellation points. An outlier sample in the so called Gaussian cloud may be having maximum magnitude among the sample points. Taking the absolute maximum value as x_{max} will result in inaccurate normalization. In view of this, a practical approach to normalize the constellation is to first estimate the cluster centers. It is easy to estimate the outermost cluster center for estimating the channel gain. The constellation points can be considered as local cluster centers within a cloud of sample points. However, the number of clusters and the corresponding number of cluster centers will depend on the modulation type.

4.3.2 Selection of the clustering algorithm

For normalizing the I-Q samples, the estimation of the cluster centers of the received signal is necessary. The cluster centers are proposed to be estimated using a clustering algorithm. Among the available clustering algorithms, the K-means, the Fuzzy K-means and the subtractive clustering algorithms are examined for using in the estimation of the cluster centers.

K-means clustering: The K-means clustering algorithm partitions a collection of data samples into K clusters and estimates the center for each cluster. In this method (developed by LIoyd in 1957 and improved by MacQeen in 1967) each data sample is allocated to belong to any one of the K clusters. The membership of the data samples is updated iteratively by minimizing the following cost function.

$$J = \sum_{j=1}^{K} \Big(\sum_{k=1}^{N_b} ||x_k - \mu_j||^2 \Big), \tag{4.15}$$

where, μ_j is the j^{th} cluster center. The partitioned clusters are defined by a $N_b \times K$ matrix $\mathbf{U}$ given by

$$u_{kj} = \begin{cases} 1, & \text{if} \quad ||x_j - \mu_k||^2 < ||x_j - \mu_i||^2, \quad i \neq k \\ 0, & \text{otherwise} \end{cases} \tag{4.16}$$

where, u_{kj} is the degree of membership of x_k in the cluster j, x_k is the k^{th} data sample, μ_j is the j^{th} cluster center and $||.||$ is the Euclidian norm expressing the similarity between any measured data and the center. The optimal value of μ_j that minimizes (4.15) is given by

$$\mu_j = \frac{1}{N_j} \sum_{k=1}^{N_j} x_k, \tag{4.17}$$

where, N_j is size of the j^{th} cluster. The iterative process for the K-means algorithm is summarized below.

- Step 1: Initialize the K cluster centers by assigning random values
- Step 2: Update the membership matrix $\mathbf{U}$ as per (4.16)

- Step 3: Compute J as per (4.15). Terminate the iterations if the value is below a certain tolerance value, or the improvement over the the previous iteration is below a certain threshold.
- Step 4: Update the cluster center as per (4.17) and go to Step 2.

Fuzzy K-means clustering (FKM): The FKM is a method of clustering which allows a sample of data to belong to two or more clusters. It is a generalized form of the K-means algorithm. This method (developed by Dunn in 1973 and improved by Bezdek in 1981) is frequently used in pattern recognition and based on minimization of the following objective function:

$$J_m = \sum_{k=1}^{N_b} \sum_{j=1}^{K} u_{kj}^m ||x_k - \mu_j||^2, \quad 1 < m < \infty \tag{4.18}$$

where m is any real number greater than 1, u_{kj}^m is the degree of membership of x_k in the cluster j. Fuzzy partitioning is carried out through the iterative optimization of 4.18, while updating the membership u_{kj} and the cluster centers μ_j. The functions are updated in the $t^{(th)}$ iteration as

$$u_{kj}^{m\,(t)} = \frac{1}{\sum_{t=1}^{K} (\frac{||x_k - \mu_j||}{||x_k - \mu_t||})^{\frac{2}{m-1}}} \quad \text{and} \quad \mu_j{}^{(t)} = \frac{\sum_{k=1}^{N_j} u_{kj}.x_k}{\sum_{k=1}^{N_j} u_{kj}^m} \tag{4.19}$$

The iterative process terminates when $\max_{kj}\{|u_{kj}^{(t+1)} - u_{kj}^t|\} < \varepsilon$, where ε is a constant, $0 \leq \varepsilon \leq 1$.

Subtractive clustering: In this method, data samples are considered as the candidates for cluster centers [77]. It is based on the estimation of the density around each data sample. In subtractive clustering, the number of clusters need not be pre-defined. The density measure at data sample x_j is given by

$$D_j = \sum_{k=1}^{N_b} \exp\Big(- \frac{||x_j - x_k||^2}{(r_a/2)^2} \Big), \quad j = 1, 2, ..., N_b \tag{4.20}$$

where, r_a is the radius of the neighborhood. Data samples outside this radius does not contribute significantly to the density function. The density measure is computed for

each data sample and the one with the highest density measure is selected as the first cluster center. Denoting the new cluster center as μ_1 and the density measure as D_1, the density measure for each data sample is updated as given below.

$$D_j = D_j - D_1 \exp\Big(-\frac{||x_j - \mu_1||^2}{(r_b/2)^2}\Big), \quad j = 1, 2, ..., N_b \tag{4.21}$$

where, $r_b = 1.5r_a$. The above density measure ensures that the estimated first cluster center is unlikely to be selected again. Once the density measures for each data sample are measured, the next cluster center μ_2 is selected. The process is repeated until a sufficient number of clusters are generated or a termination criterion is met.

In both the K-means and the FKM clustering methods, the number of clusters needs to be pre-defined. However, the FKM clustering has the advantage over K-means algorithm in terms of the convergence accuracy. On the other hand in the subtractive clustering, the selection of the neighborhood radius r_a plays a vital role in the final results. Unfortunately, the optimum value of r_a is dependent on the SNR as well as the gain of the received signal in the present case. Hence in a blind MC scenario, the application of the subtractive clustering still needs further adaptations. In our work,the FKM clustering algorithm is primarily used for estimation of the signal gain.

4.3.3 Estimation of the channel gain

The number of valid cluster centers in a received signal is an unknown parameter. Assume that K is the number of constellation points of the highest order modulation in the pool of candidate modulations. For example, the value is 16 if the set of modulations considered are BPSK, QPSK, 8QAM and 16QAM. After the convergence of the iterative clustering process, the final set of cluster centers will be formed in the vicinity of the original constellation points. Simulation results in Figure 4.2 show clustering for the QPSK and 16QAM modulations using the FKM iterations. The final cluster centers are expressed as

$$C_{final}^{(t)} = \{\mu_1, \mu_2, ...\mu_K\} \tag{4.22}$$

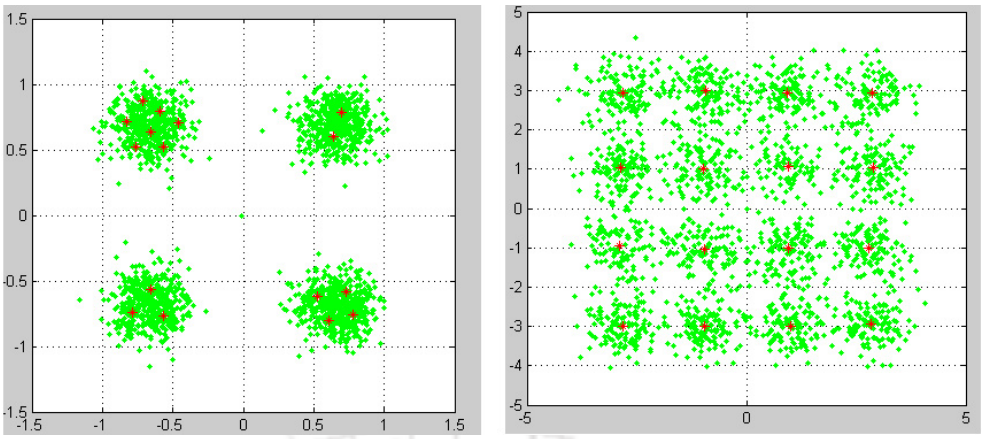

FIGURE 4.2: Final cluster centers for QPSK and 16QAM

The outermost cluster center μ_{max} is the one with the maximum distance from the origin of the I-Q space.

$$\mu_{max} = \max_{j} |||[\mu_j]|||, \quad j = 1, 2, ..., K \tag{4.23}$$

We re-write (4.14) after substituting x_{max} by μ_{max} as

$$\tilde{x}_k = \frac{x_k}{\mu_{max}}, \tag{4.24}$$

The estimated channel gain for the i^{th} modulation is given by $\hat{\alpha}^{(i)} = \mu_{max}$. This relation (4.24) approximately normalizes the demodulated constellation. The maximum likelihood based MC rule is applied using the gain normalized samples in (4.13).

4.4 Experimental Results and Discussions

In this section, the performances of the proposed gain estimation method and the QHLRT MC using the gain estimates are evaluated. We consider a pool of candidates containing both constant-amplitude as well as multi-amplitude modulations.

4.4.1 MSE of the gain estimator

The performance of the signal gain estimator has been evaluated by using the MSE of the estimator. It is calculated based in the estimation error with respect to the actual

gain. the The MSE of the estimator is given by

$$e_{MSE}^{(i)} = \frac{1}{T_I}\sum_{I=1}^{T_I}(\alpha^{(i)} - \hat{\alpha_I}^{(i)})^2 \tag{4.25}$$

where, I denotes the I^{th} iteration and T_I is the total number of iterations. In Figure 4.3, the performance of the gain estimator using the subtractive clustering is illustrated. Although, the MSE performance is very good for the appropriate selection of r_a, the performance is not guaranteed in a blind scenario under the gain uncertainty and SNR conditions. For specific cases (e.g. $r_a = 0.9$), D_j is effected by the spread of the constellation cloud, causing the MSE to deteriorate at certain range of SNRs. In Figure 4.4, the comparative performance of the gain estimator using the K-means, the FKM and the subtractive clustering is illustrated. The performance stability across the range of SNR is best for the FKM clustering among the three.

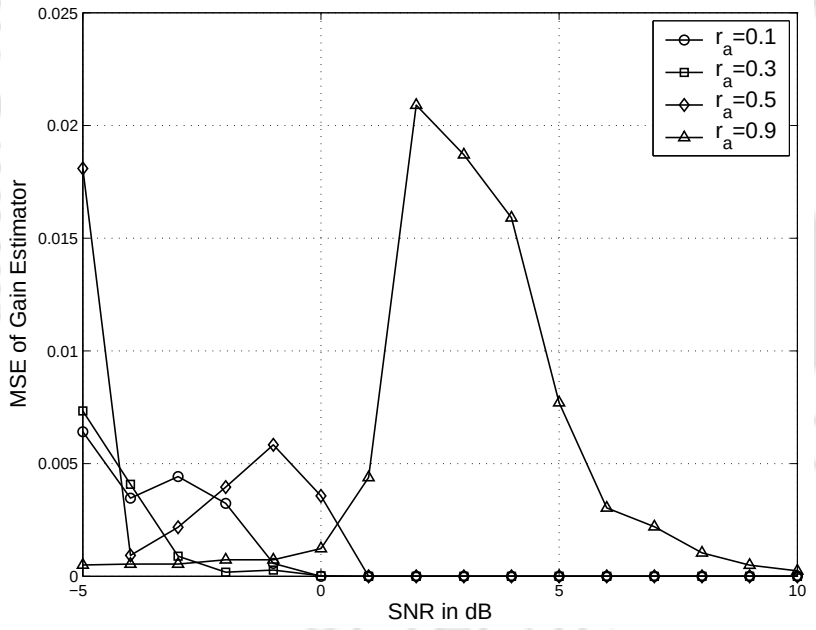

FIGURE 4.3: MSE performance of subtractive clustering based gain estimator under variations of r_a for QPSK, $N_b = 500$

For the rest of the experiments, the FKM clustering is used for the estimation of the gain. In Figure 4.5, the MSE of the proposed gain estimator is compared with the method proposed in [15, 26]. As illustrated in the figure, the proposed estimator outperforms [26] throughout the test SNR range. On the other hand, the MoM based estimator

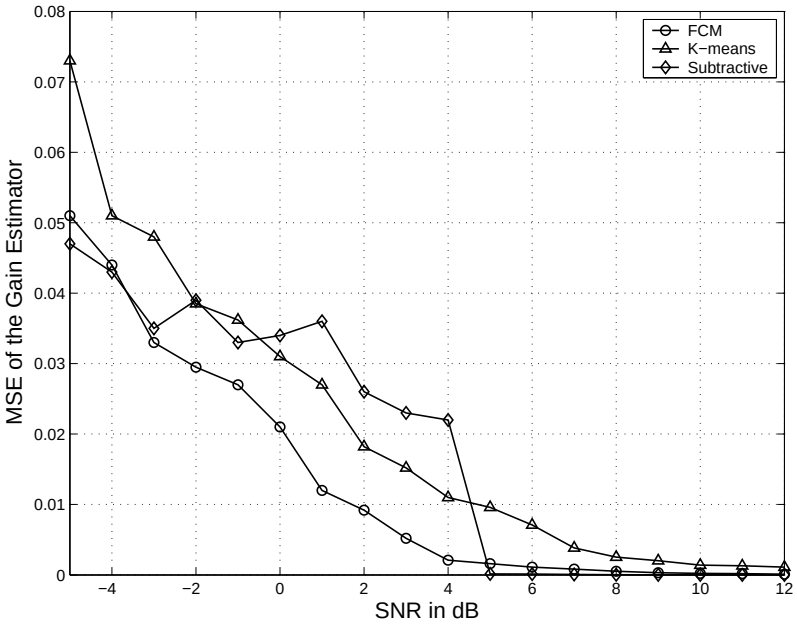

FIGURE 4.4: MSE performance comparison for 16QAM, $N_b = 1000$

[15] performs better for single amplitude constellations like QPSK. However, for multi-amplitude constellation like 16QAM, the proposed estimator performs better in general. However, since the number of centroids in the proposed estimator is pre-assigned as per the highest order modulation scheme in the candidate pool, there is a degradation of performance in the low SNR region. In Figure 4.6, the MSE of the proposed gain estimator for the QPSK modulation is plotted for various sample sizes against the same range of SNR. The performance improves as the sample length is increased. Optimum selection of sample size needs to be considered depending on the application scenario.

4.4.2 Performance of MC

The performance of the modulation classifier is measured by plotting the probability of correct classification (P_{cc}) averaged over all the candidate modulation schemes over a range of SNRs. As the analytical solution involves successive integrations, Monte Carlo simulation is convenient to plot the performance of the classifier. Recall that, P_{cc} is estimated as

$$\hat{P}_{cc} = \frac{N_C}{N_T}, \tag{4.26}$$

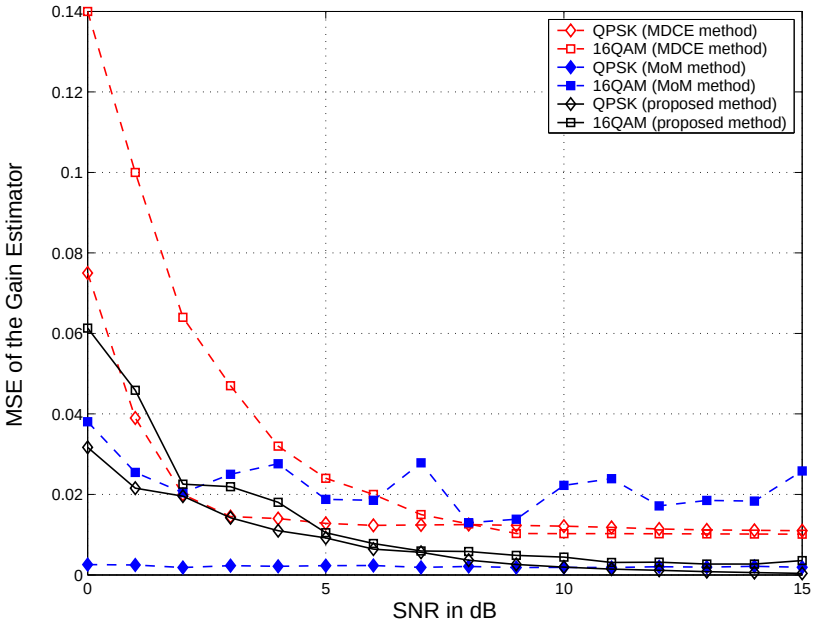

FIGURE 4.5: Comparative performances of the proposed gain estimator for $N_b = 1000$

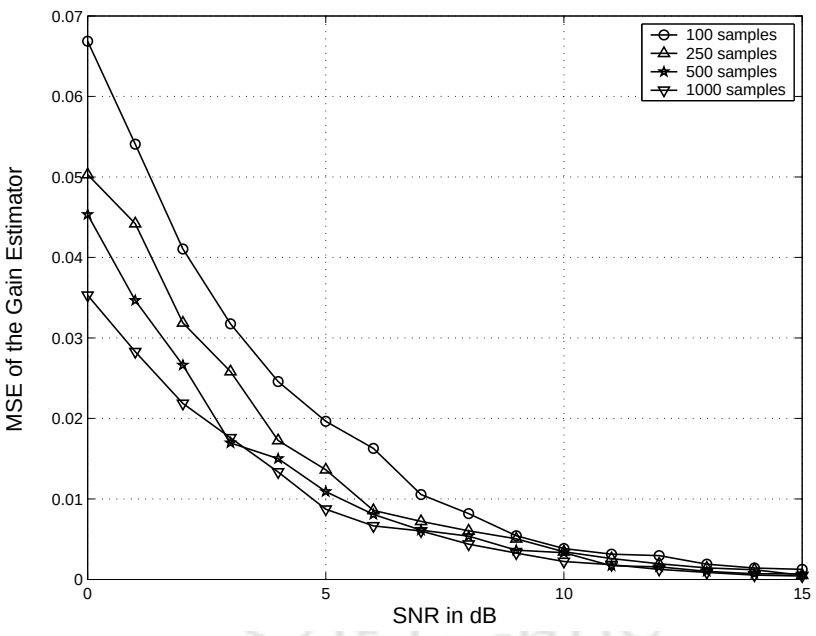

FIGURE 4.6: Performance dependence of the proposed gain estimator with the sample length for QPSK modulation

where, N_C and N_T are number of correct decisions and total number of experiments respectively.

First the performance of the likelihood based classifier with the model mismatch due to the gain uncertainty is plotted. The Monte Carlo simulation with 1000 iterations and various sample lengths are considered. Figure 4.7 shows the plot with various degrees

of gain mismatch. The gradual degradation of classifier performance is evident in the figure. It is worth mentioning that, the sensitivity of the model mismatch increases with the increase in the candidate modulation pool. In this case, a pool containing BPSK, QPSK, 8QAM and 16QAM has been considered. For example, a model mismatch of 2% has resulted in a degradation of about 3 dB in the classification performance.

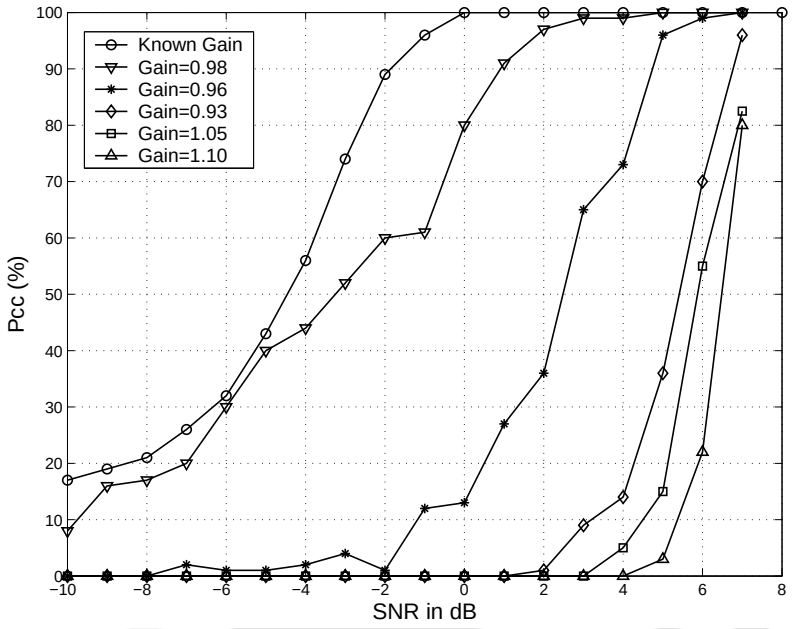

FIGURE 4.7: Comparative MC performances with accurate and erroneous amplitude scalings

Now, the performance of the likelihood based classifier with the proposed gain normalization scheme is plotted. The pool of candidate modulations include BPSK, QPSK, 8QAM and 16QAM. Figure 4.8 shows the comparative performance of the classifier, showing the ideal case with the knowledge of the received signal gain as reference. For the received signal, we consider a gain mismatch of 50% with respect to the model constellation.

The P_{cc} curve with the normalized gain is close to the performance of the classifier with known channel gain, when the noise variance is considered as a known parameter. However, there is a degradation of performance when the MoM based estimate of the noise variance is used in the likelihood function. The performance of the classifier with known gain is still better than the one with gain normalization approach at the lower SNR region. It is worth mentioning that, the degree of gain mismatch of the received signal has no noticeable influence of the estimation performance. As seen in Figure

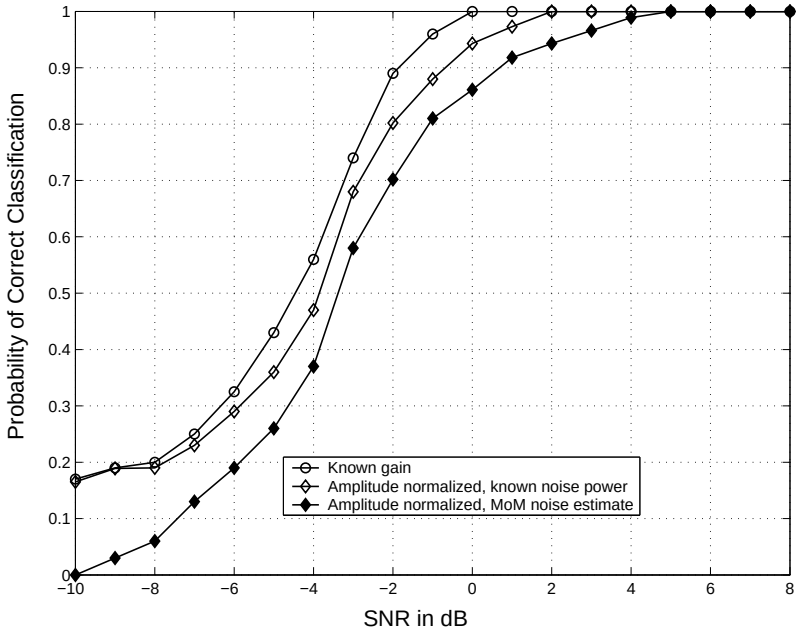

FIGURE 4.8: Comparison of classification performance with known gain and blind scenario using FCM based gain normalization, while the received modulation is QPSK

SNRs	100 samples		400 samples		1000 samples	
	KG	GN	KG	GN	KG	GN
0 dB	100%	94.3%	100%	96.5%	100%	98.9%
5 dB	100%	100%	100%	100%	100%	100%

TABLE 4.1: Average percentage of correct classification as function of SNR and Number of samples

4.9(a), at lower SNRs, the cluster centers found are spread in the constellation cloud. Hence, normalization accuracy degrades with decreasing SNR. Figure 4.9(b) shows that the final cluster centers are spaced closed together at higher SNRs, resulting in better normalization accuracy and better classification performance. Hence, at higher SNRs, the performances of both the classifiers are more closer. Table 4.1 shows the comparison of average classification accuracy as a function of SNR and number of samples for the ideal case of known gain (KG) and with the new approach using gain normalization (GN). It is assumed that the signal is received with a gain mismatch of 50%. From the table, it can be easily interpreted that P_{cc} improves as the number of samples is increased. Also, at higher SNRs, since the clustering ambiguity is reduced, the MSE of the gain estimator also reduces. This results in a reduced degree of gain mismatch and hence an improved P_{cc} is achieved.

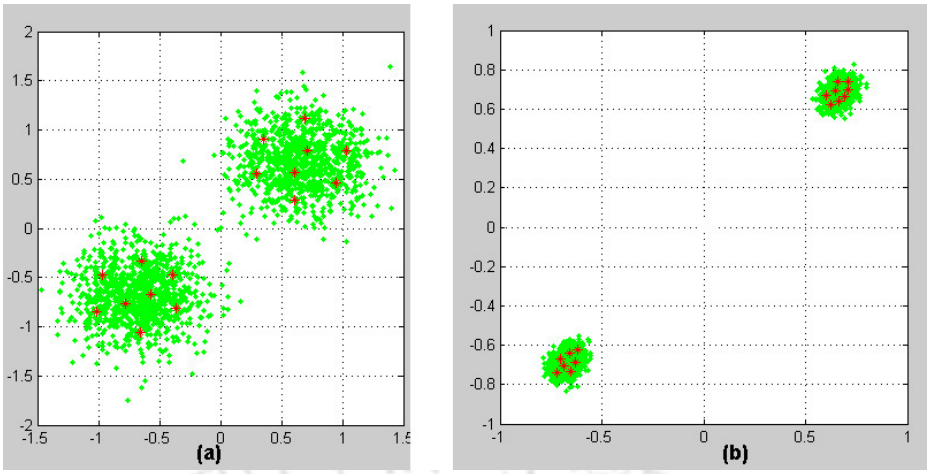

FIGURE 4.9: FKM clusting at SNR (a) 2 dB and (b) 15 dB

4.5 Summary

In this Chapter the case of gain uncertainty as one of the pre-processing issues has been addressed and a method to mitigate the same has been proposed. The proposed method has shown improved performance as compared to the MDCE method throughout the test SNR range. Also, the proposed estimator performs better for multi-amplitude modulations schemes as compared to the MoM based estimator. The better accuracy of the estimate has enabled the ML classifier to achieve improved classification performance. However, for a complete blind MC, other unknown parameters need to be taken into consideration and the performance of such estimators needs to be emphasized at the lower SNR region. Further focus is to improve the gain normalization algorithm for better classification performance in low SNR conditions.

5

Comprehensive Parameter Estimation for Blind Classification of Digital Modulations

5.1 Introduction

As discussed earlier, several authors [3–5, 17, 51] have proposed semi-blind LB classifiers, with the partial knowledge of the signal parameters. These proposals provide a good theoretical basis for further improvements, but lack the feasibility of implementation in an NDA classification scenario. Recent works in [15, 22, 24, 26] have been carried out towards the blind estimation of the unknown parameters. There is an increasing demand for a robust classifier in specific military applications like COMINT, where the

received signal is quite often severely degraded by adverse channel conditions. Hence, special focus is necessary for the improvement of the LB classification performance at a low SNR region with an additional concern about handling fading related impairments.

This chapter focuses on the QHLRT approach. Although the performance is sub-optimal as compared to the ideal case of HLRT, it is relatively a lower complexity LB classification technique [15] for practical implementation in a blind scenario. Suppose there are $\mathcal{C}$ possible modulations. Consider the modulated signal model in the AWGN and an unknown channel as discussed in Chapter 1, given by

$$r_c(t) = e^{j2\pi(f_c+\Delta f)t}e^{j\phi}\sum_{k=-\infty}^{\infty} s_k^{(i)}h(t-kT_s-t_0)+n_g(t),, \tag{5.1}$$

Further, the matched filtered output of the signal as modeled in Chapter 1 is reproduced here.

$$\mathbf{x} = \alpha^{(i)}e^{j\psi^{(i)}}\mathbf{s}^{(i)}+\mathbf{n} \tag{5.2}$$

Note that, $\alpha^{(i)}$ is the channel gain and $\psi^{(i)}$ is the resultant phase offset. Suppose $\mathbf{x}_1, \mathbf{x}_2, \cdots, \mathbf{x}_{N_b}$ are N_b samples of the received signal. The log likelihood function in the QHLRT framework for the hypothesis $H^{(i)}$ as defined in Equation (2.11)

$$l(\mathbf{x_1}, \mathbf{x_2}, ..., \mathbf{x_{N_b}}|H^{(i)})_{QHLRT} = \sum_{k=1}^{N_b}\ln\left[\sum_{m=1}^{M^{(i)}}\frac{1}{M^{(i)}\pi N^{(i)}}exp\left\{-\frac{1}{N^{(i)}}\left|x_k-\alpha^{(i)}e^{j\psi^{(i)}}s_m^{(i)}\right|^2\right\}\right], \tag{5.3}$$

Among the unknown parameters T_s, α, ψ and N are to be estimated for the QHLRT classification. The estimation of T_s in adverse signal conditions has been illustrated in Chapter 3. In this Chapter, we deploy the estimator for T_s for the use in the demodulation process to derive the matched filtered base-band signal in the I-Q plane. As described in the previous Chapters, the relatively simple MoM based estimations of α, ψ and N have been used in the QHLRT based MC [15, 24]. However, performance degradation for the use of these estimators in a generic pool of candidate modulations with single and multi-amplitude constellations is the main concern. The estimation of α and ψ using the MDCE method [26] was aimed at reducing the complexity in an alternate LB classification method of the NPLF. However, the need for improvement in the overall

classification performance at the low SNR region is still a strong motivation towards the development comprehensive blind estimators for the unknown parameters.

This chapter presents a QHLRT based MC method in a blind scenario. For the estimation of $\alpha^{(i)}$, $\psi^{(i)}$ and $N^{(i)}$, we first determine the cluster centers of the received constellation using the expectation maximization (EM) algorithm considering the signal as a GMM. The EM algorithm converges to get the estimates of the cluster centers and the covariance matrix for each cluster. The covariance matrices provide the estimate of $N^{(i)}$. $\alpha^{(i)}$ and $\psi^{(i)}$ are derived from the estimated cluster centers using geometrical transformations. To establish the theoretical performance limit, the Crammer Rao lower bounds (CRLB) [78] for $\widehat{\alpha}^{(i)}$ and $\widehat{\psi}^{(i)}$ are derived. Experimental results are presented at a slow fading scenario, showing the estimation performance as compared to the earlier methods. Finally, the estimated values of the unknown parameters are inserted in (5.3) to obtain the QHLRT classification. The performance of the proposed QHLRT classifier is compared with the theoretical limit of the HLRT as well as with the performance of the existing algorithms to illustrate the improvements achieved by the proposed method.

5.2 Proposed Approach to the Estimation of the Unknown Parameters

In this section, an alternative approach is proposed to estimate the signal gain $\alpha^{(i)}$, the phase offset $\psi^{(i)}$ and the noise variance $N^{(i)}$. We exploit the fact that $\alpha^{(i)}$ and $\psi^{(i)}$ are functions of the received constellation centers [26]. Hence, by estimating the cluster centers of the received constellations, it is possible to geometrically derive $\alpha^{(i)}$ and $\psi^{(i)}$. In Chapter 4, the cluster centers are estimated using the fuzzy K-means clustering method. However, since the number of clusters is fixed as per the highest order candidate modulation schemes, the variance of the estimator is high at low SNR conditions. Table 5.1 provides the summary for the suitability of choosing the clustering algorithm for the new method. The complexity is defined for the case of 2-dimensional constellation parameter with N_b samples, $M^{(i)}$ clusters, I iterations for convergence and $\mathcal{C}$ candidate modulation schemes. Among the listed clustering algorithms, the K-means, the FKM

Algorithm	Number of clusters	Complexity
K-means	Pre-defined	$O((\mathcal{C}+1)N_b M^{(i)} I)$ [79]
Fuzzy K-means	Pre-defined	$O((\mathcal{C}+1)N_b {M^{(i)}}^2 I)$ [80, 81]
Subtractive clustering	Not pre-defined	$O(N_b I)$ [77, 82]
Hierarchical clustering	Not pre-defined	$O(N_b^3)$ [83]
EM	Pre-defined	$O((\mathcal{C}+1)N_b M^{(i)} I)$ [84]

TABLE 5.1: Summary of clustering algorithms

and the EM algorithms require the number of clusters to be pre-defined. The same is not necessary for the subtractive and the hierarchical clustering algorithms. This makes the subtractive and the hierarchical clustering algorithms the potential candidates for use in the blind scenario. As brought out in Chapter 4, the subtractive clustering performance is dependent on the selection of the neighborhood radius r_a. Also, the optimum value of r_a is dependent on the SNR as well as the gain of the received signal. On the other hand, the complexity of the hierarchical clustering is high and arriving at a termination criterion for the iterations is a non-trivial problem in a blind scenario. Exploring further, the clustering complexity of the K-means and the EM algorithms are less than the FKM. Among these two, the EM algorithm can additionally provide the estimate of the noise variance apart from the cluster centers.

In the proposed method, the cluster means and the variances are estimated by employing the EM algorithm. As a motivation for the approach, the received constellation in the AWGN can be assumed as a GMM with the number of clusters, individual cluster means and cluster variances as unknown parameters. Since the EM estimate of the noise variance can be considered close to the ML estimate [85], it may be employed to derive the noise power, which finally contributes to the performance of the QHLRT classifier. Figure 5.1 illustrates the 3-D histogram of a 16QAM base-band signal modeled as a GMM. The EM algorithm also requires a pre-defined number of clusters to converge. In the proposed method, this issue is overcome by introducing a pre-processing step, where the actual number of clusters is estimated by examining the Gaussianity of the estimated clusters.

The computational performance of the EM, the K-means and the FKM algorithms in

the context of the current problem is examined. In Figure 5.2, the experimental computation time of the EM algorithm for the proposed method is compared with other algorithms. Among the three clustering algorithms considered, the overall computational performance of the EM algorithm for the same number of iterations falls in the average region. However the additional information of the noise power estimate makes the EM algorithm more attractive for employing in the estimation process. As shown in

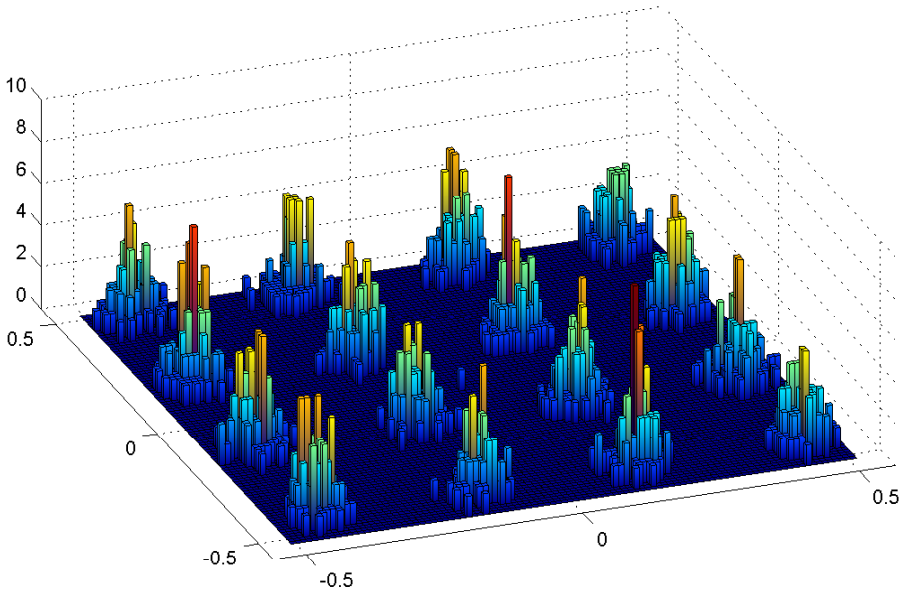

FIGURE 5.1: 3-D histogram of a 16QAM signal

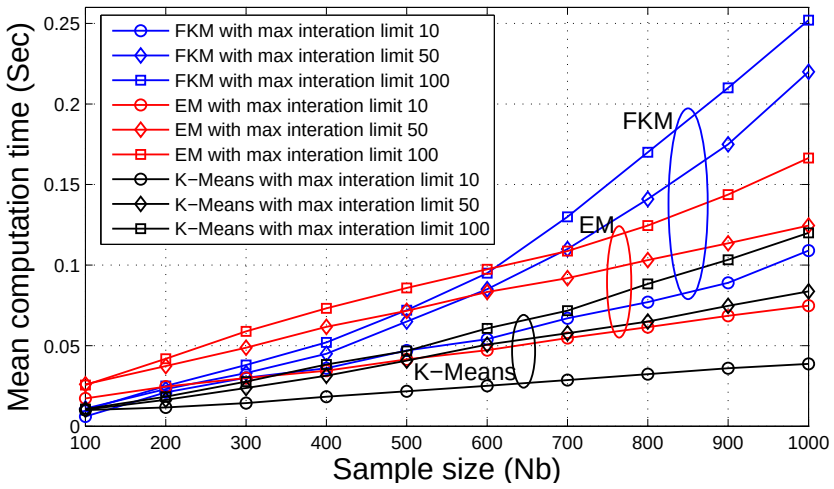

FIGURE 5.2: Computation time for an Intel Xeon CPU with 2 GHz processor in a fading channel $\mathbf{h} = [1\ 0.3\ 0.2]T$

Table 5.1, the preprocessing step introduces additional computational complexity. However, it is a trade off for the estimation performance. It is possible to limit the number of iterations of the EM algorithm to further reduce the computation time. In Figure 5.3, it is evident that the convergence time of the EM algorithm is dependent on the convergence factor (in %) and the maximum number of iterations defined a-priori. However, above certain value of convergence factor, the number of iterations does not contribute significantly to the computation time. This fact can be used to optimize the number of iterations, without any significant compromise on the overall estimation performance, thereby optimizing the computation time.

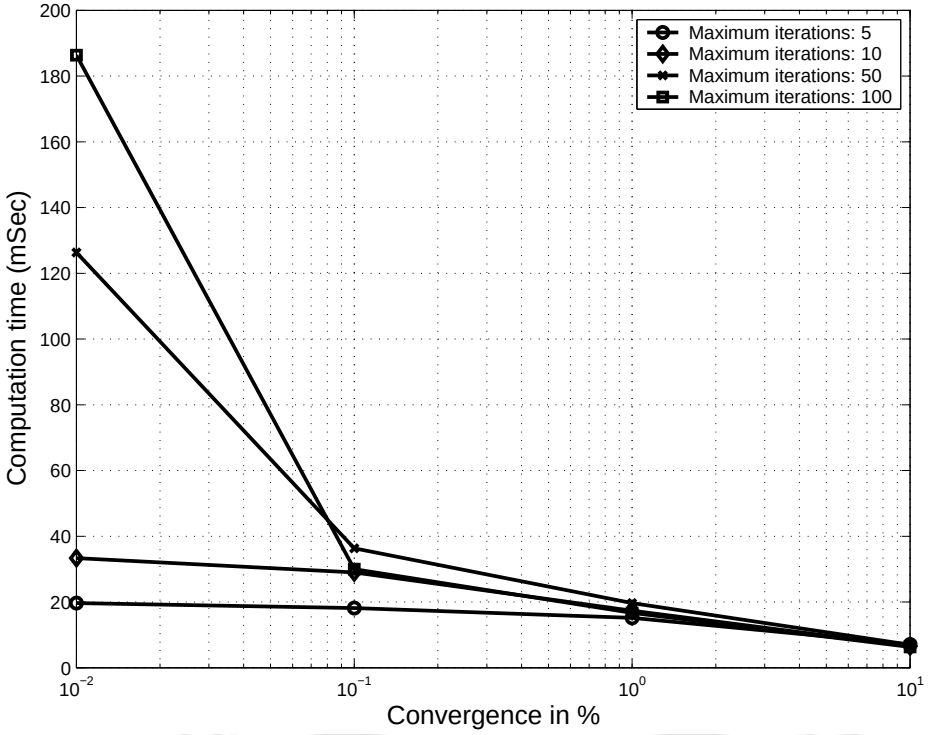

FIGURE 5.3: Convergence time of EM algorithm with respect to the number of iterations, $N_c = 2000$, calculated in an Intel Xeon CPU with 2 GHz processor

5.2.1 Expectation Maximization Algorithm

The received constellation follows a bivariate GMM with real and imaginary parts, so that the n^{th} sample is represented as $x_n = x_{I,n} + jx_{Q,n}$. The PDF of the k^{th} Gaussian

cluster is given by

$$p_k(\mathbf{x}_n) = \frac{1}{(2\pi)|\mathbf{\Sigma}_k|} \exp\Big\{ -\frac{1}{2}\Big(\mathbf{x}_n - \boldsymbol{\mu}_k\Big)^T \mathbf{\Sigma}_k^{-1}\Big(\mathbf{x}_n - \boldsymbol{\mu}_k\Big)\Big\}, \tag{5.4}$$

where, $\mathbf{x}_n = \begin{pmatrix} x_{I,n} \\ x_{Q_n} \end{pmatrix}$ represents the real and imaginary parts of the n^{th} sample as a vector, $\boldsymbol{\mu}_k = \begin{pmatrix} \mu_{I,k} \\ \mu_{Q,k} \end{pmatrix}$ is the k^{th} cluster center, $\mathbf{\Sigma}_k$ is the corresponding covariance matrix and $|.|$ denotes the determinant. Now the EM algorithm performs the following two steps:

Expectation step: In the t^{th} iteration, the probability $\omega_{k,n}^{(t)}$ that $\mathbf{x}_n$ belonging to k^{th} cluster is given by

$$\omega_{k,n}^{(t)} = \frac{p_k(\mathbf{x}_n)P(\omega_k)}{\sum_{l=1}^{M^{(i)}} p_l(\mathbf{x}_n)P(\omega_l)} \tag{5.5}$$

where, $P(\omega_k)$ is the prior probability of the k^{th} cluster signifying the fraction of the total data belonging to cluster k.

Maximization step: For a received sample length of N_b, the ML estimates of the unknown parameters are calculated for the $(t+1)^{th}$ iteration as

$$P(\omega_k)^{(t+1)} = \frac{1}{N_b}\sum_{n=1}^{N_b} \omega_{k,n}^{(t)} \quad , \tag{5.6}$$

$$\boldsymbol{\mu}_k^{(t+1)} = \frac{\sum_{n=1}^{N_b} \omega_{k,n}^{(t)} \mathbf{x}_n}{\sum_{n=1}^{N_b} \omega_{k,n}^{(t)}} \quad , \tag{5.7}$$

and

$$\mathbf{\Sigma}_k^{(t+1)} = \frac{\sum_{n=1}^{N_b} \omega_{k,n}^{(t)} (\mathbf{x}_n - \boldsymbol{\mu}_k^{(t)})(\mathbf{x}_n - \boldsymbol{\mu}_k^{(t)})^T}{\sum_{n=1}^{N_b} \omega_{k,n}^{(t)}} \tag{5.8}$$

The ML estimates of the $(t+1)^{th}$ iteration are in turn used in the $(t+1)^{th}$ iteration of the expectation step and so and so forth. The iterations are continued until the convergence criterion $||\mu_{\mathbf{k}}{}^{(t+1)} - \mu_{\mathbf{k}}{}^{(t)}|| < \epsilon$ is achieved. The value of ϵ is defined based on the budget of computational resources.

5.2.2 Estimation of the Number of Clusters

To estimate the number of clusters, for a candidate pool containing $\mathcal{C}$ types of modulations, the EM convergence is applied $\mathcal{C}$ times, with the number of clusters corresponding to the candidate modulation schemes. Since the true clusters are Gaussian, the degree of Gaussianity of the estimated clusters can be verified by the *kurtosis* of each cluster. The excess kurtosis is employed, which is defined by [86]

$$Kurt = E\Big[\Big(\frac{X-\mu}{\sigma}\Big)^4\Big] - 3, \tag{5.9}$$

where, μ is the mean and σ is the standard deviation of the random variable X. For a Gaussian, $Kurt = 0$. Hence, the minimum value of the kurtosis provides the optimum condition for Gaussianity. Since the received constellation is a bi-variate Gussian mixture, the kurtosis of the k^{th} cluster corresponding to the i^{th} hypothesis is computed along the real and the imaginary axes as

$$Kurt_{I,k}^{(i)} = \frac{\frac{1}{N_k}\sum_{n=1}^{N_k}\Big(x_{I,n} - \mu_{I,k}^{(i)}\Big)^4}{s_{I,k}^{(i)\,4}} - 3, \tag{5.10}$$

and

$$Kurt_{Q,k}^{(i)} = \frac{\frac{1}{N_k}\sum_{n=1}^{N_k}\Big(x_{Q,n} - \mu_{Q,k}^{(i)}\Big)^4}{s_{Q,k}^{(i)\,4}} - 3, \tag{5.11}$$

where, N_k is the number of elements in the k^{th} cluster, $\mu_{I,k}$ and $\mu_{Q,k}$ are the real and imaginary parts of the k^{th} cluster mean, $s_{I,k}$ and $s_{Q,k}$ are standard deviations of the real and imaginary components respectively. The variance of the kurtosis is minimized by averaging the kurtosis of all the clusters. This is given by

$$Kurt^{(i)} = \frac{1}{2M^{(i)}}\sum_{k=1}^{M^{(i)}}\Big(|Kurt_{I,k}^{(i)}| + |Kurt_{Q,k}^{(i)}|\Big) \tag{5.12}$$

The number of clusters for the received signal is estimated by finding the corresponding hypothesis as

$$i^* = \arg\min_i Kurt^{(i)} \tag{5.13}$$

When the number of actual base-band clusters is equal to the assumed number of clusters, the histogram of the individual clusters tend towards Gaussianity. Figure 5.4 depicts the condition. The histogram of one of the clusters after EM convergence is plotted to illustrate the shape of the PDF, considering only the real valued components. However, due to the symmetry of the constellation shape, the PDF along the imaginary part also exhibit similar shape. On the other hand, for a mismatch condition, the actual number of constellation clusters and the assumed numbers are different. In such cases, the Gaussianity of the individual clusters tend to reduce. This scenario is illustrated in Figure 5.5.

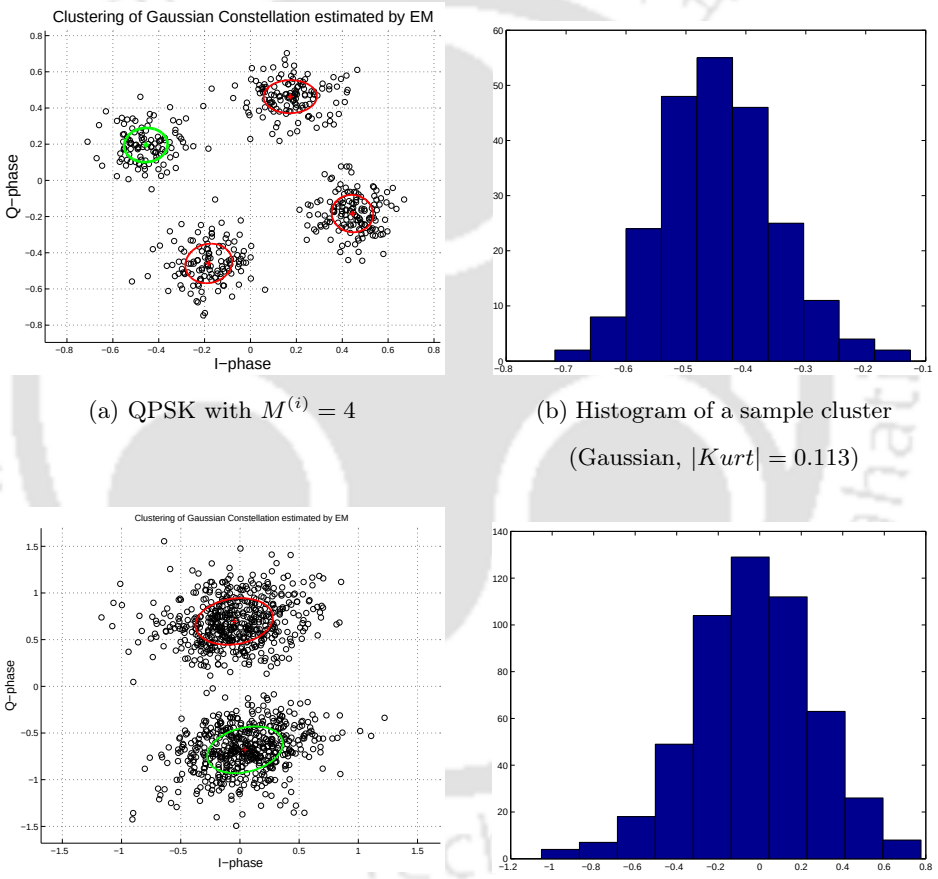

(a) QPSK with $M^{(i)} = 4$

(b) Histogram of a sample cluster (Gaussian, $|Kurt| = 0.113$)

(c) BPSK with $M^{(i)} = 2$

(d) Histogram of a sample cluster (Gaussian, $|Kurt| = 0.184$)

FIGURE 5.4: Convergence of the EM algorithm in a matched cluster condition under a fading channel $\mathbf{h} = [1\ 0.3\ 0.2]^T$, SNR 3 dB

The cluster estimation performance using kurtosis is shown in Figure 5.6. The Gaussianity of the clusters improves with the increase in the sample size, thereby improving the estimation performance. Although, there is a possibility that the modulation scheme

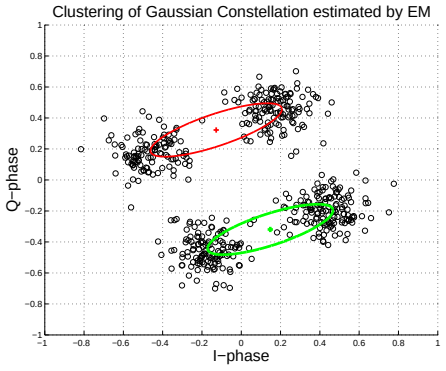

(a) QPSK with $M^{(i)} = 2$

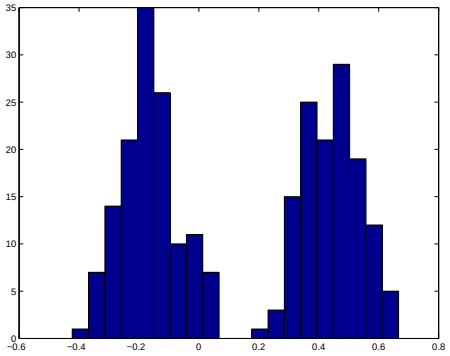

(b) Histogram of a sample cluster (non-Gaussian combination, $|Kurt| = 1.688$)

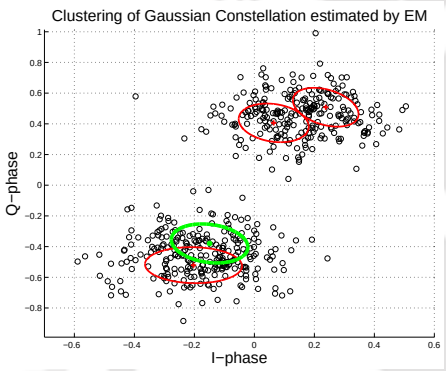

(c) BPSK with $M^{(i)} = 4$

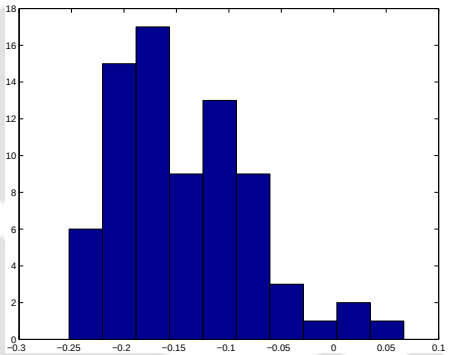

(d) Histogram of a sample cluster (non-Gaussian, $|Kurt| = 0.724$)

FIGURE 5.5: Convergence of the EM algorithm in a clustering mismatch condition under a fading channel $\mathbf{h} = [1, 0.3, 0.2]^T$, SNR 3 dB

can be directly interpreted from the number of constellations estimated at this stage, the classification decision is best derived from the decision theoretic stage only. Moreover, the ambiguities between modulation schemes with the same number of symbols, e.g. 8PSK and 8QAM etc, can not be resolved at this stage. To proceed with the estimation of the signal gain and the phase-offset, the cluster centers corresponding to the best convergence as per (5.13) are expressed as $\mu_k = \mu_{I,k} + j\mu_{Q,k}, \quad k = 1, 2, \ldots, M^{(i)}$.

5.2.3 Estimation of Gain $\widehat{\alpha}^{(i)}$

In Chapter 4, the channel gain has been estimated using the FKM algorithm with a pre-assigned number of clusters. This resulted in the performance degradation at the low SNR region. By using the pre-processing stage to estimate the number of clusters,

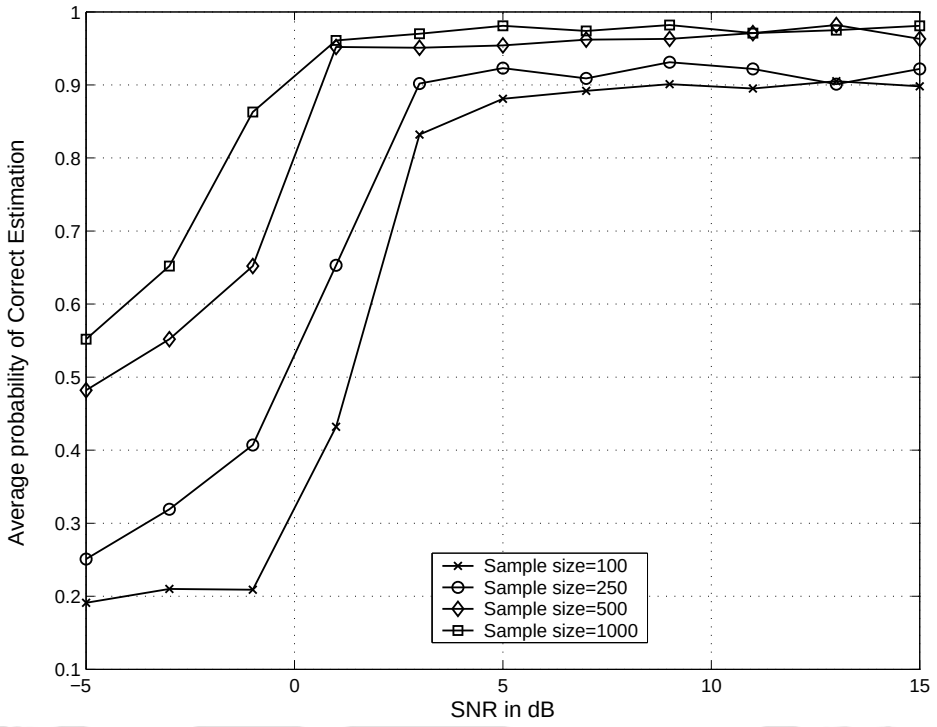

FIGURE 5.6: Estimation performance using kurtosis

the variance of the gain estimator, especially at the low SNR region, has been reduced here. As illustrated in Chgapter 4, the signal gain is estimated as the ratio between the amplitudes of the outermost cluster center and the unity magnitude constellation point of the ideal symbols. The outermost cluster center is given by

$$\mu_{max} = \arg\max_{k} ||\mu_k||, \quad k = 1, 2, \ldots, M^{(i)} \tag{5.14}$$

and

$$\mu_{max} = \mu_{I,max} + j\mu_{Q,max} \tag{5.15}$$

If the unity magnitude constellation point of the ideal symbols is represented as $S_I + jS_Q$, the signal gain is given by

$$\widehat{\alpha}^{(i)} = \frac{\sqrt{\mu_{I,max}^2 + \mu_{Q,max}^2}}{\sqrt{S_I^2 + S_Q^2}} = \sqrt{\mu_{I,max}^2 + \mu_{Q,max}^2} \tag{5.16}$$

since $\sqrt{S_I^2 + S_Q^2} = 1$.

5.2.4 Estimation of Phase Offset $\widehat{\psi}^{(i)}$

We assume geometric symmetry of the candidate constellations in the I-Q plane. The symbol of the model constellation nearest to μ_{max} is given by

$$S_{nearest} = \arg\min_{S_m} ||\mu_{max} - S_m||, \quad m = 1, 2, ..., M_{outer} \tag{5.17}$$

where, M_{outer} is the number of symbol points in the outermost constellation ring. The estimate of the random phase is obtained by the simple geometrical transformation

$$\begin{aligned}
\widehat{\psi}^{(i)} &= \arg(S_{nearest}) - \arg(\mu_{max}) \\
&= \arg(S_I + jS_Q) - \arg(\mu_{I,max} + j\mu_{Q,max}) \\
&= \arccos \frac{S_I\mu_{I,max} + S_Q\mu_{Q,max}}{\sqrt{\mu_{I,max}^2 + \mu_{Q,max}^2}\sqrt{S_I^2 + S_Q^2}} \\
&= \arccos \frac{S_I\mu_{I,max} + S_Q\mu_{Q,max}}{\sqrt{\mu_{I,max}^2 + \mu_{Q,max}^2}}
\end{aligned} \tag{5.18}$$

Due to the non-linear transformation involved in the gain and the phase offset estimators, a bias is introduced in the respective estimates. The bias in the gain estimator can be expressed as $Bias[\hat{\alpha}] = E[\hat{\alpha}] - \alpha$. As shown in Figure 5.8, the significance of the bias reduces with the increase in the SNR and sample size. The phase correction of the received signals is shown in Figure 5.7 for various channel gain scenarios. In the case of square-symmetric constellations like QPSK, 16QAM etc, the phase correction can be carried out by taking unit magnitude ideal constellation points at four quadrants in the I-Q plane. However, the same is not directly applicable for circular symmetric constellations like 8PSK, 16PSK etc, non-square symmetric ones like 32QAM and rectangular constellations, since none of the actual constellation points coincide with the ideal points. To mitigate this, a phase offset is introduced to the ideal constellation points, so that at least one of the ideal constellation point coincides with the ideal unit magnitude reference.

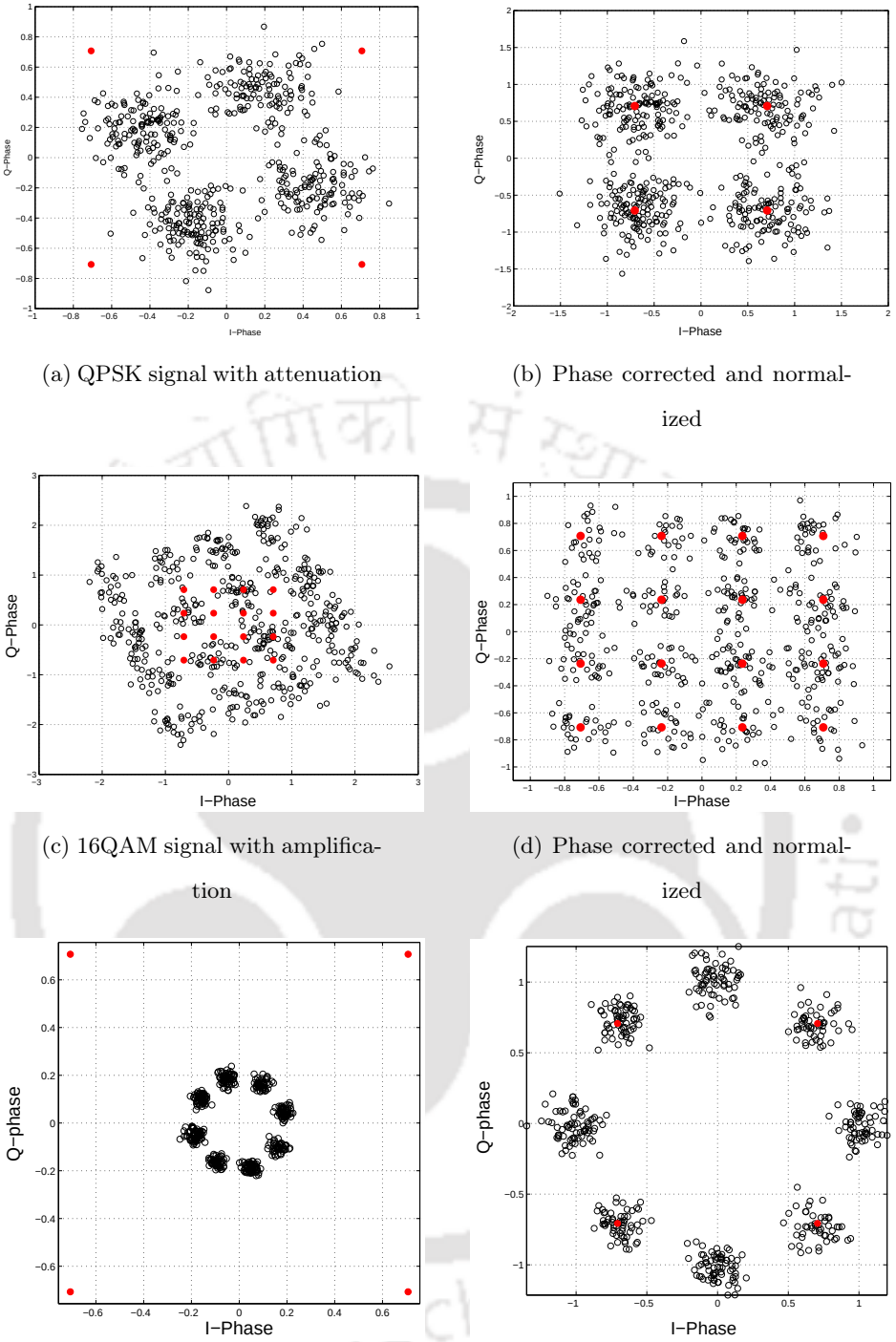

(a) QPSK signal with attenuation

(b) Phase corrected and normalized

(c) 16QAM signal with amplification

(d) Phase corrected and normalized

(e) 8PSK signal with attenuation

(f) Phase corrected and normalized

FIGURE 5.7: Amplitude and phase correction in a fading channel $\mathbf{h} = [1, 0.3, 0.2]^T$

5.2.5 Estimation of the Noise Power $\widehat{N}^{(i)}$

After convergence of the EM process, the covariance matrices for each cluster are obtained as per (5.8). Since the received constellation is symmetric along the real and imaginary

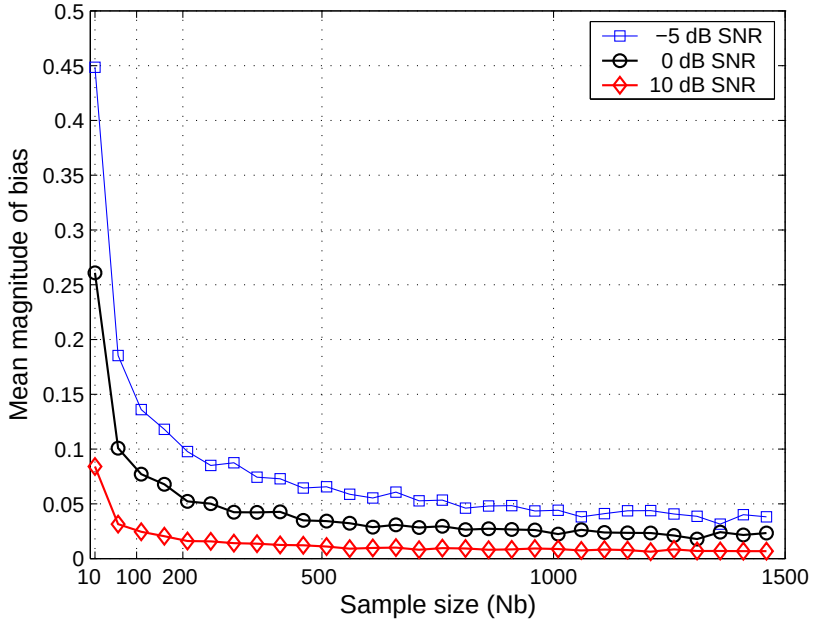

FIGURE 5.8: Bias for the gain estimator

axes, the noise power is estimated by averaging the variances of all the clusters along real and imaginary axes. The covariance elements in $\mathbf{\Sigma}_j$ being insignificant, are neglected. The estimated noise power $\widehat{N}^{(i)}$ is given by

$$\widehat{N}^{(i)} = \frac{1}{M^{(i)}} \sum_{j=1}^{M^{(i)}} \Big(\mathbf{\Sigma}_j(1,1) + \mathbf{\Sigma}_j(2,2) \Big) \tag{5.19}$$

The EM estimation of the noise power is an alternate to the widely used MoM based method. The proposed method is suitable for single as well as multi-amplitude modulations in the context of blind MC.

5.3 Performance Analysis of the Gain and the Phase Estimators

In this section, we evaluate the theoretical performance bounds of $\hat{\alpha}^{(i)}$ and $\hat{\psi}^{(i)}$ by deriving the CRLB. First, the efficiency and unbiasedness of the cluster center estimator are examined. The received constellation is modeled as a Gaussian mixture (GM). The constellation points can be considered as independent and an arbitrary cluster is picked

up for analysis. Since the problem is to estimate the k^{th} cluster center, the unknown parameter vector is $\boldsymbol{\theta} = [\mu_{I,k}\ \mu_{Q,k}]^T$.

5.3.1 CRLB of the Cluster Center Estimator

The likelihood function for the k^{th} cluster is given by

$$p(\boldsymbol{x};\boldsymbol{\theta}) = \frac{1}{(2\pi\sigma^2)^{N_k/2}} \exp\left[-\frac{1}{2\sigma^2}\sum_{n=1}^{N_k}\left\{\left(x_{I,n}-\mu_{I,k}\right)^2 + \left(x_{Q,n}-\mu_{Q,k}\right)^2\right\}\right] \tag{5.20}$$

Taking logarithm,we get the log-likelihood function as

$$\ln p(\boldsymbol{x};\boldsymbol{\theta}) = -\ln(2\pi\sigma^2)^{N_k/2} - \frac{1}{2\sigma^2}\sum_{n=1}^{N_k}\left\{\left(x_{I,n}-\mu_{I,k}\right)^2 + \left(x_{Q,n}-\mu_{Q,k}\right)^2\right\} \tag{5.21}$$

The estimates of the real and imaginary parts of the cluster center is given by

$$\widehat{\mu}_{I,k} = \frac{1}{N_k}\sum_{n=1}^{N_k} x_{I,n} \tag{5.22}$$

$$\widehat{\mu}_{Q,k} = \frac{1}{N_k}\sum_{n=1}^{N_k} x_{Q,n} \tag{5.23}$$

Clearly, these are unbiased estimates for $\mu_{I,k}$ and $\mu_{Q,k}$ respectively. Note that the Fisher Information matrix (FIM) $\boldsymbol{I}(\boldsymbol{\theta})$ is given by

$$\boldsymbol{I}(\boldsymbol{\theta}) = \begin{pmatrix} -E\left[\frac{\delta^2 \ln p(\boldsymbol{x};\boldsymbol{\theta})}{\delta\mu_{I,k}^2}\right] & -E\left[\frac{\delta^2 \ln p(\boldsymbol{x};\boldsymbol{\theta})}{\delta\mu_{I,k}\delta\mu_{Q,k}}\right] \\ -E\left[\frac{\delta^2 \ln p(\boldsymbol{x};\boldsymbol{\theta})}{\delta\mu_{Q,k}\delta\mu_{I,k}}\right] & -E\left[\frac{\delta^2 \ln p(\boldsymbol{x};\boldsymbol{\theta})}{\delta\mu_{Q,k}^2}\right] \end{pmatrix} \tag{5.24}$$

We derive the elements of $\boldsymbol{I}(\boldsymbol{\theta})$ as follows

$$\frac{\delta \ln p(\boldsymbol{x};\boldsymbol{\theta})}{\delta\mu_{I,k}} = \frac{1}{\sigma^2}\sum_{n=1}^{N_k}\left(x_{I,n}-\mu_{I,k}\right)$$

and

$$\frac{\delta \ln p(\boldsymbol{x};\boldsymbol{\theta})}{\delta\mu_{Q,k}} = \frac{1}{\sigma^2}\sum_{n=1}^{N_k}\left(x_{Q,n}-\mu_{Q,k}\right)$$

Therefore,

$$\boldsymbol{I}(\boldsymbol{\theta}) = \begin{pmatrix} \frac{N_k}{\sigma^2} & 0 \\ \\ 0 & \frac{N_k}{\sigma^2} \end{pmatrix} \tag{5.25}$$

Now, the existence of CRLB for the estimator of cluster center is examined.

$$\frac{\delta \ln p(\boldsymbol{x};\boldsymbol{\theta})}{\delta \boldsymbol{\theta}} = \begin{pmatrix} \frac{1}{\sigma^2}\sum_{n=1}^{N_k}\left(x_{I,n} - \mu_{I,k}\right) \\ \\ \frac{1}{\sigma^2}\sum_{n=1}^{N_k}\left(x_{Q,n} - \mu_{Q,k}\right) \end{pmatrix} \tag{5.26}$$

Rearranging the above equation,

$$\frac{\delta \ln p(\boldsymbol{x};\boldsymbol{\theta})}{\delta \boldsymbol{\theta}} = \begin{pmatrix} \frac{N_k}{\sigma^2} & 0 \\ \\ 0 & \frac{N_k}{\sigma^2} \end{pmatrix} \begin{pmatrix} \widehat{\mu}_{I,k} - \mu_{I,k} \\ \\ \widehat{\mu}_{Q,k} - \mu_{Q,k} \end{pmatrix} \tag{5.27}$$

Equation (5.27)is in the form

$$\frac{\delta \ln p(\boldsymbol{x};\boldsymbol{\theta})}{\delta \boldsymbol{\theta}} = \boldsymbol{I}(\boldsymbol{\theta})\left(\widehat{\boldsymbol{\theta}} - \boldsymbol{\theta}\right) \tag{5.28}$$

which ensures that the estimator for the cluster center attains CRLB [78]. The corresponding CRLBs for the estimators are

$$var(\widehat{\mu}_{I,k})^{(CRLB)} = \frac{\sigma^2}{N_k} \tag{5.29}$$

$$var(\widehat{\mu}_{Q,k})^{(CRLB)} = \frac{\sigma^2}{N_k} \tag{5.30}$$

Under the blind scenario, where the number of clusters and the degree of belongingness of individual symbols to the actual cluster centers are not known, it is a fair assumption that the estimates of cluster centers and CRLB of variance using the EM algorithm are close to the theoretical values. With this, the analysis is now extended to the estimator of signal gain and the phase-offset, which are functions of the outermost cluster center in the received constellation. Here, without any loss of generality, the k^{th} cluster center is considered as the outermost one. Also, the nearest among the outermost ideal

constellation points is considered as (S_I, S_Q).

5.3.2 CRLB of the Gain Estimator

The signal gain is a function of the cluster center and given by

$$\alpha = f_1(\mu_{I,k}, \mu_{Q,k}) = \frac{\sqrt{\mu_{I,k}^2 + \mu_{Q,k}^2}}{\sqrt{S_I^2 + S_Q^2}} \tag{5.31}$$

Since the ideal constellation points are normalized, $\sqrt{S_I^2 + S_Q^2} = 1$. Taking partial derivatives of f_1 with respect to $\mu_{I,k}$ and $\mu_{Q,k}$ we have

$$\frac{\delta f_1(\boldsymbol{\theta})}{\delta \mu_{I,k}} = \frac{\delta}{\delta \mu_{I,k}} \left(\mu_{I,k}^2 + \mu_{Q,k}^2\right)^{1/2} = \mu_{I,k} \tag{5.32}$$

Similarly,

$$\frac{\delta f_1(\boldsymbol{\theta})}{\delta \mu_{Q,k}} = \mu_{Q,k} \tag{5.33}$$

Using the property of parameter transformation [78], the CRLB of the gain estimator is given by

$$var(\widehat{\alpha}) \geq \frac{\delta f_1(\boldsymbol{\theta})}{\delta \boldsymbol{\theta}} \boldsymbol{I}^{-1}(\boldsymbol{\theta}) \frac{\delta f_1(\boldsymbol{\theta})^T}{\delta \boldsymbol{\theta}}, \tag{5.34}$$

where the Jacobian is given by

$$\frac{\delta f_1(\boldsymbol{\theta})}{\delta \boldsymbol{\theta}} = \begin{pmatrix} \frac{\delta f_1(\boldsymbol{\theta})}{\delta \mu_{I,k}} & \frac{\delta f_1(\boldsymbol{\theta})}{\delta \mu_{Q,k}} \end{pmatrix}, \tag{5.35}$$

so that

$$\frac{\delta f_1(\boldsymbol{\theta})}{\delta \boldsymbol{\theta}} \boldsymbol{I}^{-1}(\boldsymbol{\theta}) \frac{\delta f_1(\boldsymbol{\theta})^T}{\delta \boldsymbol{\theta}} = \begin{pmatrix} \mu_{I,k} & \mu_{Q,k} \end{pmatrix} \begin{pmatrix} \frac{\sigma^2}{N_k} & 0 \\ 0 & \frac{\sigma^2}{N_k} \end{pmatrix} \begin{pmatrix} \mu_{I,k} \\ \mu_{Q,k} \end{pmatrix} = \frac{\sigma^2}{N_k} \left[\mu_{I,k}^2 + \mu_{Q,k}^2\right] \tag{5.36}$$

Hence, the CRLB for the gain estimator is given by

$$var(\widehat{\alpha})^{(CRLB)} = \frac{\sigma^2}{N_k}\left[\mu_{I,k}^2 + \mu_{Q,k}^2\right] \tag{5.37}$$

5.3.3 CRLB of the Phase-offset Estimator

The estimate of the phase offset is a function of the cluster center and given by

$$\psi^{(i)} = f_2(\mu_{I,k}, \mu_{Q,k}) = \arg(S_I + jS_Q) - \arg(\mu_{I,k} + j\mu_{Q,k}), \tag{5.38}$$

or

$$\widehat{\psi}^{(i)} = \arccos\frac{S_I\mu_{I,k} + S_Q\mu_{Q,k}}{\sqrt{\mu_{I,k}^2 + \mu_{Q,k}^2}} \tag{5.39}$$

Using the property of parameter transformation, the CRLB of the phase offset estimator is given by

$$var(\widehat{\psi}^{(i)}) \geq \frac{\delta f_2(\boldsymbol{\theta})}{\delta\boldsymbol{\theta}}\boldsymbol{I}^{-1}(\boldsymbol{\theta})\frac{\delta f_2(\boldsymbol{\theta})^T}{\delta\boldsymbol{\theta}}, \tag{5.40}$$

where the Jacobian is

$$\frac{\delta f_2(\boldsymbol{\theta})}{\delta\boldsymbol{\theta}} = \begin{pmatrix} \frac{\delta f_2(\boldsymbol{\theta})}{\delta\mu_{I,k}} & \frac{\delta f_2(\boldsymbol{\theta})}{\delta\mu_{Q,k}} \end{pmatrix} \tag{5.41}$$

Let

$$u = \frac{S_I\mu_{I,k} + S_Q\mu_{Q,k}}{\sqrt{\mu_{I,k}^2 + \mu_{Q,k}^2}}, \tag{5.42}$$

$$\begin{aligned}\frac{\delta f_2(\boldsymbol{\theta})}{\delta\mu_{I,k}} &= -\frac{1}{\sqrt{1-u^2}} \times \frac{\delta u}{\delta\mu_{I,k}} \\ &= -\frac{S_I}{\sqrt{1-u^2}}\frac{\delta}{\delta\mu_{I,k}}\left(\frac{\mu_{I,k}}{\sqrt{\mu_{I,k}^2 + \mu_{Q,k}^2}}\right) \\ &= -\frac{S_I}{\sqrt{1-u^2}}\left[\frac{\left(\mu_{I,k}^2 + \mu_{I,k}^2\right)^{1/2} - \mu_{I,k}}{\mu_{I,k}^2 + \mu_{I,k}^2}\right]\end{aligned} \tag{5.43}$$

Substituting the value of u and further simplifying

$$\frac{\delta f_2(\boldsymbol{\theta})}{\delta\mu_{I,k}} = -\frac{S_I(\mu - \mu_{I,k})}{\mu^{3/2}(\mu - S_I\mu_{I,k} - S_Q\mu_{Q,k})^{1/2}}, \tag{5.44}$$

where, $\mu = \sqrt{\mu_{I,k}^2 + \mu_{Q,k}^2}$. Similarly,

$$\frac{\delta f_2(\boldsymbol{\theta})}{\delta \mu_{Q,k}} = -\frac{S_Q(\mu - \mu_{Q,k})}{\mu^{3/2}(\mu - S_I\mu_{I,k} - S_Q\mu_{Q,k})^{1/2}} \tag{5.45}$$

Now, let

$$\alpha_1 = -\frac{S_I(\mu - \mu_{I,k})}{\mu^{3/2}(\mu - S_I\mu_{I,k} - S_Q\mu_{Q,k})^{1/2}}$$
$$\alpha_2 = -\frac{S_Q(\mu - \mu_{Q,k})}{\mu^{3/2}(\mu - S_I\mu_{I,k} - S_Q\mu_{Q,k})^{1/2}},$$

so that,

$$\frac{\delta f_2(\boldsymbol{\theta})}{\delta \boldsymbol{\theta}} \boldsymbol{I}^{-1}(\boldsymbol{\theta}) \frac{\delta f_2(\boldsymbol{\theta})^T}{\delta \boldsymbol{\theta}} = \begin{pmatrix} \alpha_1 & \alpha_2 \end{pmatrix} \begin{pmatrix} \frac{\sigma^2}{N_k} & 0 \\ 0 & \frac{\sigma^2}{N_k} \end{pmatrix} \begin{pmatrix} \alpha_1 \\ \alpha_2 \end{pmatrix} = \frac{\sigma^2}{N_k}\left[\alpha_1^2 + \alpha_2^2\right] \tag{5.46}$$

Substituting the values of α_1 and α_2,

$$\frac{\delta f_2(\boldsymbol{\theta})}{\delta \boldsymbol{\theta}} \boldsymbol{I}^{-1}(\boldsymbol{\theta}) \frac{\delta f(\boldsymbol{\theta})^T}{\delta \boldsymbol{\theta}} = \frac{\sigma^2}{N_k}\left[\frac{S_I^2(\mu - \mu_{I,k})^2}{\mu^3(\mu - S_I\mu_{I,k} - S_Q\mu_{Q,k})} + \frac{S_Q^2(\mu - \mu_{Q,k})^2}{\mu^3(\mu - S_I\mu_{I,k} - S_Q\mu_{Q,k})}\right] \tag{5.47}$$

After simplifying , the CRLB for the phase offset estimator is given by

$$var(\widehat{\psi}^{(i)})^{(CRLB)} = \frac{\sigma^2}{N_k}\left[\frac{S_I^2(\mu - \mu_{I,k})^2 + S_Q^2(\mu - \mu_{Q,k})^2}{\mu^3(\mu - S_I\mu_{I,k} - S_Q\mu_{Q,k})}\right] \tag{5.48}$$

5.4 ML Classification

After plugging in the estimates $\widehat{\alpha}^{(i)}$, $\widehat{\psi}^{(i)}$ and $\widehat{N}^{(i)}$, (5.3) is re-written as

$$l(\mathbf{x_1}, \mathbf{x_2}, ..., \mathbf{x_{N_b}}|H^{(i)})_{QHLRT} = \sum_{k=1}^{N_b} \ln\left[\sum_{m=1}^{M^{(i)}} \frac{1}{M^{(i)}\pi\widehat{N}^{(i)}} exp\left\{-\frac{1}{\widehat{N}^{(i)}}\left|x_k - \widehat{\alpha}^{(i)}e^{j\widehat{\psi}^{(i)}}s_m^{(i)}\right|^2\right\}\right] \tag{5.49}$$

The MC is carried out using the decision rule

$$\hat{H} = \arg\max_{H^{(i)}} l(\mathbf{x_1}, \mathbf{x_2}, ..., \mathbf{x_{N_b}}|H^{(i)})_{QHLRT} \tag{5.50}$$

With f_s, $\alpha^{(i)}$, $\psi^{(i)}$ and $N^{(i)}$ as unknown parameters, the overall computational complexity of the proposed method is $\mathcal{O}\Big[\frac{N_c}{\Delta\omega}\log\frac{N_c}{L} + (\mathcal{C}+1)N_bM^{(i)}I + \sum_{i=1}^{\mathcal{C}} N_bM^{(i)}\Big]$. The first term in the summation represents the computational complexity for the symbol rate estimation. The second term is for the estimation of $\alpha^{(i)}$, $\psi^{(i)}$ and $N^{(i)}$, while the third term corresponds to the QHLRT MC.

5.5 Experimental Results and Discussion

In this section the simulation results are presented for the individual performance of the estimators and the QHLRT classifier using the proposed estimates. The performance comparisons of the estimators with existing proposals at various complexity and channel conditions are illustrated. The QHLRT classification using the proposed estimates is compared with that of the theoretical and MoM based approaches. In addition, the better classification performance of the QHLRT based approach has been illustrated with respect to a fourth-order cumulant based classifier using the new estimators.

5.5.1 Simulation Setup

We consider a pool of modulated signals containing BPSK, QPSK, 8PSK, 8QAM, 16QAM and 32QAM. Multipath fading is simulated with a three-tap FIR filter $\mathbf{h} = [1\ h_2\ h_3]^T$. The first co-efficient accounts for the line of sight component, whereas h_2 and h_3 account for the variance of the gain of the multipath components. In a typical COMINT signal interception scenario, a slow-fading Rician channel, which is time invariant within the sample duration is considered. During the Monte Carlo simulation, the channel variation is applied between the iterations. The variance of the estimators are analyzed using various sample sizes to assess the performance against computational complexity. Monte Carlo simulation is employed with 1000 iterations to plot the probability of correct classification P_{cc} across a range of SNR values. We apply the symbol rate estimator developed

in Chapter 3. For application in the QHLRT MC, the I-Q demodulation is implemented using the estimate of the symbol rate.

5.5.2 Performance of the Gain Estimator

The MSE of the gain estimator (Equation 4.25) for various modulation schemes is plotted against the SNR in Figure 5.9, for the proposed gain estimator. We observe that the MSE performance improves as the modulation order is reduced. This is attributed to the decreasing ambiguity between the symbol boundaries at low SNR for the lower order modulations.

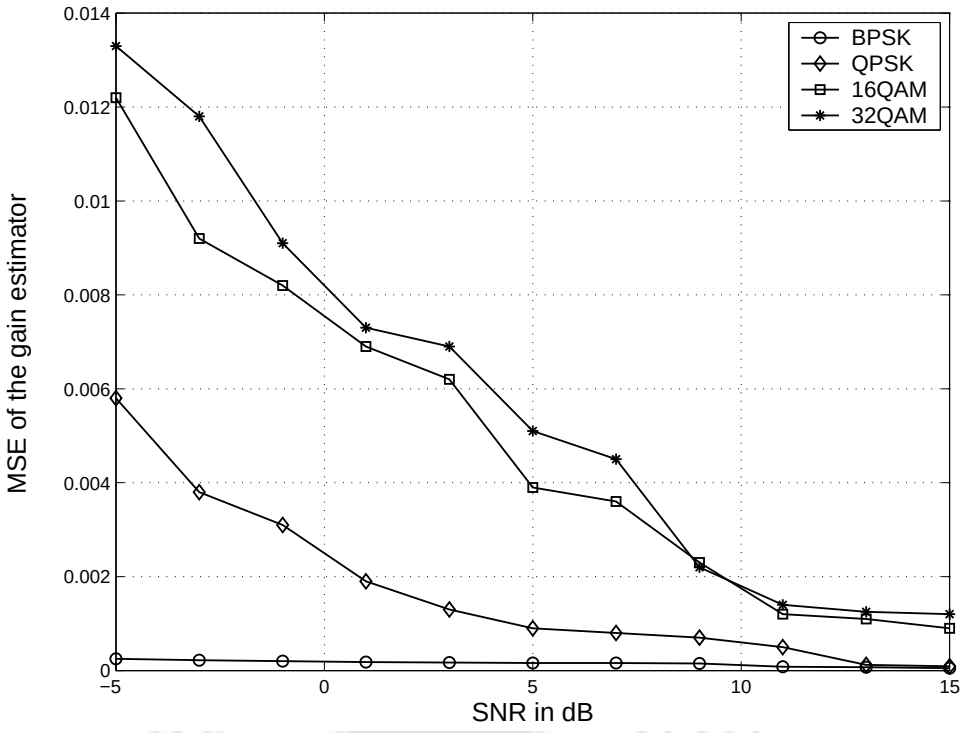

FIGURE 5.9: MSE of the gain estimator at a flat fading channel with channel response $\mathbf{h} = [1\ 0.3\ 0.2]^T$, base band sample size $N_b = 1000$

In Figure 5.10, the variance of the gain estimator is plotted across a range of signal gains for various sample sizes. The gain variance increases as the sample size decreases, since the Gaussianity of the clusters decreases for smaller sample sizes. This has the final implication on the estimation of the number of clusters in the received signal. In addition, as per Equation (5.37) the variance increases in general as the signal gain increases. In Figure 5.11 the performance of the proposed gain estimator is compared

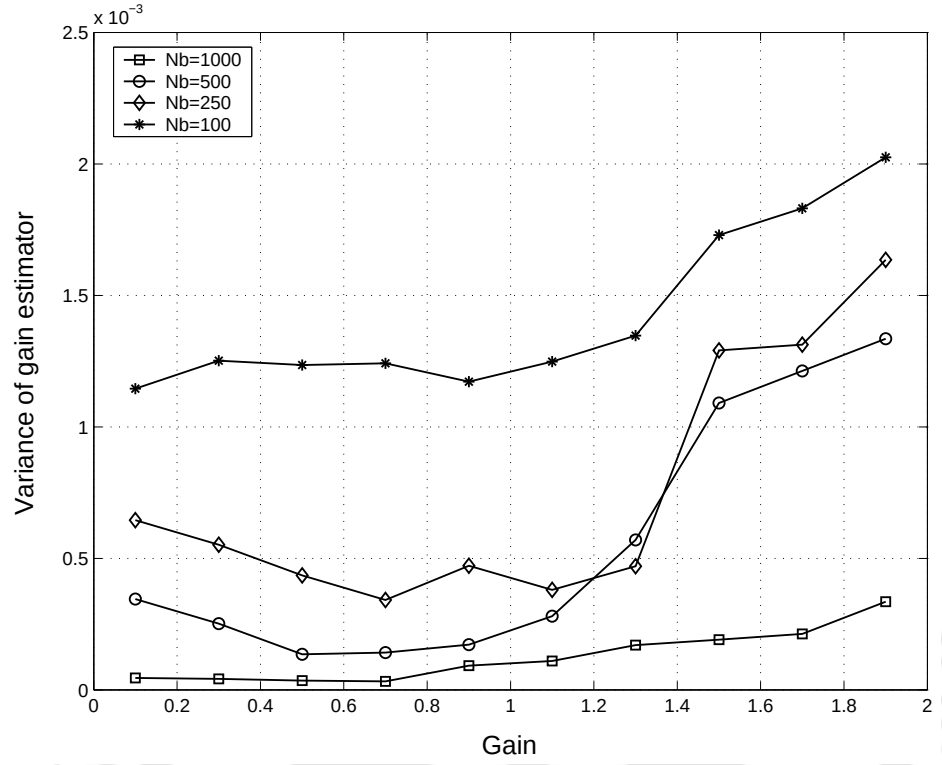

FIGURE 5.10: Variance of the gain estimator against the signal gains at channel response $\mathbf{h} = [1\ 0.3\ 0.2]^T$

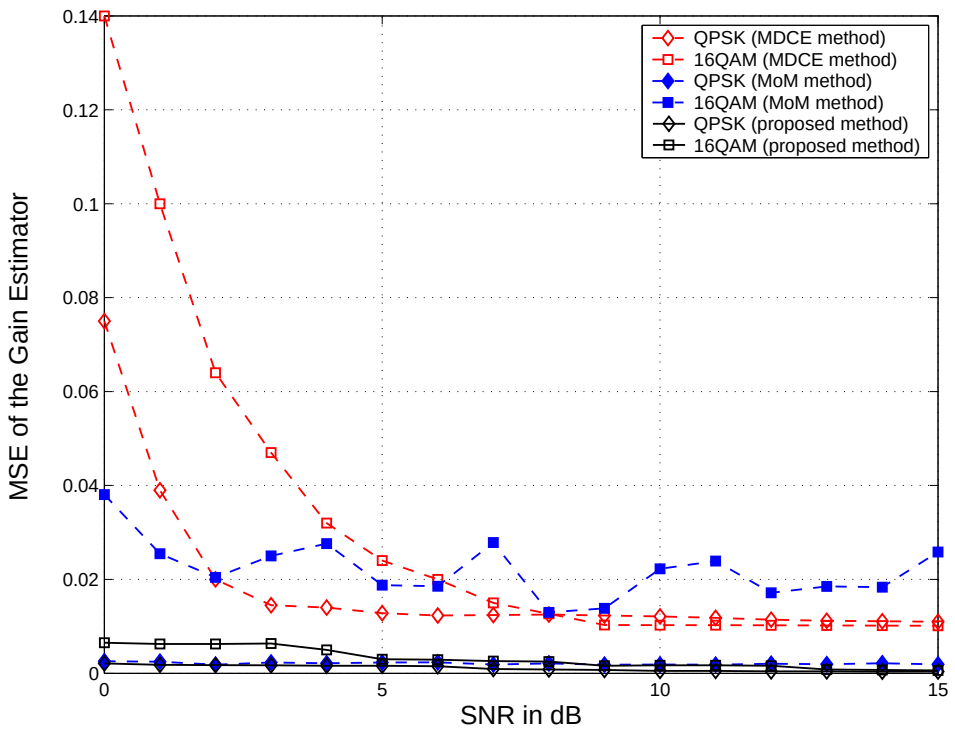

FIGURE 5.11: Comparison of MSE of gain estimator between centroid estimation by MDCE method and the new approach, $N_b = 1024$

with the same using the MDCE [26] and MoM method [15, 24]. As shown in Figure 5.12, a significant improvement of performance is achieved from the approach proposed in Chapter 4. As evident from the plot, the proposed estimator outperforms the MDCE method of [26] especially in the low SNR region. At the same time the proposed estimator performs better as compared to the MoM based algorithms throughout the range of SNR considered.

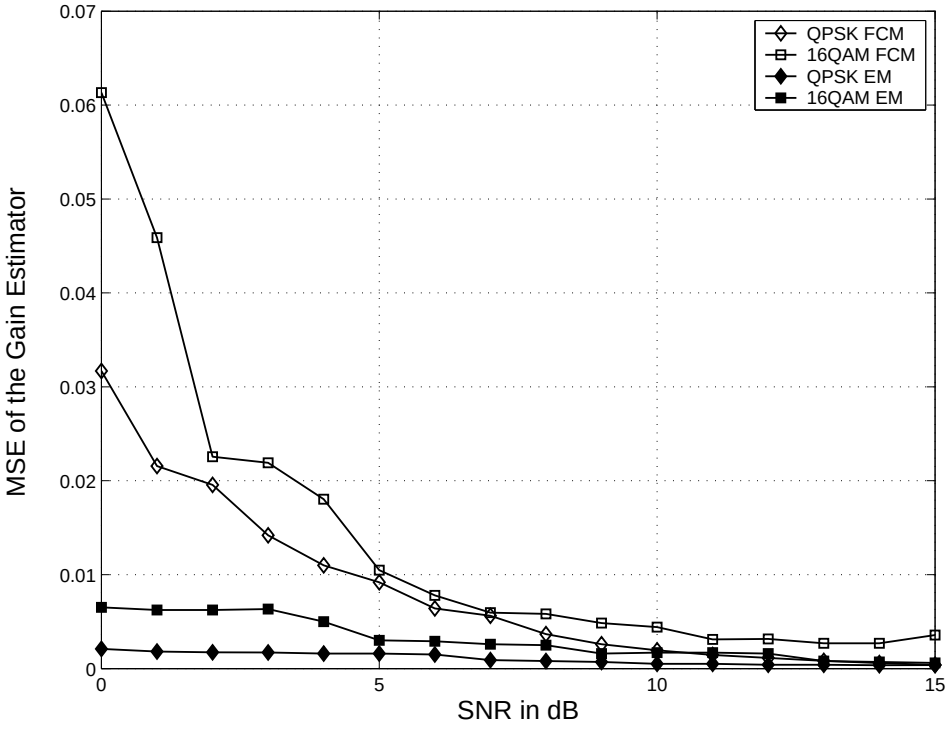

FIGURE 5.12: Comparison of the MSE performance of the gain estimator using fixed number of clusters (Chapter 4) and the method proposed in this chapter

5.5.3 Performance of the Phase-offset Estimator

The MSE of the phase-offset estimator is plotted in Figure 5.13 for various modulation schemes. The degradation in the MSE performance for the higher order modulations at low SNR region is due to the same reason as explained for the performance of the gain estimator in the previous Section.

Figure 5.14 shows the performance advantage with the present approach of predicting the number of clusters against the performance of the gain estimator proposed in Chapter 4, where the number of clusters were pre-defined as per the highest order candidate

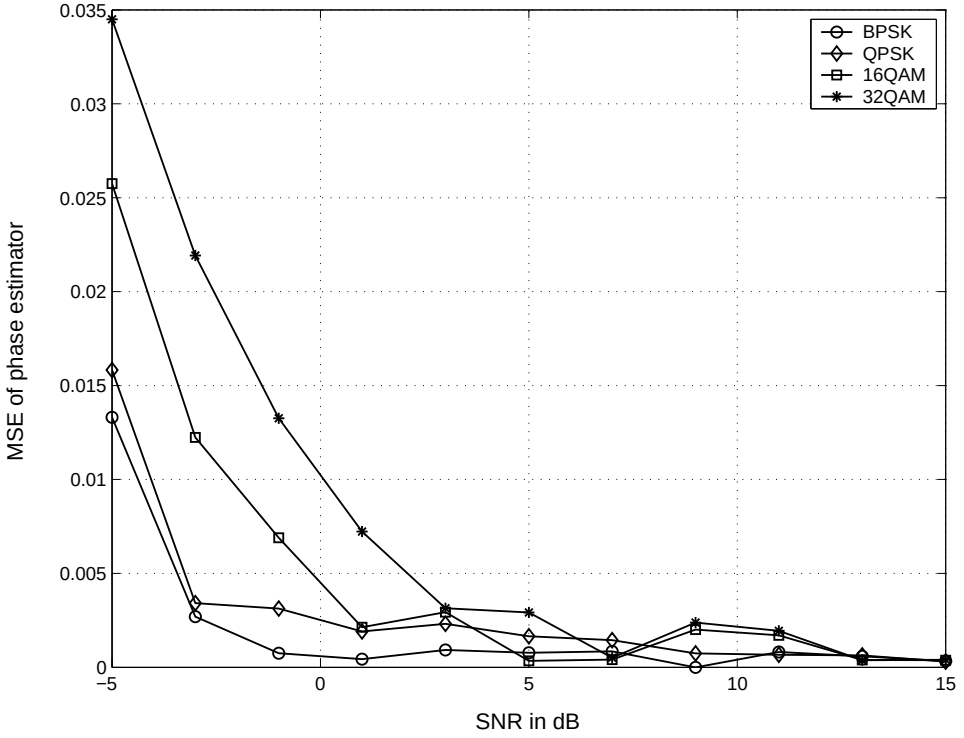

FIGURE 5.13: MSE of phase offset estimator at a flat fading channel $\mathbf{h} = [1\ 0.3\ 0.2]^T$ with base band sample size $N_b = 1024$

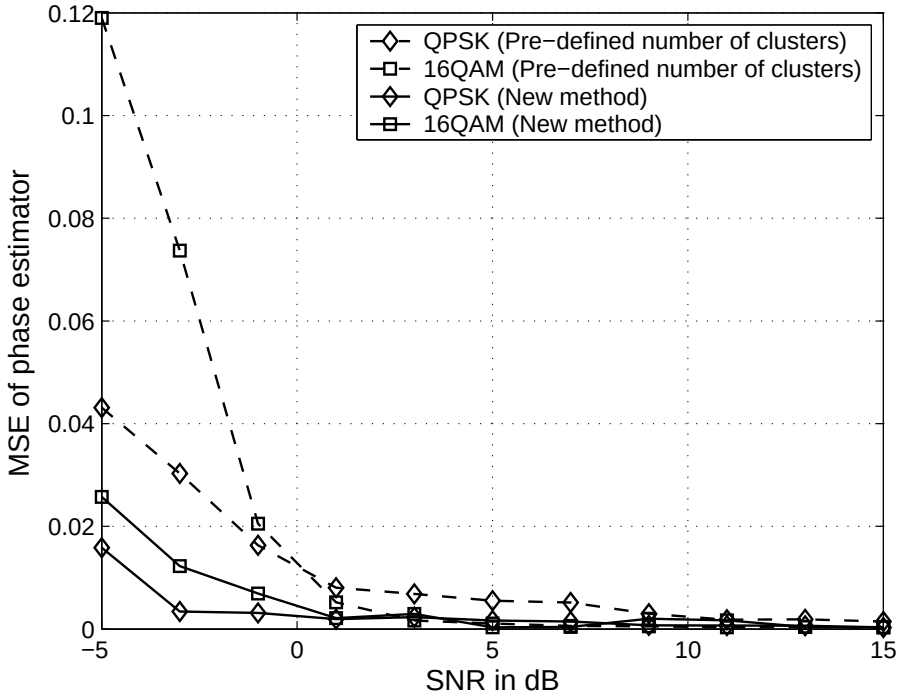

FIGURE 5.14: Comparison of MSE of phase offset estimator between pre-defined number of clusters and the new adaptive approach

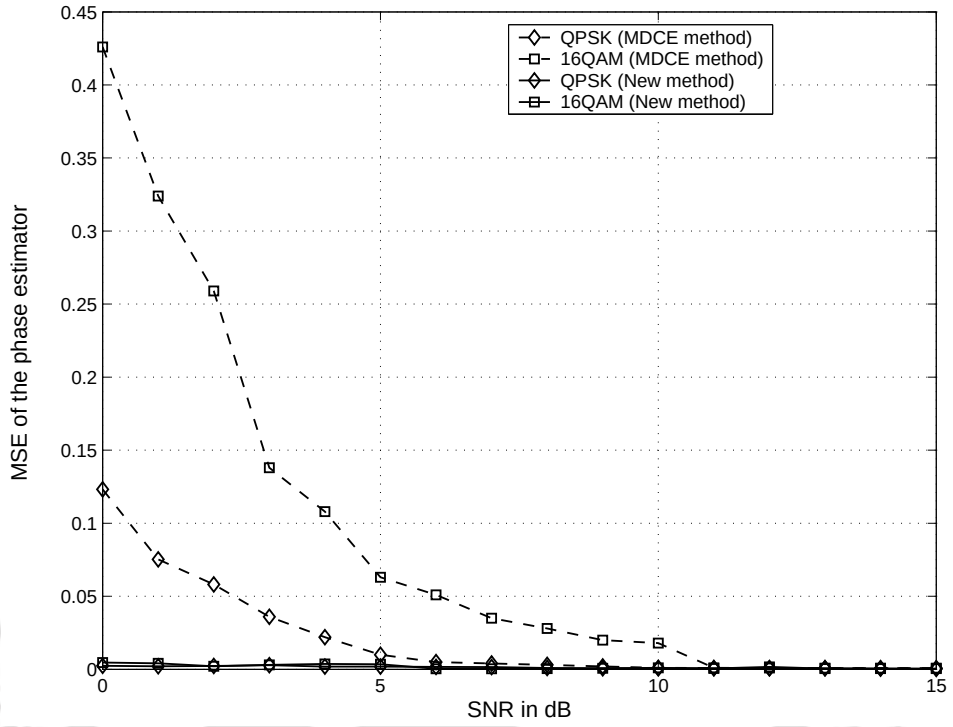

FIGURE 5.15: Comparison of the MSE of phase-offset estimator between MDCE method and the new adaptive approach

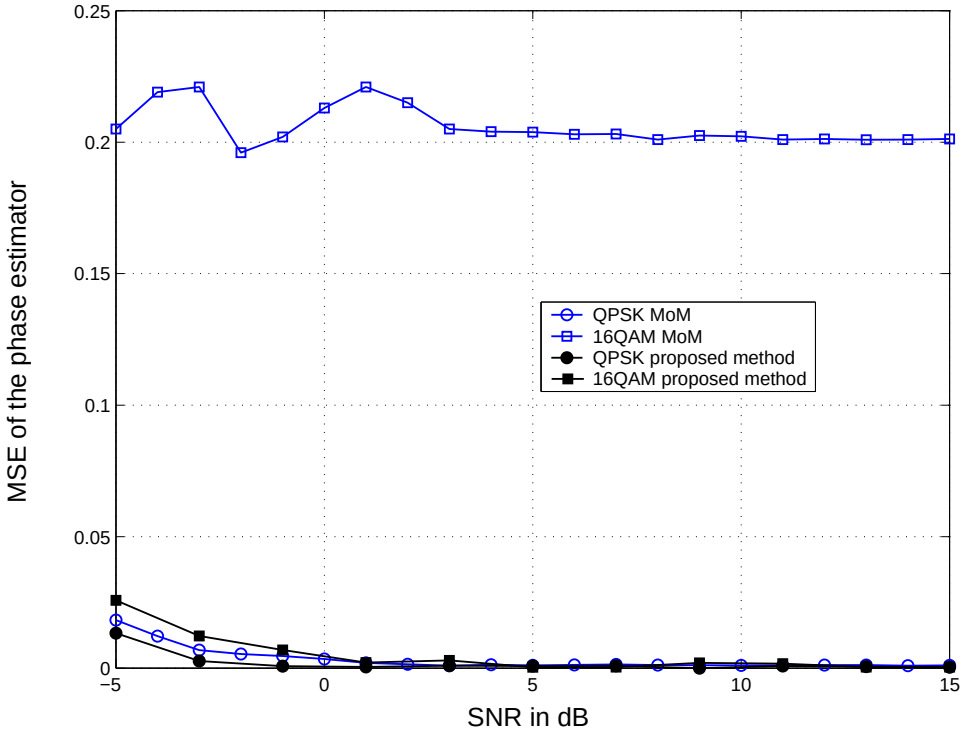

FIGURE 5.16: Comparison of the MSE of phase-offset estimator by the MoM method and the proposed approach

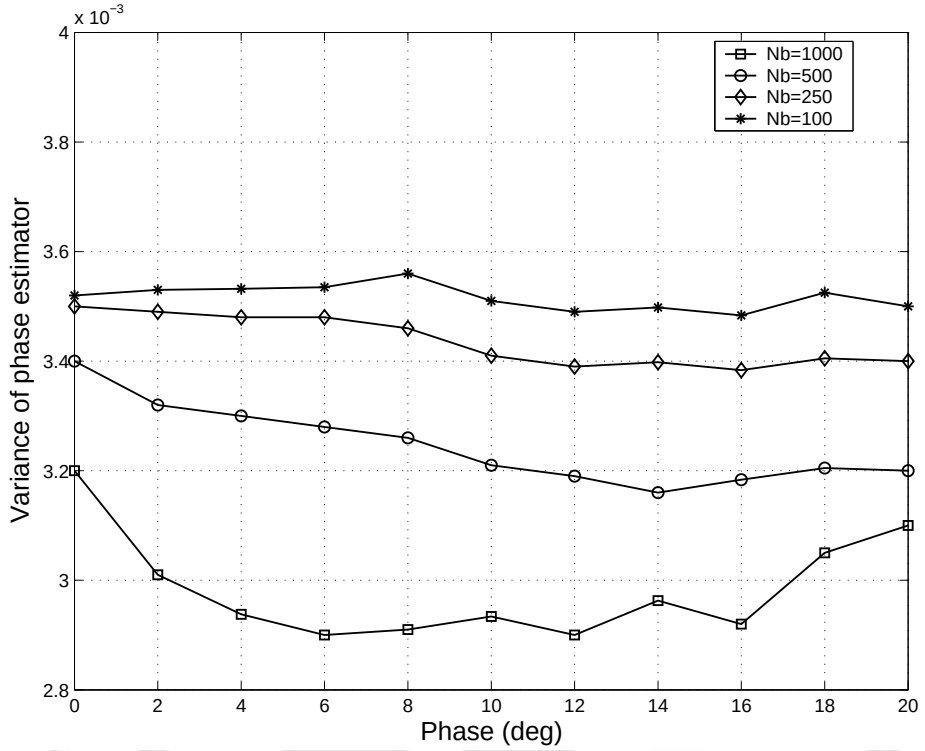

FIGURE 5.17: Variance of the proposed phase-offset estimator against the unknown parameter at channel response $\mathbf{h} = [1\ 0.3\ 0.2]^T$

modulation scheme. The new scheme shows advantage in the low SNR region. Further, the proposed estimator is compared with the method used in [26] in Figure 5.15. The improvement with the proposed estimator is evident especially in the low SNR region. Another comparison with the MoM based phase estimator [15] is made in Figure 5.16. The performance of the estimator is equivalent to the proposed estimator for single amplitude modulations like QPSK. However, the MoM based phase-offset estimator is significantly unreliable for multi-amplitude modulations like 16QAM. The variance of the phase-offset estimator is presented for various base-band sample sizes in Figure 5.17. The variance increases for smaller sample sizes, due to the decrease in the Gaussianity of individual clusters.

5.5.4 Performance of the Noise Power Estimator

The performance of the noise power estimator in a fading channel is shown in Figure 5.18. The comparative performance of the noise power estimator is illustrated in Figure

5.19. The MoM based estimator of [15] performs well for single amplitude PSK modulations. However, the proposed estimator outperforms the MoM based estimator for multi-amplitude QAM modulated signals.

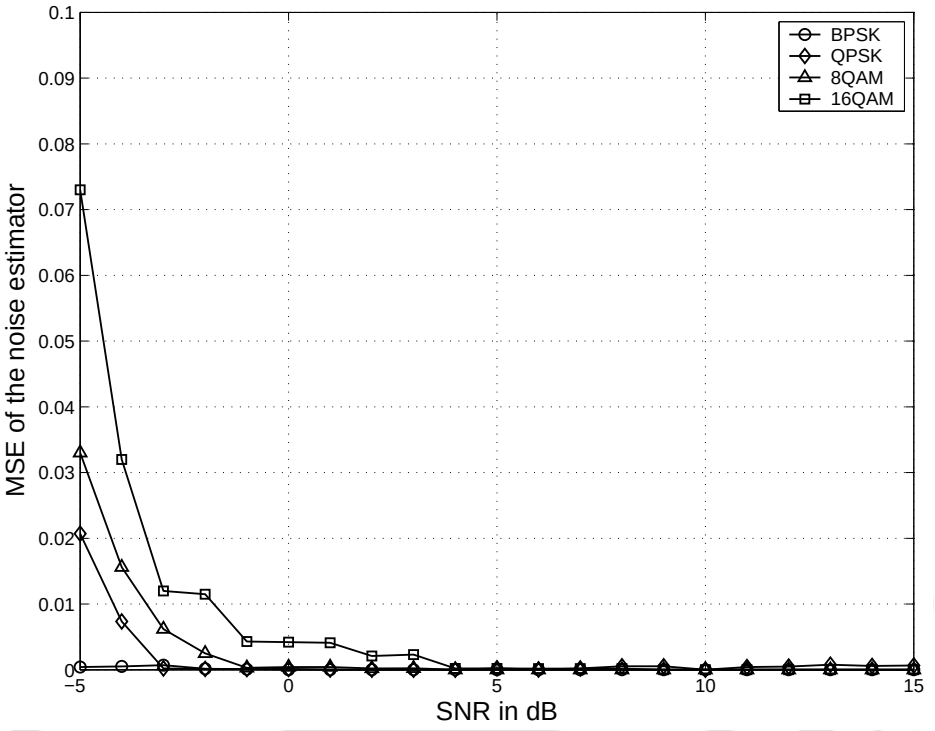

FIGURE 5.18: MSE performance of the noise estimator at fading channel $\mathbf{h} = [1\ 0.3\ 0.2]^T$

5.5.5 Probability of Correct Classification

Monte Carlo simulation is carried out to plot the probability of correct classification for a pool of modulations. Various cases have been considered from the main modulation pool containing BPSK, QPSK, 8PSK, 8QAM, 16QAM and 32QAM. The QHLRT classification case has been considered with known gain, phase-offset and noise power as the upper bound of classification performance. The demodulation is carried out with the estimation of the symbol rate using a carrier sample size of 1000. In Figure 5.20, the probability of correct classification is plotted for the pool of modulations. Figure 5.21 shows the comparative classification performance with the results of [15], considering the case of only BPSK and QPSK as candidate modulations. The plot shows that the proposed method exhibits better performance in the low SNR region as compared to the

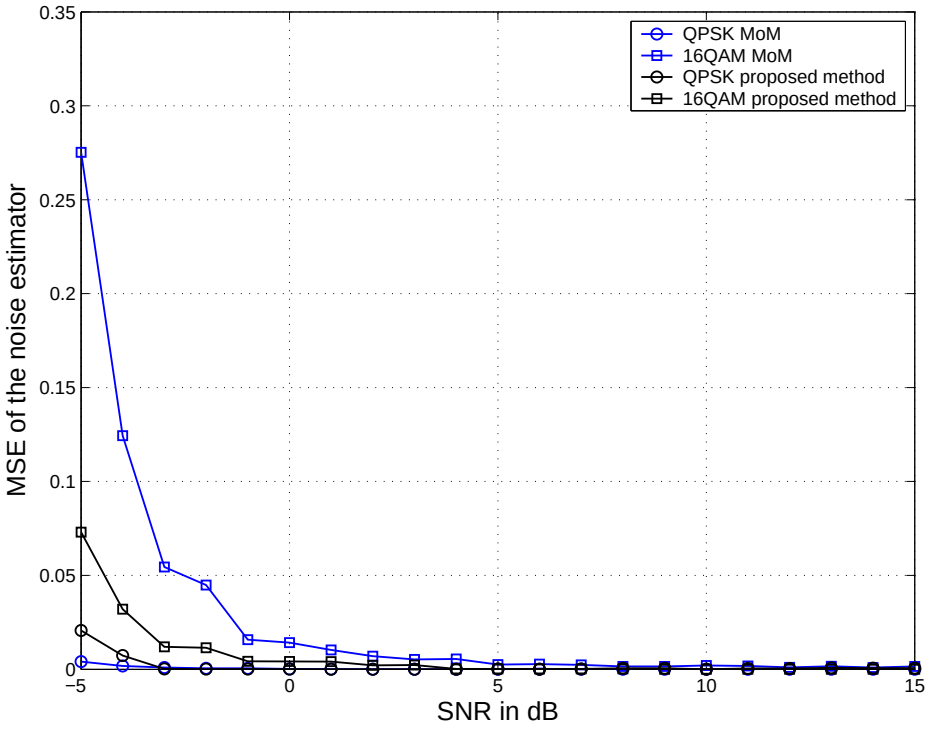

FIGURE 5.19: Comparative MSE performance of the noise estimator at fading channel $\mathbf{h} = [1\ 0.3\ 0.2]^T$

	BPSK	QPSK	8PSK	8QAM	16QAM	32QAM
BPSK	100%	0	0	0	0	0
QPSK	0	100%	0	0	0	0
8PSK	0	0	93%	7%	0	0
8QAM	0	2%	0	95%	1%	2 %
16QAM	0	0	0	0	93%	7%
32QAM	0	0	0	2%	8%	90%

TABLE 5.2: Classification confusion matrix for fading channel $\mathbf{h} = [1\ 0.3\ 0.2]^T$, $N_b = 1000$ at 0 dB SNR

QHLRT classifier employing the MoM based estimations. Also, the performance of the new classifier is closer to the ideal QHLRT upper bound. This improvement is attributed to the reduction in variance of the proposed parameter estimators.

In Table 5.2, the MC performance is represented in terms of the confusion matrix for the pool containing BPSK, QPSK, 8PSK, 8QAM, 16QAM and 32QAM. Consider a slow, flat fading scenario at a low SNR of 0 dB. In Figure 5.22, the comparative MC performance

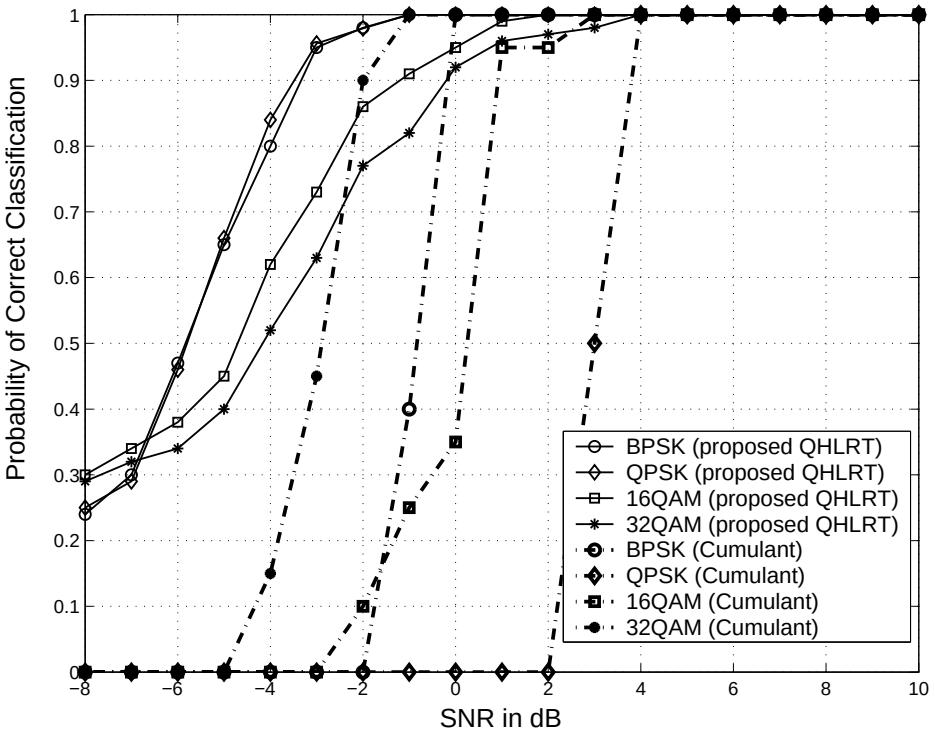

FIGURE 5.20: Probability of correct classification in a fading channel $\mathbf{h} = [1\ 0.3\ 0.2]^T$ with base-band sample size $N_b = 500$

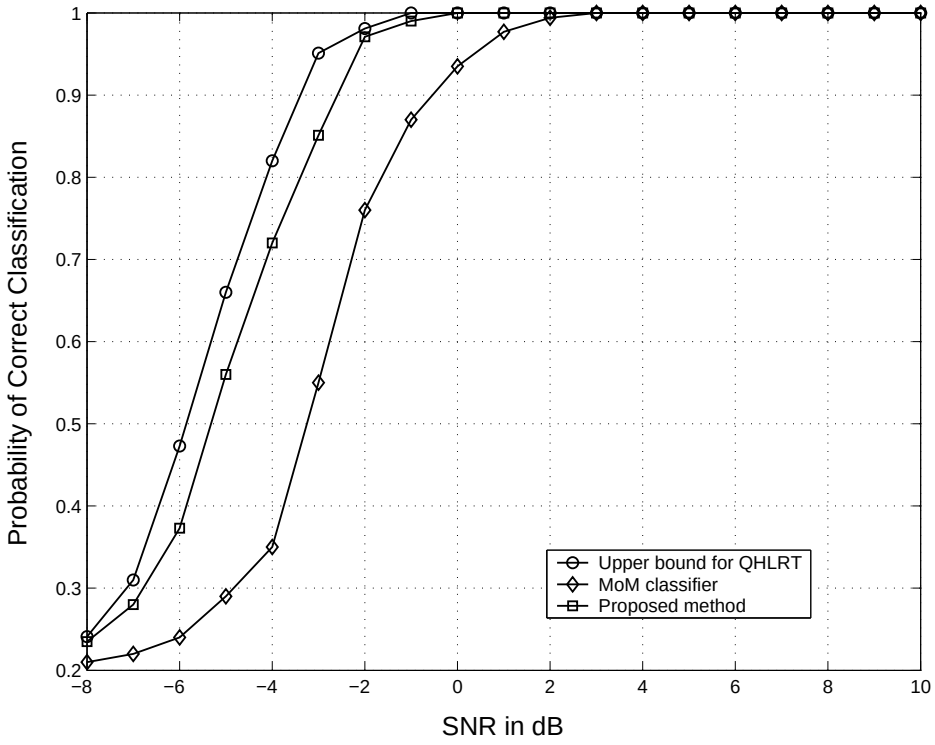

FIGURE 5.21: Comparative performance in a fading channel $\mathbf{h} = [1\ 0.3\ 0.2]^T$, $N_b = 100$

is represented as a function of the Rician fading factor. Recall that, the Rician factor is defined as the ratio of the received power level of the line of sight component to the resultant received power of the reflected components. The Rician factor signifies the severity of the fading scenario. For a basic pool containing BPSK and QPSK, the MC performance of the proposed method achieves ideal level for almost the entire test range. The average MC performance for a bigger pool is degraded due to the introduction of

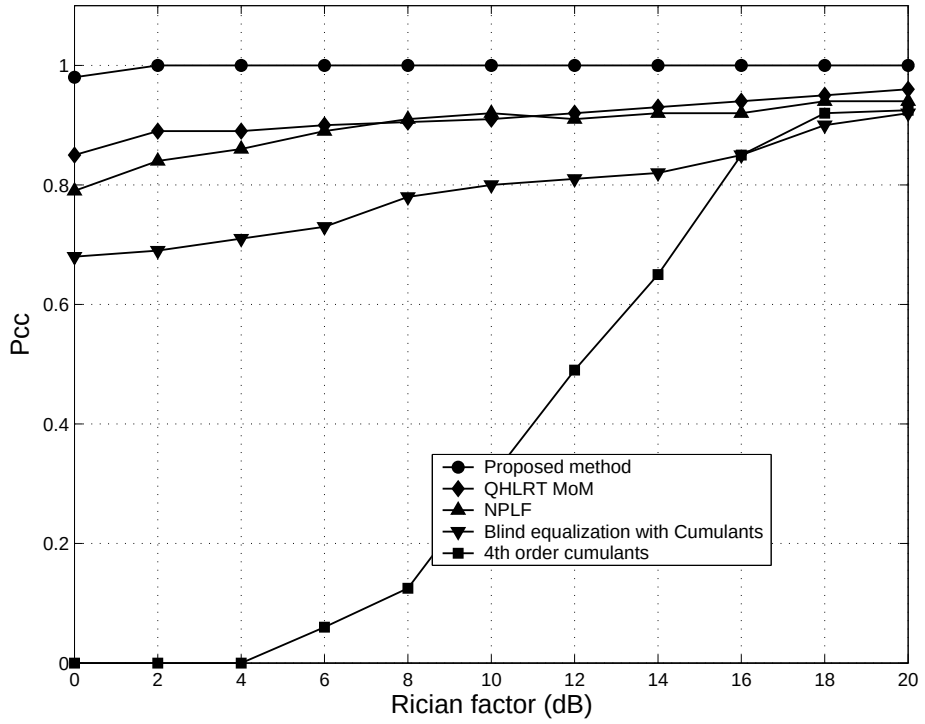

FIGURE 5.22: Comparative classification performance of BPSK and QPSK pool in Rician fading, $N_b = 1000$

additional confusion in the LB decision making. The performances at 0 dB SNR for various sample sizes are illustrated in Figure 5.23. As observed from the figure, the classification accuracy can be improved at the cost of bigger sample size. Depending on the application, the tradeoff between accuracy and the computation complexity can be made.

5.5.6 Effect of Non-Gaussian Impulse Noise

The proposed method is subjected to non-Gaussian impulse noise of various severity levels to asses the robustness. Consider the noise model of (2.12) with $N_a = 2$. The

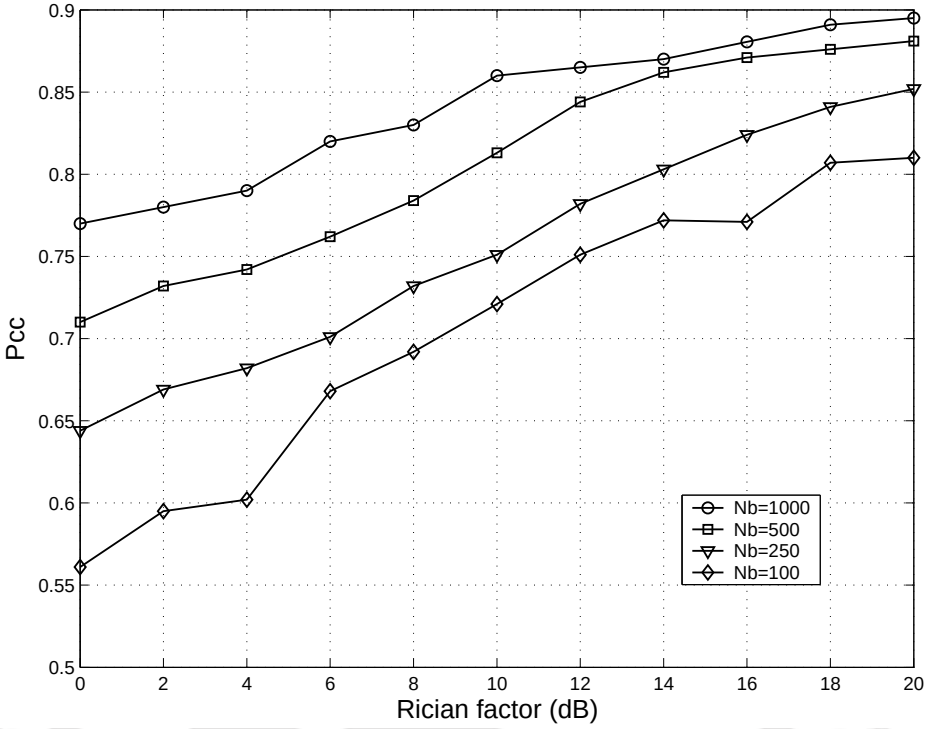

FIGURE 5.23: Classification performance of BPSK, QPSK, 8PSK, 8QAM, 16QAM and 32QAM pool in Rician fading

noise model is rewritten as

$$p(n_k) = \frac{\lambda_1}{2\pi\sigma_1^2} exp\Big(-\frac{|n_k|^2}{2\sigma_1^2}\Big) + \frac{\lambda_2}{2\pi\sigma_2^2} exp\Big(-\frac{|n_k|^2}{2\sigma_2^2}\Big) \tag{5.51}$$

Figure 5.24 illustrates the effect of non-Gaussian noise on the classification performance of the proposed method. The simulation is carried out in a pool containing BPSK, QPSK, 8QAM and 16QAM. The *Pcc* while the incoming modulation is QPSK is taken arbitrarily as an example. The severity of the non-Gaussian noise is attributed to λ_n and the ratio of the variances of the contributing Gaussian components [22]. It is noteworthy that for certain urban areas, severity of the non-Gaussian noise may be significant. From the figure it is observed that, within the practical limits of severity, the proposed method withstands the non-Gaussian impulse noise well. Under very high severities of impulse noise, Gaussianity of the individual clusters tend to reduce. This causes overall degradation in the estimation accuracy, finally resulting in the model mismatch in the QHLRT classifier. However, as the SNR improves, the effect of impulse noise becomes negligible in general.

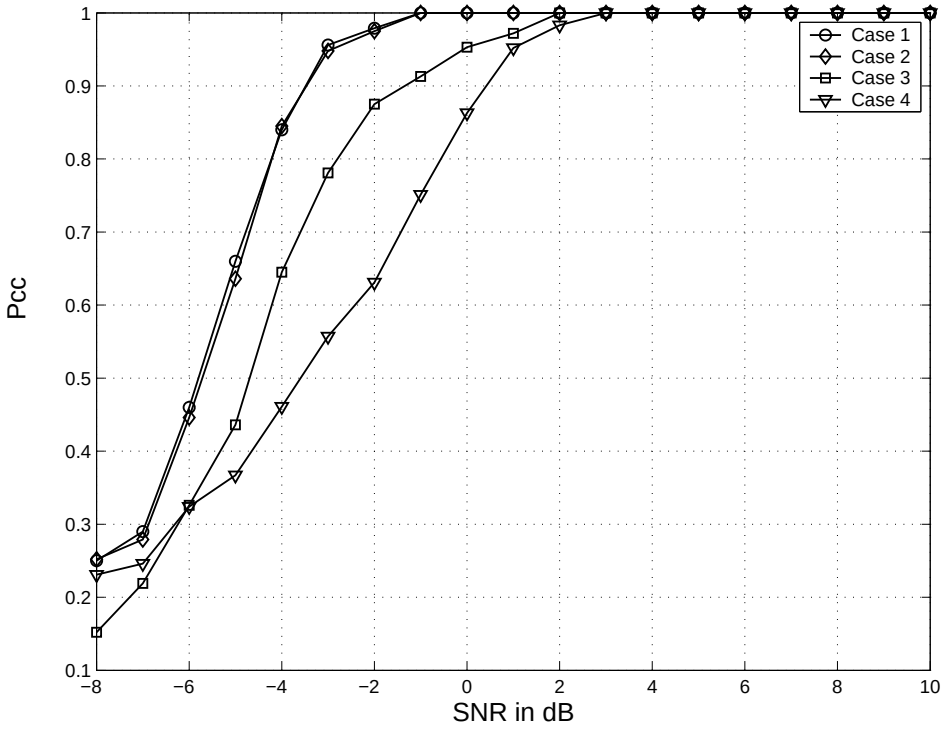

FIGURE 5.24: Classification performance in non-Gaussian noise with $\frac{\sigma_2^2}{\sigma_1^2} = 100$. Case 1: $\lambda_1 = 1$, $\lambda_2 = 0$; Case 2: $\lambda_1 = 0.9$, $\lambda_2 = 0.1$; Case 3: $\lambda_1 = 0.8$, $\lambda_2 = 0.2$; Case 4: $\lambda_1 = 0.7$, $\lambda_2 = 0.3$

5.5.7 Effect of Maximum Phase Rician Channel

The performance of the proposed classifier is evaluated in maximum phase Rician channel. In this case, the gross signal energy in the reflected multipath components is higher than the direct component. A slow, flat fading scenario is considered with a candidate pool containing BPSK, QPSK, 8QAM and 16QAM. Figure 5.25 illustrates the performance of the proposed classifier against various values of the Rician factor for the maximum phase scenario. The robustness of the classifier is observed at the low SNR cases.

5.5.8 Performance comparison with FB approach

The fourth-order cumulant based classifier [35] is considered under the FB framework. The cumulant based classifier is highly susceptible to model mismatch due to phase rotation. However, it is almost immune to the gain uncertainty. Like other FB classifiers, the performance of the cumulant based classifier is sub-optimal even in the ideal case

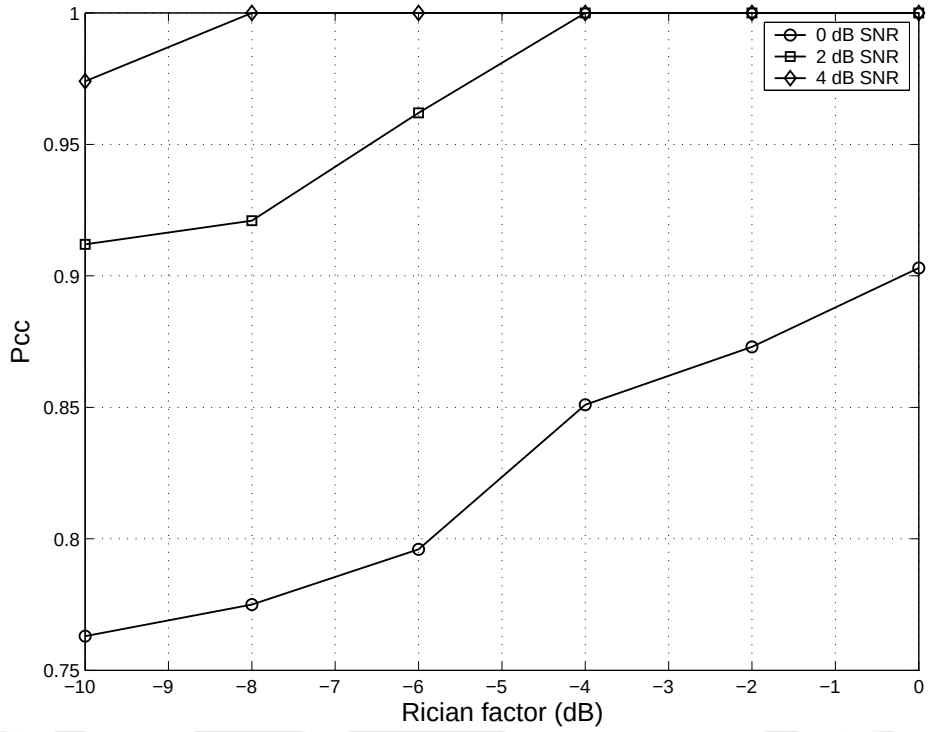

FIGURE 5.25: Effect of maximum phase Rician channel for classification of QPSK in the pool

of the knowledge of the parameters. Here, the proposed phase correction is applied to the received signal constellation and classify the modulations within the candidate pool. Figure 5.20 illustrates the comparison of the classification performance with respect to the proposed QHLRT based approach. From the plots, it is evident that the cumulant based classifier can be employed in a model mismatch scenario when used with the phase-offset correction. However, the QHLRT classifier outperforms the cumulant based classifier even the with the common pre-processing steps of gain and phase-offset corrections.

5.5.9 Performance comparison with non-blind and semi-blind MC

In Figure 5.26, the achieved results are reviewed in comparison to the non-blind and several semi-blind scenarios. Average probability of correct classification is considered in a pool containing BPSK, QPSK, 8QAM and 16QAM under a slow flat fading channel $[1\ 0.3\ 0.2]^T$. The carrier and the base-band sample sizes considered are 4096 and 1024 respectively. The semi-blind scenario with only f_s as unknown parameter is observed to

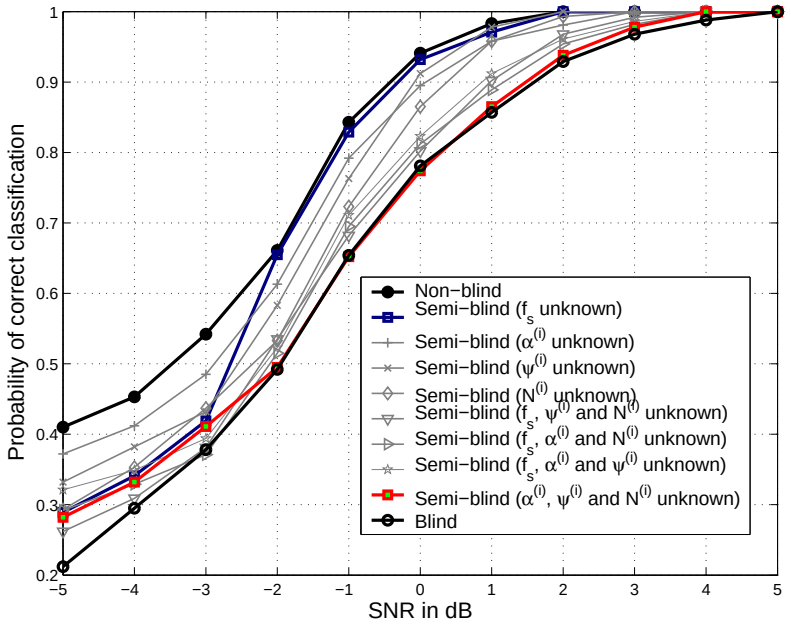

FIGURE 5.26: Performance comparison for non-blind, semi-blind and blind scenarios

be the closest to the non-blind MC performance above SNR of about -2 dB. On the other hand, the performance for the semi-blind scenario with $\alpha^{(i)}$, $\psi^{(i)}$ and $N^{(i)}$ and unknown parameter is the closest to the blind MC performance. This provides us an idea about the importance of estimation accuracy of certain parameters. In this case, the knowledge and the lack of knowledge of f_s play a significant role in the performance of the MC as compared to the other parameters. For the proposed method, the estimation accuracy of f_s at SNR values above a threshold makes the MC performance independent of the this parameter.

5.6 Summary

In this Chapter a QHLRT based classifier has been proposed for the linear digital modulation schemes. Considering a blind scenario, new estimators for the channel gain, the phase-offset and the noise power are presented. The CRLBs for the gain and the phase estimators are established as the performance bound. Although the above estimators are not efficient due to the non-linear transformations involved, the MSE performance at blind scenario makes them practically useful. The simulation results establish that the proposed blind estimators perform better in the low SNR conditions in a slow fading

channel as compared to the existing estimators. Further, the probability of correct classification of the proposed QHLRT classifier employing the new estimators is very close to the theoretical QHLRT upper bound. The new classifier also outperforms the existing QHLRT classifier using the MoM based estimators. The method has demonstrated immunity up to a moderate level of non-Gaussian impulse noise. Further, the proposed phase correction method may be employed as a pre-processing stage in certain FB classifiers like the cumulant based algorithm to mitigate the model mismatch due to the fading channel. However, from the performance point of view, the LB approach remains the best choice. The performance of the estimators and the MC being directly correlated to the sample length, the complexity of the method is a significant factor to consider. Although there is a scope for future work to reduce the computational complexity of the proposed algorithm, the superior results at adverse channel conditions may be a trade off between better performance and time complexity. The performance bounds of the noise power estimator may be considered for investigation in future.

6

Mitigation of Frequency Selective Fading Effects

6.1 Introduction

Multipath fading is one of the primary causes of model mismatch in the LB MC due to the distortion caused in the received signal. The adverse channel conditions pose a major challenge to the classification accuracy [42] of blind MC. Apart from the fading channel, imperfections in the receiver such as the carrier frequency offset, the phase offset, the timing offset etc. introduce additional distortions in the signal. The combined effect of the multipath fading and the receiver imperfections produces the resultant distortion

in the base-band I-Q signal. This overall channel effect left out in the baseband signal is termed as the *residual base-band fading* [21].

In blind MC, no prior information on the signal parameters and the propagation channel is available. In the event of the ISI in the residual channel, equalization is the primary mitigation approach available. Blind equalization has been addressed in conventional communication systems [87, 88] to avoid the use of a training sequence, so that a better throughput is ensured. In such a co-operative scenario, the modulation scheme being known, a decision directed least mean square (DDLMS) approach is very commonly employed [87]. Decision making for the DDLMS algorithm is straight-forward with the number of levels of the base band symbols as the known parameter. For the blind scenario, the performance of the DDLMS algorithm deteriorates due to the uncertainty of the symbols in a generic case containing single amplitude (e.g. QPSK, 8PSK) and multi-amplitude (e.g. 16QAM, 32QAM etc.) modulations. If a specific cost function is employed as in the conventional DDLMS, the MSE increases [89] as the order of the modulations is changed.

We explore further towards the other blind equalization approaches used in the conventional communication systems like the constant modulus algorithm (CMA) [90] and the modified CMA (M-CMA) [91]. In the CMA approach, the ISI is mitigated by minimizing a cost function based on the magnitudes of the sample vectors. Although the CMA can handle the PSK and the QAM constellations, the phase correction is not possible. In M-CMA, by considering a cost function that retains the phase information of the sample vectors, both the blind equalization and the phase correction can be carried out. However, both the algorithms provide noisy outputs, and their direct application in blind MC is not suitable at low SNR conditions. In [42], a blind equalizer is used to address the channel distortion in the base-band signal, while the channel is considered as a slow, flat fading one. The iterative equalization process is coupled with the optimization of two cost functions, the first one is based on the cumulant based MC performance, while the second one is based on symbol detection. This is one of the practical approaches for the blind MC applications, when a minimum phase channel is considered. However, the mitigation of the ISI introduced by the frequency selective fading still needs special attention in the context of blind MC. In majority of applications, MC faces the challenge of

identifying the modulation scheme under multi-path propagation effect and the channel noise. Issues due to the channel noise, the phase offset and the unknown channel gain have been addressed in [22, 24, 26] and Chapter 5. Frequency selective fading due to the multi-path effect causes distortion and random scaling in the received signal. In the LB approach, the resulting ISI deteriorates the MC performance due to the model mismatch in the likelihood function. For severe channel distortion, LB classification completely fails if mitigation measures are not taken [42].

In subsequent sections of this Chapter, a study is performed on the effect of the channel distortion due to the frequency selective fading in blind MC. The LB approach is invariably adopted due to the availability of the optimum solution. Starting with a simpler case of real valued channel coefficients, a suitable mitigation approach is formulated for blind MC. Here, a modulation-specific DDLMS algorithm is employed, which is supported by the gain normalization of the received signal. The proposed method is further extended towards the more practical case of complex channel coefficients, where the signal distortion is a combined effect of the ISI and the phase offset. A new equalizer scheme containing the conventional modified constant modulus algorithm (M-CMA) [91] and the modulation specific DDLMS is formulated as a generic pre-processing stage in blind MC. A pool of possible modulation schemes is considered to evaluate the performance of the new scheme. Experimental results are presented for establishing the utility of the proposed method in the QHLRT based blind MC.

6.2 Performance of LB MC under ISI

For a frequency selective fading scenario, the base-band signal model is given by [35]

$$x_k = \alpha^{(i)} \sum_{l=-\infty}^{\infty} s_l^{(i)} h(kT_s - lT_s + \epsilon_T T_s) e^{(j2\pi\Delta f k T_s + j\theta_n)} + n_k \tag{6.1}$$

where x_k is the k^{th} sample of the received complex signal, ϵ_T represents timing error and the other symbols represent their usual meaning. Assume that T_s has been estimated without any significant error and the effects of ϵ_T, Δf and θ_n are negligible. Also assume

that the channel gain $\alpha^{(i)}$ is normalized. The received signal model now can be simplified in the vector form as

$$x_k = \mathbf{h}^H \mathbf{s}_k^{(i)} + \mathbf{n}_k \tag{6.2}$$

where $\mathbf{x}_k = [x_k \ x_{k-1}...x_{k-L+1}]^T$ is the vector of the received complex signal, $\mathbf{s}_k^{(i)} = [s_k^{(i)} \ s_{k-1}^{(i)}...s_{k-L+1}^{(i)}]^T$ is the transmitted complex symbol vector, $\mathbf{h} = [h_0 \ h_1...h_{L-1}]^T$ denotes the vector of the complex channel response with length L, $\mathbf{n}_k$ is the complex AWGN with power spectral density N and H represents the Hermitian transpose operator. Ideally, $\mathbf{x}_k$ needs to be equalized using an FIR filter with the weight vector $\mathbf{w}_k = [w_{0,k} \ w_{1,k}...w_{L-1,k}]^T$, such that the output $z_k = \mathbf{w}_k^H \mathbf{x}_k$ is free from ISI. To ensure that the received and the library signals are matched in terms of scaling and orientation without the ISI, the equalizer output is used in the QHLRT log-likelihood function. For $H^{(i)}$, the QHLRT log-likelihood function of Equation 2.11 can be re-written as

$$L_{QHLRT}(\mathbf{z}|H^{(i)}) = \sum_{k=1}^{N_b} \ln \left[\sum_{m=1}^{M^{(i)}} \frac{1}{M^{(i)} \pi N^{(i)}} \times exp\left\{ -\frac{1}{N^{(i)}} \left| z_k - s_m^{(i)} \right|^2 \right\} \right] \tag{6.3}$$

The MC decision is arrived at by

$$\hat{H} = \arg\max_i L_{QHLRT}(\mathbf{z}|H^{(i)}) \tag{6.4}$$

As evident from (6.3) and (6.4), the QHLRT decision depends on the removal of the ISI in the equalized signal z_k. Hence, the mitigation against the ISI involves the appropriate formulation of the blind equalization process. Since $\mathbf{x}_k$ is a function of the channel impulse response $\mathbf{h}$, the received base-band signal is distorted depending on the severity of the residual fading. As a result of fading, the received signal constellation suffers distortion and random scaling as shown in Figure 6.1. Unlike flat-fading scenarios with resulting rotation of the received constellation, the frequency selective fading introduces additional distortion due to the ISI. Figures 6.1a and 6.1b illustrate the ISI in the base-band signal for two different cases of fading severities. As the channel coefficients are real valued, there is no phase-offset in these cases. In Figures 6.1c and 6.1d, the combined effect of ISI and the phase offset is shown, while considering the complex valued channel coefficients.

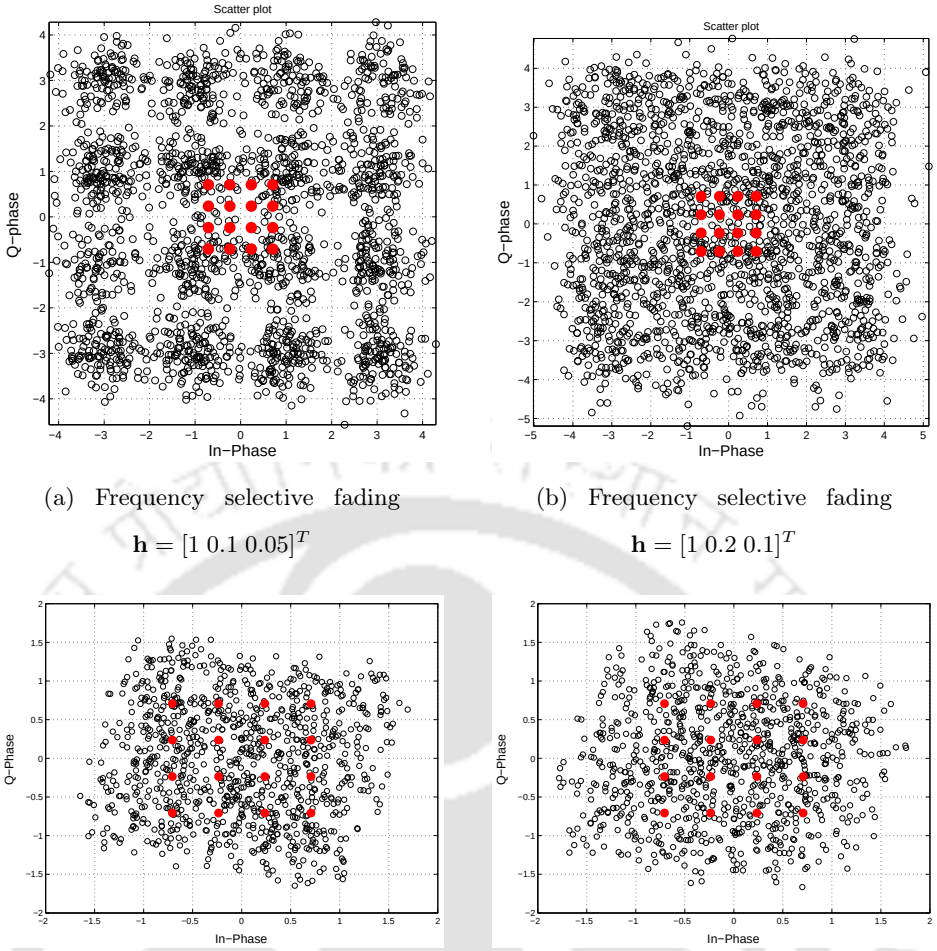

(a) Frequency selective fading $\mathbf{h} = [1\ 0.1\ 0.05]^T$

(b) Frequency selective fading $\mathbf{h} = [1\ 0.2\ 0.1]^T$

(c) Frequency selective fading $\mathbf{h} = [1 - j0.2\ \ 0.3 + j0.05\ \ 0.2 - j0.06]^T$

(d) Frequency selective fading $\mathbf{h} = [1 - j0.3\ \ 0.5 + j0.07\ \ 0.2 - j0.03]^T$

FIGURE 6.1: Distortion in received signal at SNR 10 dB

To examine the effect of the frequency selective fading on the QHLRT based MC, a scenario is created using a pool of modulation containing BPSK, QPSK, 8QAM and 16QAM. The probability of correct classification is plotted across a range of SNRs using the Monte Carlo simulation. Figure 6.2 shows the performance of the LB classifier for the classification of QPSK among the candidate pool in a residual fading channel with various levels of severities. The performance of the MC method is effected as per the severity of the model mismatch caused by the fading channel. As observed in the figure, the effect of a complex channel is more severe for blind MC. In the lower SNRs, there is an uncertainty of the MC decision and due to the predominance of noise. As the SNR increases, the ISI becomes the primary cause of the model mismatch. Hence, for severe

cases of ISI, the MC decision degrades consistently at higher SNRs.

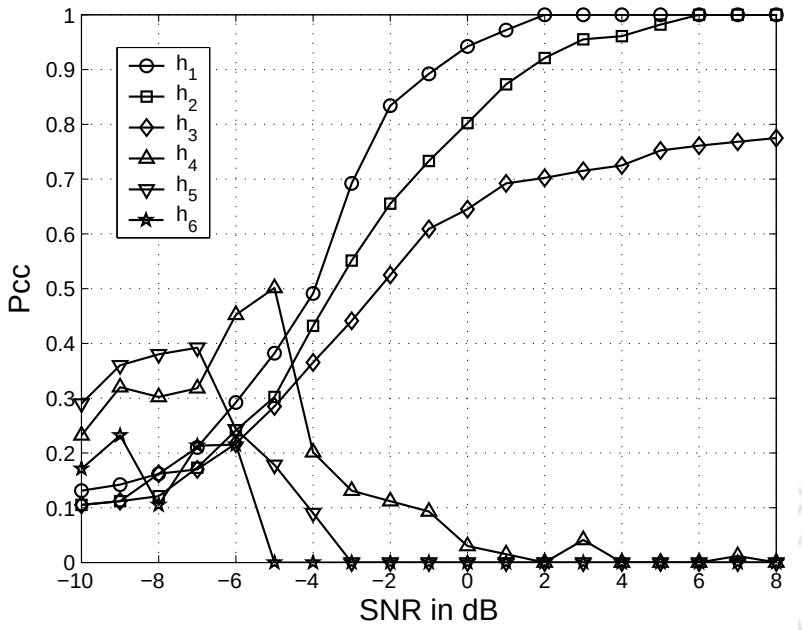

FIGURE 6.2: Performance of LB classifier in frequency selective fading channel. $\mathbf{h}_1 = [1\ 0\ 0]^T$, $\mathbf{h}_2 = [1\ 0.1\ 0.05]^T$, $\mathbf{h}_3 = [1\ 0.2\ 0.1]^T$, $\mathbf{h}_4 = [0.7\ 0.3\ 1.0]^T$, $\mathbf{h}_5 = [1 - j0.2\ 0.3 + j0.05\ 0.2 - j0.06]^T$, $\mathbf{h}_6 = [1 - j0.3\ 0.5 + j0.07\ 0.2 - j0.03]^T$

As illustrated in the analysis of the two situations of fading with the real and the complex valued channel coefficients, the estimation of the fading channel becomes the necessary pre-processing for the LB classification. In the subsequent sections in this chapter, we formulate the mitigation measures to improve the performance of the blind LB MC.

6.3 Proposed Scheme for Mitigation of the ISI in Real Channel

As a measure to mitigate the effect of frequency selective fading, a combined scheme with blind equalization and amplitude normalization is adopted. There are two main approaches to the blind adaptive equalization, the first one is based on the stochastic gradient descent (SGD) and the higher order statistics (HOS) based method [92] being the second one. The first method is considered here and the same is adapted for blind MC. The SGD approach iteratively minimizes a chosen cost function over the choices of equalizer coefficients [93]. The equalization scheme is illustrated in Figure 6.3. Without

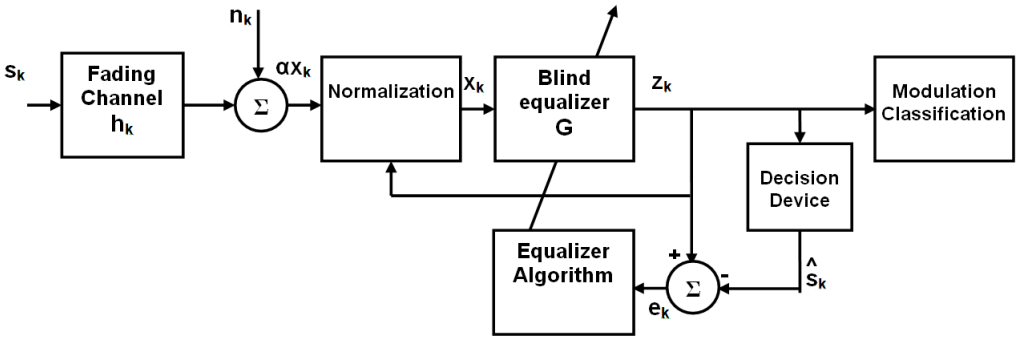

FIGURE 6.3: Blind DDLMS scheme in Likelihood Based MC

the loss of generality, the input $\alpha^{(i)}x_k$ is considered to be normalized to obtain x_k as the input to the equalizer. The equalizer coefficients need to be adjusted such that the output of the equalizer z_k can be quantized to yield a reliable estimate of the channel input $s_k^{(i)}$. The decision device is a quantizer, which forces the value of the output symbol level to the nearest library symbol magnitude. The output of the decision device is represented by

$$\hat{s}_k^{(i)} = Q(z_k) \tag{6.5}$$

Theoretically, the equalizer takes the form of an infinite impulse response (IIR) filter. However, for practical convenience, the adaptive equalizer is implemented by FIR filters. Since, the performance of the MC scheme is dependent on the length of the equalizer [42], the selection of L is important. The experimental evaluation in [42] established that, after a threshold length, the performance does not improve significantly. Hence, the value of L is selected such that, the optimum performance is achieved without adding to further computational complexity. The conventional DDLMS algorithm [87] is employed to minimize the MSE cost function asymptotically. The channel coefficients being real, the advantage of the symmetry of the constellation is taken and a modulation-specific DDLMS cost function corresponding to $H^{(i)}$ is introduced and defined as

$$J_{DDLMS}^{(i)} = E\Big(z_{I,k}{}^{(i)} - Q^{(i)}(z_{I,k}{}^{(i)})\Big)^2, \tag{6.6}$$

where, $z_{I,k}$ is the in-phase component of $z_k^{(i)}$ and $Q^{(i)}(.)$ quantizes $z_{I,k}$ to the corresponding nearest symbol magnitude. Now, taking the gradient of the cost function with

respect to $\mathbf{w}_k^{(i)}$,

$$\begin{aligned}\frac{\delta J_{DDLMS}^{(i)}}{\delta \mathbf{w}_k^{(i)}} &= 2E\Big[\Big\{{z_{I,k}}^{(i)} - Q^{(i)}(z_{I,k}^{(i)})\Big\}\frac{\delta z_{I,k}^{(i)}}{\delta \mathbf{w}_k^{(i)}}\Big] \\ &= 2E\Big[\Big\{z_{I,k}^{(i)} - Q^{(i)}(z_{I,k}^{(i)})\Big\}\frac{\delta}{\delta \mathbf{w}_k^{(i)}}{\mathbf{w}_k^{(i)}}^H \mathbf{z}_{I,k}\Big] \\ &= 2E\Big[\mathbf{z}_{I,k}\Big\{z_{I,k}^{(i)} - Q^{(i)}(z_{I,k}^{(i)})\Big\}^*\Big] \\ &= 2E\Big(\mathbf{z}_{I,k}e_k^{(i)*}\Big), \quad \text{where the instantaneous error} \quad e_k^{(i)} = z_{I,k}^{(i)} - Q^{(i)}(z_{I,k}^{(i)})\end{aligned} \tag{6.7}$$

We consider the stochastic gradient to update the weight vector $\mathbf{w}_k^{(i)}$ as

$$\mathbf{w}_k^{(i)} = \mathbf{w}_{k-1}^{(i)} - \mu \mathbf{z}_{I,k}e_k^{(i)*} \tag{6.8}$$

where $\mu = \frac{\mu_1}{2}$. Using the iterative process, the blind equalizer asymptotically minimizes the MSE

$$E\{|e_k^{(i)}|^2\} = E|z_{I,k}^{(i)} - \hat{s}_k^{(i)}|^2 \tag{6.9}$$

The iterations are continued till the MSE becomes very small so that the equalizer output $z_{I,k}^{(i)}$ is a close estimate of the original channel input $s_k^{(i)}$. Hence, by appropriate selection of $Q^{(i)}(.)$, the blind equalizer is able to track variations in the channel dynamics.

Selection of the Decision function: Unlike conventional communication system, where the IQ constellation pattern is known, there is no prior knowledge of the constellation pattern in blind MC. In this scenario, the decision functions corresponding to all the modulations among the candidate pool need to be considered. The decision boundaries for each modulation is derived based on the normalized signal model. This makes it necessary to normalize the received signal before starting the equalization process.

For gain normalization, the estimation of the constellation points is necessary. The normalization algorithm has been described in details in Chapter 4 for simplicity. Due to the ISI, in the beginning of the equalization process, only coarse normalization is possible depending on the severity of the fading. However, the normalization can be fine tuned after the equalization process, with an additional cycle of processing.

The decision function is designed such that the distance of the equalizer output from any of the symbol values of the assumed constellation model is minimum. The Euclidian distance of $z_{I,k}^{(i)}$ from the model constellation points for any of the $\mathcal{C}$ modulation schemes is expressed as

$$d(l) = ||z_{I,k}^{(i)} - s_l^{(i)}||, \quad l = 1, 2, \ldots M^{(i)} \tag{6.10}$$

where $s_l^{(i)}$ is the l^{th} constellation point and $M^{(i)}$ is the number of constellation points in the assumed modulation scheme. The decision function $Q(.)$ can be expressed as

$$Q(z_{I,k}) = s_{I_{min}}^{(i)}, \quad I_{min} = \arg\min_l(d(l)) \tag{6.11}$$

The decision function for the BPSK and the QPSK modulations is shown in Figure 6.4 with 0.7071 and -0.7071 as decision boundaries. A list of decision boundaries for various

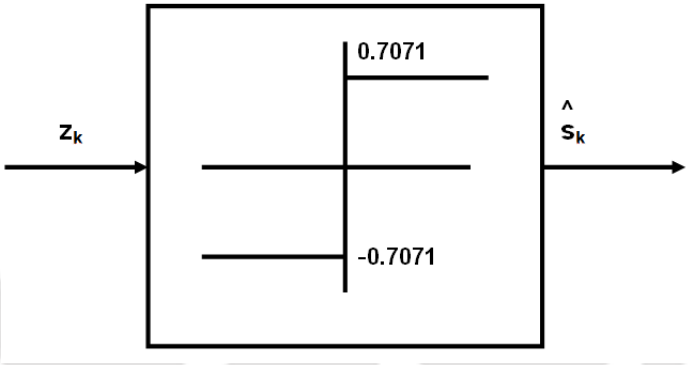

FIGURE 6.4: Decision function for BPSK and QPSK modulations

modulation schemes is provided in Table 6.1. Since the constellations are considered symmetric, the decision boundaries for the real components alone are shown. Out of the pool of assumed modulation schemes, blind equalization is carried out for each of the $\mathcal{C}$ constellation models. The implementation scheme is illustrated in Figure 6.5. Although the DDLMS approach is efficient for convergence in a blind scenario, the cost function employed does not carry the phase information of the received samples. This makes the method sensitive to the phase offset when the channel coefficients are complex.

Modulation	Decision boundaries
BPSK	±0.7071
QPSK	±0.7071
8PSK	±0.7071, 0, ±1
8QAM	±0.7071, 0
16QAM	±0.2357, ±0.7071
32QAM	±0.1414, ±0.4242, ±0.7071
64QAM	±0.101, ±0.303, ±0.505, ±0.7071

TABLE 6.1: Decision boundaries for various modulations

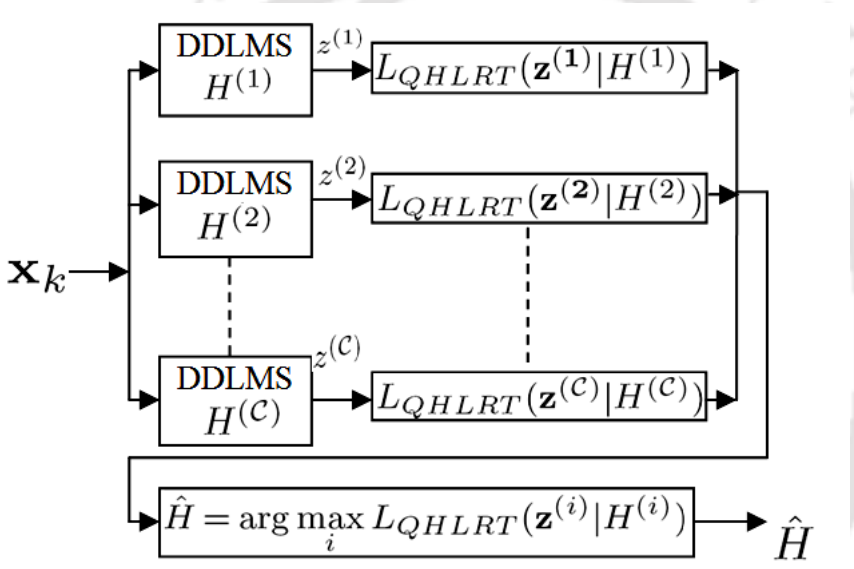

FIGURE 6.5: Equalization scheme for real channel

6.4 Mitigation of the ISI and Phase-Offset: Complex Channel Coefficients

6.4.1 Constant modulus algorithm

Towards a generic solution to the blind equalization problem in the MC context, first the CMA is explored. The CMA cost function is given by

$$J_{CMA} = E\left\{\left(|z_k|^2 - R\right)^2\right\}, \tag{6.12}$$

where, $R = \frac{E|x_k|^4}{E|x_k|^2}$ is a constant for the observation interval. The constant modulus criterion was formulated especially to address the constant amplitude constellations, which also have the utility for the multi-amplitude scenario at comfortable levels of SNR. Due to the single modulus cost function, the CMA converges reasonably well only for the single amplitude modulations (e.g. QPSK). Further, it does not correct the phase offset in a complex channel [94].

6.4.2 Modified CMA

The shortcomings of the CMA are addressed in the modified-CMA (M-CMA) cost function, and it is the next available choice for the blind MC to mitigate the ISI and resolve the phase ambiguity even for the multi-modulus scenarios (e.g. 16QAM). The cost function for the M-CMA is given by

$$J_{MCMA} = E\left\{\left(|z_{I,k}|^2 - R_I\right)^2 + \left(|z_{Q,k}|^2 - R_Q\right)^2\right\}, \tag{6.13}$$

where, the subscripts I and Q denote the in-phase and quadrature-phase baseband components, $R_I = \frac{E|x_{I,k}|^4}{E|x_{I,k}|^2}$ and $R_Q = \frac{E|x_{Q,k}|^4}{E|x_{Q,k}|^2}$ are constants. The M-CMA minimizes the individual cost functions involving the in-phase and the quadrature-phase components. Unlike the CMA, it is able to minimize the dispersion of both the components in the I-Q plane, thereby correcting the phase-offset. The cost function is minimized by taking gradient of (6.13) with respect to $\mathbf{w}_k$ as

$$\frac{\delta J_{MCMA}}{\delta \mathbf{w}_k} = E\left(e_k \mathbf{x}_k^*\right) \tag{6.14}$$

The error term e_k is given by

$$e_k = 2[z_{I,k}(z_{I,k}^2 - R_I) + j z_{Q,k}(z_{Q,k}^2 - R_Q)] \tag{6.15}$$

Using the SGD method, the M-CMA weight vector is recursively updated as

$$\mathbf{w}_k = \mathbf{w}_{k-1} - \mu \mathbf{x}_k e_k^* \tag{6.16}$$

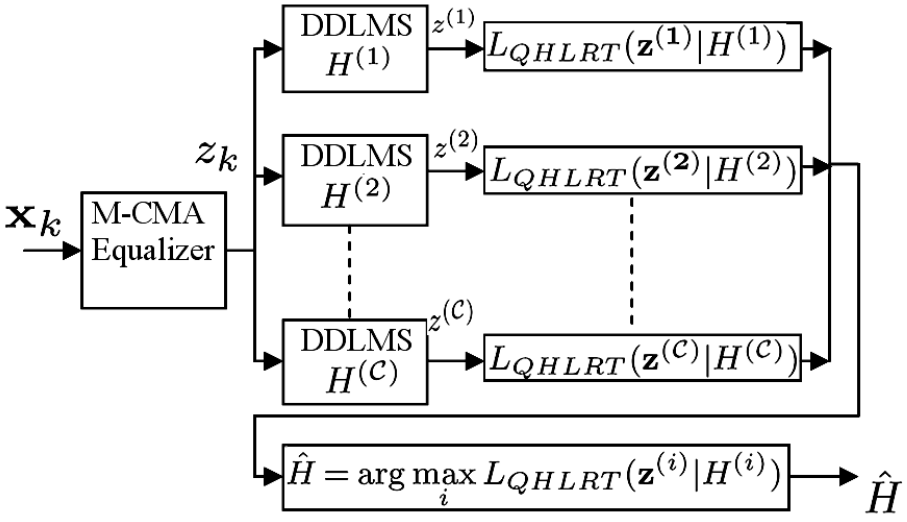

FIGURE 6.6: Proposed generic scheme for MC in a complex channel

where μ is the appropriately chosen step size. The M-CMA is suitable for the mitigation of the ISI and the phase-offset for the constant and the multi-modulus scenarios. This makes it a potential pre-processing stage for the use in the QHLRT classifier. On the disadvantages, the method inherently introduces equalization noise in the recovered signal [95], making it unsuitable under low SNR conditions.

6.4.3 Proposed Scheme for the Complex Channel

The DDLMS approach deteriorates considerably when the channel coefficients are complex. On the positive side, it is experimentally observed that, on formulating a DDLMS cost function using both the in-phase and the quadrature-phase components, effective mitigation of the ISI and the phase-offset can be achieved until the phase-offset pushes the symbols beyond the quadrant boundaries in the severe cases of fading. On the other hand, the low SNR performance of the M-CMA for multi-modulus case still needs improvement for the blind MC scenario. We propose a scheme with the M-CMA as the pre-processing stage, followed by the modulation specific DDLMS equalization as shown in Figure 6.6. The cost functions employed in the proposed method are shown in Figure 6.7. As illustrated in the figure, the M-CMA cost function does not consider the decision boundaries for multi-amplitude modulations. But the phase correction is effective in M-CMA based equalization [91]. Once the phase offset is mitigated, the modulation specific cost function for the DDLMS stage forces the equalizer to converge within the

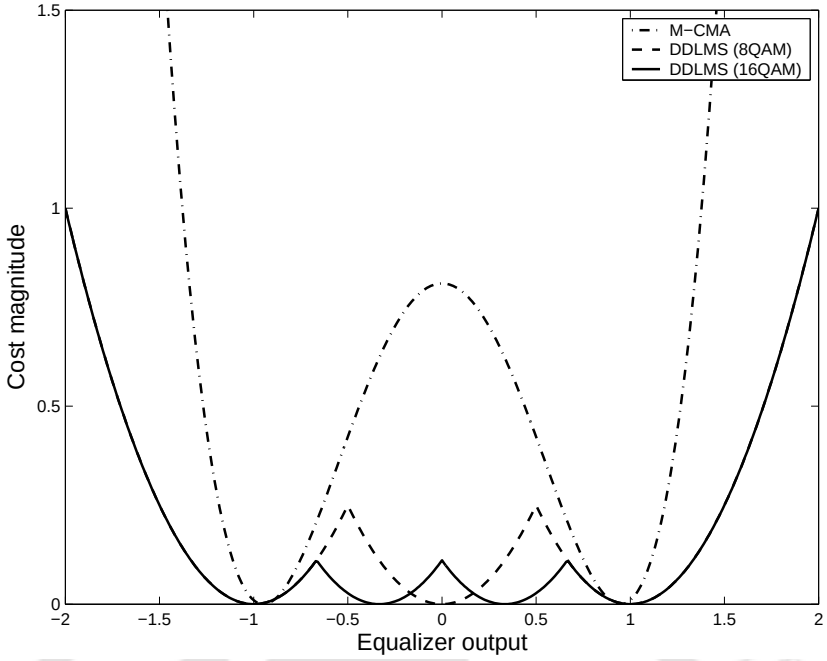

FIGURE 6.7: Cost functions for the M-CMA and the DDLMS algorithms

decision boundaries. The input to the M-CMA is normalized to minimize the gain uncertainty. We define the following modulation specific DDLMS (MD) cost function for the i^{th} branch in Figure 6.6 corresponding to $H^{(i)}$. It is given by

$$J_{MD}^{(i)} = E\left\{ \left(z_{I,k}^{(i)} - Q^{(i)}(z_{I,k}^{(i)}) \right)^2 + \left(z_{Q,k}^{(i)} - Q^{(i)}(z_{Q,k}^{(i)}) \right)^2 \right\}, \tag{6.17}$$

where, $Q^{(i)}(.)$ quantizes the in-phase and the quadrature-phase components of $z_k^{(i)} = z_{I,k}^{(i)} + j z_{Q,k}^{(i)}$ to the nearest symbol components. The quantization is independently applied on the in-phase and the quadrature-phase components. Now, taking the gradient of $J_{MD}^{(i)}$ with respect to $\mathbf{w}_k^{(i)}$, we get

$$\begin{aligned} \frac{\delta J_{MD}^{(i)}}{\delta \mathbf{w}_k^{(i)}} &= 2E\left[\left(z_{I,k}^{(i)} - Q^{(i)}(z_{I,k}^{(i)}) \right) \frac{\delta z_{I,k}^{(i)}}{\delta \mathbf{w}_k^{(i)}} + \left(z_{Q,k}^{(i)} - Q^{(i)}(z_{Q,k}^{(i)}) \right) \frac{\delta z_{Q,k}^{(i)}}{\delta \mathbf{w}_k^{(i)}} \right] \\ &= 2E\left[\mathbf{z}_k \left\{ \left(z_{I,k}^{(i)} - Q^{(i)}(z_{I,k}^{(i)}) \right)^* + \left(z_{Q,k}^{(i)} - Q^{(i)}(z_{Q,k}^{(i)}) \right)^* \right\} \right] \end{aligned} \tag{6.18}$$

We employ the stochastic gradient to update the weight vector $\mathbf{w}_k^{(i)}$ as

$$\mathbf{w}_k^{(i)} = \mathbf{w}_{k-1}^{(i)} - \mu \mathbf{z}_k e_k^{(i)*}, \quad \mu = \frac{\mu_1}{2} \tag{6.19}$$

where instantaneous error is given by $e_k^{(i)} = z_k^{(i)} - Q^{(i)}(z_k^{(i)})$.

6.5 MC decision

The likelihood function is calculated for each hypothesis using (6.3). The MC decision is arrived at by (6.4). In the generic case of a complex channel, equalization is achieved in two cascaded stages. As shown in the MC scheme of Figure 6.6, the M-CMA stage performs the phase correction and the first level of mitigation against the ISI. The modulation specific equalizers in the next stage perform the final equalization. Each equalized output is used to calculate the value of the respective log-likelihood function for use in the final MC decision.

6.6 Experimental results and discussion

6.6.1 Equalization for real valued channel

Simulations are carried out with 1000 base-band samples. The channel is simulated by a three tap FIR filter $\mathbf{h} = [h_1 \ h_2 \ h_3]^T$, where each element of the vector represents the real valued channel coefficients. The candidate modulation pool comprises BPSK, QPSK, 8QAM and 16QAM. The noise power $N^{(i)}$ can be estimated by using the method proposed in Chapter 5 and also by using the method of moments [15] for using in (6.3). In this experiment, the MoM estimate is used to limit the computation time. The performance of the proposed scheme is studied using Monte Carlo simulation method to calculate probability of correct classification P_{CC} against SNR. The comparison is made with the optimum classifier with complete knowledge of the channel response. Cases with various channel conditions are experimented. The equalizer length of 10 [42] is considered to achieve optimum performance.

Figure 6.8 shows that, blind channel estimation for MC is possible within a certain limit of channel distortion. The method performs well for minimum phase multipath channels. However the iterative algorithm does not converge in severe multi-path scenarios, where the direct signal path is small as compared to the delayed reflected paths (maximum

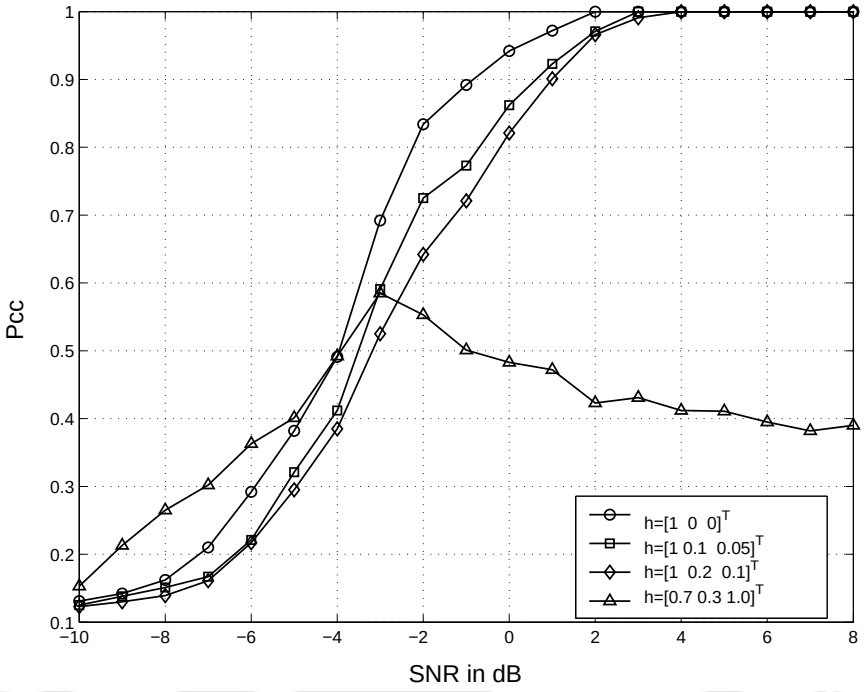

FIGURE 6.8: Comparative performance of the proposed scheme for real channel

phase channel). This case is illustrated under the fading channel $\mathbf{h} = [0.7\ 0.3\ 1.0]^T$ in Figure 6.8. The classification performance even at the higher SNR does not improve due to the model mismatch caused by the unresolved ISI.

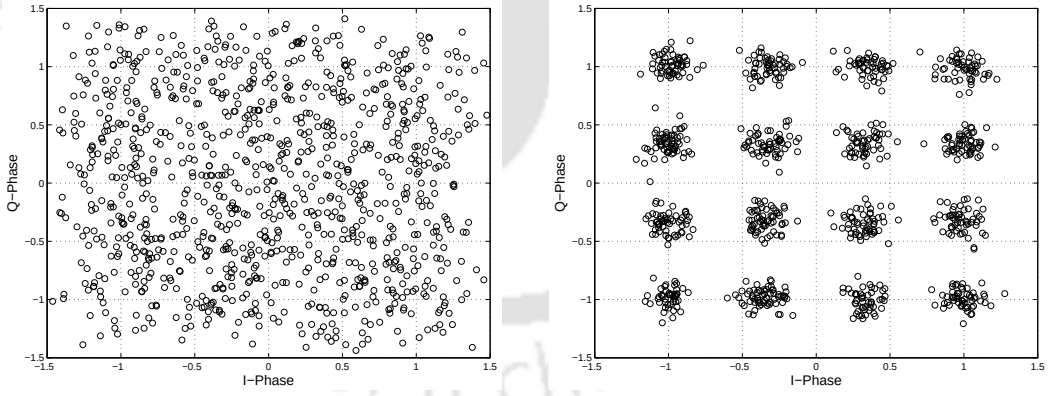

(a) Received Signal (b) Equalized Signal

FIGURE 6.9: Blind equalization using modulation specific DDLMS for 16QAM signal

Figure 6.9 (a) shows the received signal constellation for a 16QAM signal after subjected to channel distortion by impulse response $\mathbf{h} = [0.8\ 0.2\ 0.1]^T$ at 10 dB SNR. Figure 6.9 (b) is the normalized constellation of the equalizer output. Thus the proposed equalization scheme effectively mitigates the ISI for a real channel. Figure 6.10 shows the instanta-

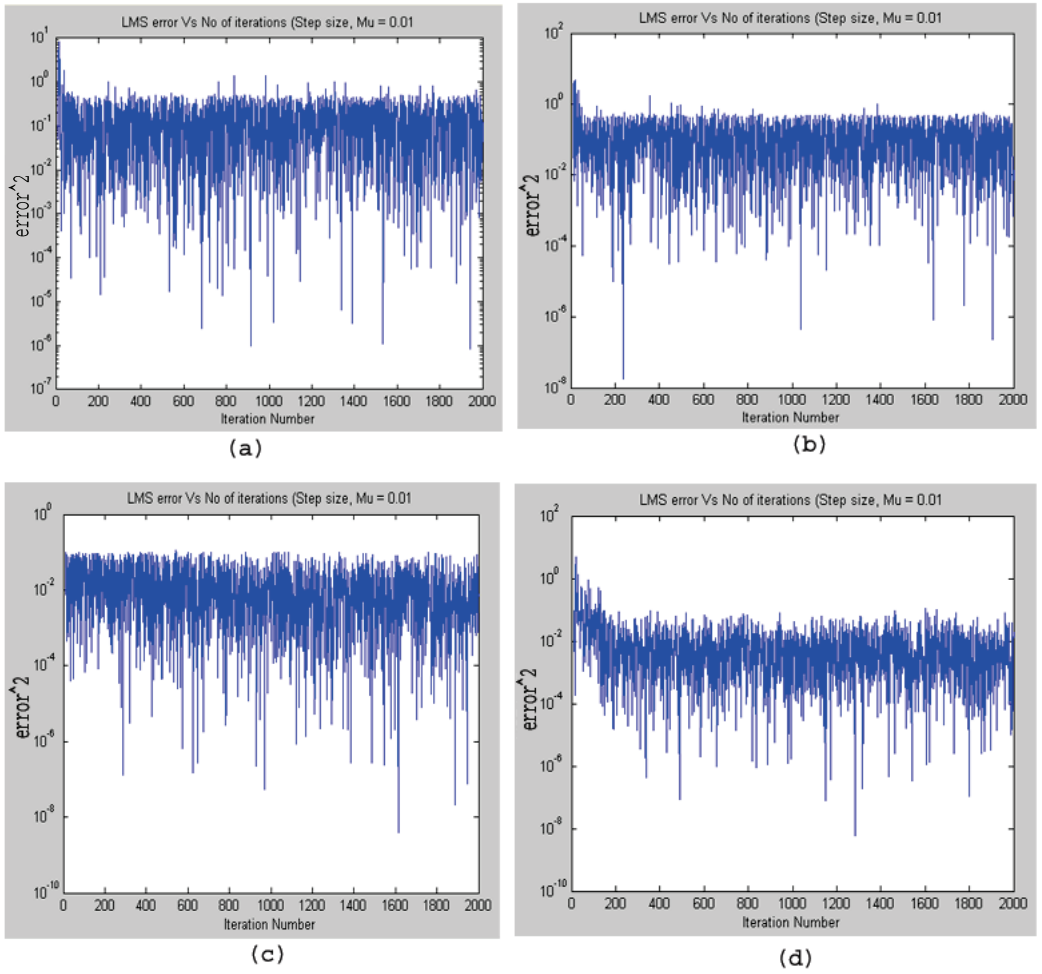

FIGURE 6.10: Instantaneous squared error against the number of iterations: (a) BPSK, (b) QPSK, (c) 8QAM, (d)16QAM, channel response $\mathbf{h} = [0.8\ 0.2\ 0.1]^T$

neous squared error magnitude for a range of iteration steps for different constellation models, when the original signal is 16QAM. The decaying characteristics of the instantaneous error-square is observed in Figure 6.10d. In the proposed scheme, modulation specific DDLMS equalizers are maintained for all the candidates. The input signal is subjected to the modulation specific equalization process in the respective branches as shown in Figure 6.5. If the input modulation of the received signal does not match with the equalizer model in any of the branches, the ISI may not be mitigated. However, in one of the equalizer branch, the received modulation will have a match with the equalizer model and the equalizer weights will be optimally estimated after the convergence of the adaptive process. The equalized output from the matching branch will be the closest to

the constellation model of the corresponding hypothesis. This principle is exploited in the proposed QHLRT MC.

6.6.2 Equalization for complex channel

We consider a complex channel represented by a three-tap FIR filter $[h_{1,r} + jh_r\ h_{2,r} + jh_r h_{3,r} + jh_r]^T$. The real part of each fading co-efficient is represented by an independent Gaussian random variable with mean assigned as per the fading severity and variance $\sigma^2_{h_r} = 0.05$. The imaginary part is represented by a zero-mean independent Gaussian random variable of same variance to simulate the random phase offset. The random channel co-efficients are considered fixed for each observation interval. Let the equalizer length be $L = 10$ as earlier. The mitigation of the ISI is illustrated for two different cases of fading severities in Figure 6.11. As observed in Figure 6.11a and 6.11b that effective mitigation of the ISI is achieved even for more severe cases of fading. Clearly, the performance of the generic scheme of Figure 6.6 is better as compared to the modulation specific DDLMS scheme proposed for the real channels. This improvement ensures better QHLRT MC performance in the subsequent stage. Monte Carlo simulations are carried out to estimate the probability of correct classification of the QHLRT classifier for the same candidate pool in a range of SNRs. Figure 6.12 shows the average probability of correct classification when the received signals are QPSK and 16QAM within the candidate pool. The experiment is performed in two cases of fading severities, while the equalization is carried out by the M-CMA alone and the proposed scheme. A distinct improvement in the performance of the QHLRT MC using the proposed equalizer scheme has been observed. However, the improvement is more prominent for the multi-modulus case. On the other hand, the classification performance deteriorates with the increasing severity of the complex fading channel. Table 6.2 shows the confusion matrix considering square symmetric candidates QPSK, 8QAM, 16QAM and 64 QAM. Since the performance of the blind equalization process deteriorates for higher order modulations, this has the implication on the QHLRT MC performance. Also, the confusion in the MC decision increases with the number of candidate modulation schemes.

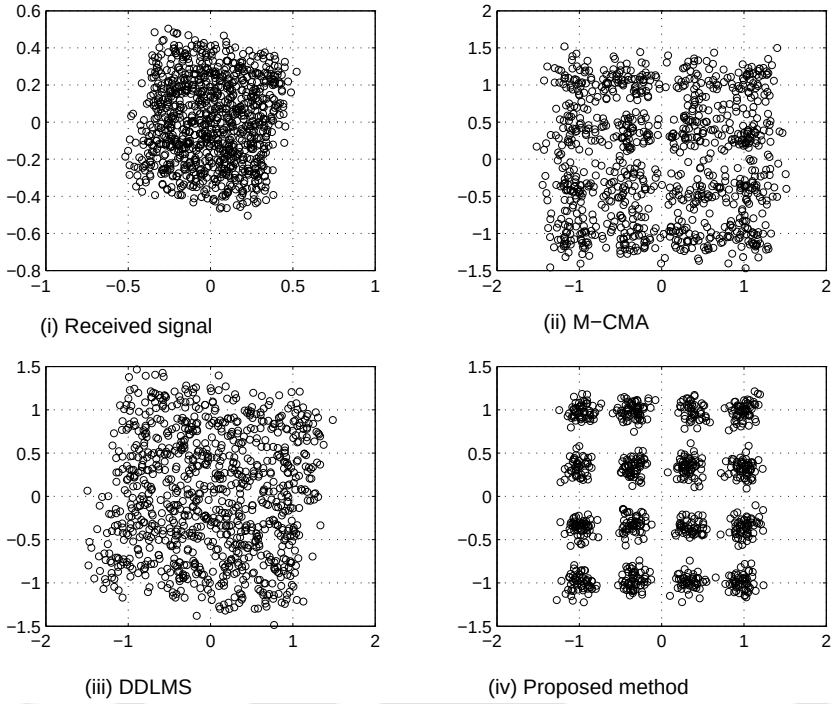

(a) $\mathbf{h} = [1 - j0.2\ 0.3 + j0.05\ 0.2 - j0.06]^T$

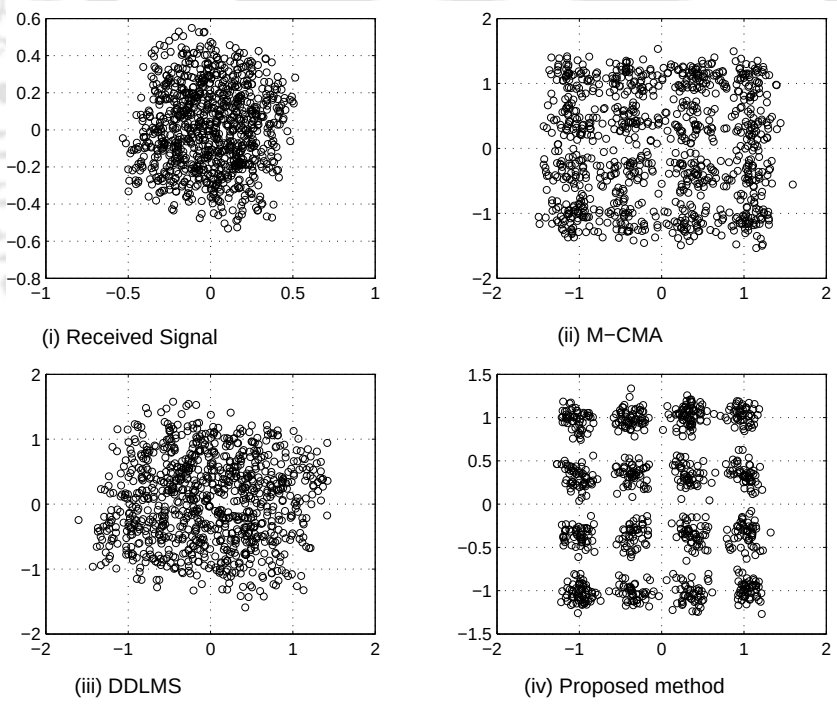

(b) $\mathbf{h} = [1 - j0.3\ 0.5 + j0.07\ 0.2 - j0.03]^T$

FIGURE 6.11: Processing of a 16QAM signal at 20 dB SNR

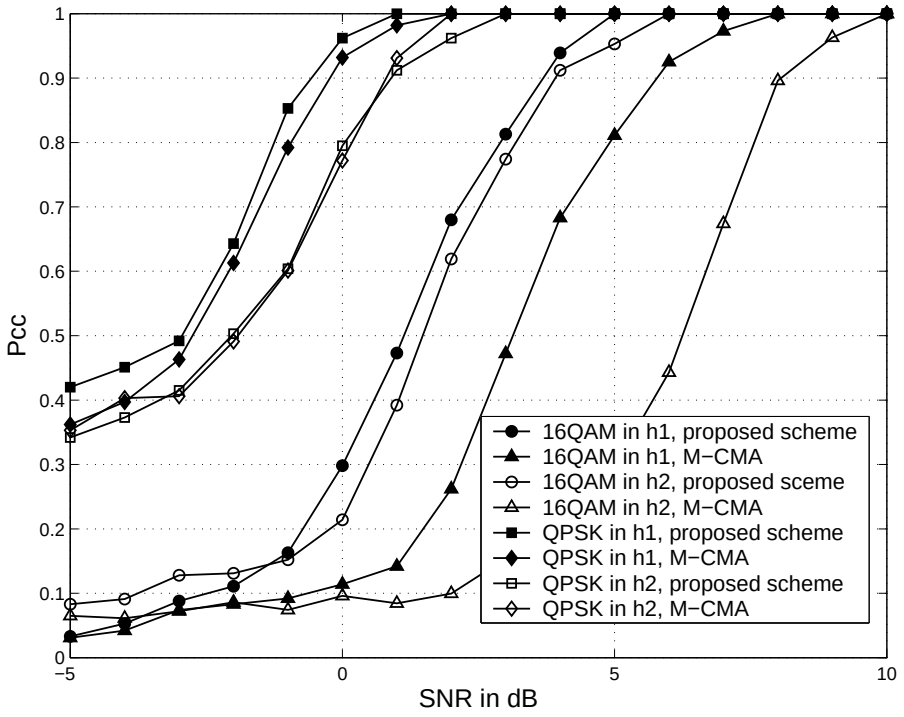

FIGURE 6.12: Probability of correct classification of QPSK and 16QAM signals, with $h_1 = [1 - j0.2\ 0.3 + j0.05\ 0.2 - j0.06]^T$ and $h_2 = [1 - j0.3\ 0.5 + j0.07\ 0.3 - j0.03]^T$

	QPSK	8QAM	16QAM	64QAM
QPSK	100%	0	0	0
8QAM	0	100%	0	0
16QAM	2	0	91%	6%
64QAM	3	0%	25	72%

TABLE 6.2: Classification confusion matrix for fading channel $h_1 = [1 - j0.2\ 0.3 + j0.05\ 0.2 - j0.06]^T$ at 5 dB SNR

6.7 Summary

In this Chapter, the relatively less addressed issue of mitigating the frequency selective fading in the context of blind MC has been discussed. Although this issue has been addressed for the conventional communication applications, adapting the same for the blind MC scenario is not straight forward under the uncertainty of the modulation type. To mitigate this problem, first a modulation specific DDLMS equalization scheme is proposed as a pre-processing step for the QHLRT MC, by considering a channel with real valued coefficients. Subsequently, a more generic scheme is proposed using a cascaded

arrangement containing an M-CMA stage followed by a network of modulation specific DDLMS in the complex domain. The new scheme has shown better mitigation for ISI in a generic pool of modulations. The phase correction in the complex channel is also addressed by the scheme. Apart from the blind MC scenario, the scheme may find application in the conventional communication system to mitigate ISI without a training sequence. The primary focus on the blind equalization performance for the multi-modulus modulation schemes has shown significant improvement over the existing methods. Implementation of the proposed method in a practical MC deployment may provide further insight into the problem.

7

Practical Implementation of Blind MC

7.1 Background of the Application

Over the last two decades, the communication technology has evolved considerably. The migration of the technology is primarily driven by aspects like the data rate, secrecy and the quality of service. The MC has to overcome the challenges and meet the demands of the specific application under the diverse types of communication signals. It is generally accepted that, to achieve the maximum effectiveness, the design and implementation of the MC has to be tailored to the specific application. In Table 7.1, the commonly

Application area	**Modulations used**	**Carrier mode**
Military radios	BPSK, QPSK, DQPSK, OQPSK, 8PSK, 8QAM, 16QAM, 64QAM	Single carrier, frequency hopping (FH), spread spectrum (SS)
Civilian terrestrial microwave links	QPSK, DQPSK, OQPSK, 16QAM, 64QAM	Single carrier
Aviation	AM	Single carrier
Satellite Communication	BPSK, QPSK, 8PSK, 8QAM, 16APSK, 16QAM, 32QAM, 64QAM	Single carrier
2G mobile networks	QPSK, $\frac{\pi}{4}$DQPSK, GMSK	Single carrier
3G mobile networks	QPSK (typically)	Single carrier and multi-carrier CDMA
4G LTE mobile networks	QPSK, 16QAM, 64QAM	OFDM and MIMO-OFDM
Wi-Max	BPSK, QPSK, 16QAM, 64QAM	OFDM and MIMO-OFDM

TABLE 7.1: Commonly used modulations schemes

used modulation schemes in various applications of the modern communication systems are listed [96, 97].

In this chapter, a case study is presented on the design and implementation of the MC for COMINT applications. A brief description on the broad operational and functional requirements is presented to illustrate their importance in the design of the MC scheme. Subsequently, the broad architecture of the system and the functional flow are explained. The achieved MC performance is analyzed based on the data collected from the trial deployment of the COMINT system.

7.2 Operational and Functional Requirements

7.2.1 Operational Requirements

The COMINT system is required to detect, analyze and process the long distance signals from the military radios, the microwave terrestrial links and the satellite communication signals within the specified frequency band of operation. The system should be suitable for deployment in static and mobile platforms, including military transport aircrafts.

7.2.2 Functional Requirements

The system is required to operate on real-time or recorded signals, depending on the deployment scenario. The signal of interest (SOI) is selected from a real-time source like an interception receiver or a recording unit for off-line analysis. An automatic MC stage is required to estimate the symbol rate and identify the modulation type of the SOI. The demodulator needs to be automatically configured using the estimation of the MC module. The demodulated signal needs to be processed further at the base-band level.

7.3 Design Considerations

7.3.1 Formulation of the design

Based on the operational and functional requirements, the design of the automatic MC module is carried out. From the types of target signals, the pool of candidate modulations has been finalized. Provision is made for progressive inclusion of new modulation schemes. The hardware resources are planned depending on the signal bandwidth, the availability of the sample size and the possible constraints on the analysis time. Since the system needs to operate with very low quality long distance signals with various nuisance factors associated with the mobility of the platform, robust parameter estimation methods are required to be used for an optimum performance of the MC module. Considering these aspects, the broad technical requirements are formulated as shown in Table 7.2.

Requirement	**Design considerations**
Target signals: military radios, the microwave terrestrial links and the satellite communication signals	BPSK, QPSK (with variants), 8PSK, 8QAM, 16QAM, 32QAM, 64QAM, 16APSK
Signal bandwidth	20 KHz to 40 MHz
MC method	LB (QHLRT)
Pre-processing	Estimation of the symbol rate, I-Q demodulation, gain normalization, phase-offset correction, estimation of the noise power
Minimum analysis sample duration	1 mSec (considering FH signals with 1000 hops/sec)
Maximum duration for decision	1 Sec (non-critical)

TABLE 7.2: Formulation of the MC design

7.3.2 System Implementation

The broad system architecture to be implemented is shown in Figure 7.2. A PXI-e based pre-amplifier and receiver unit is used as the front end for reception of the signal of interest. The gain control signal from the demodulator output provides the trigger for the automatic gain control (AGC) to keep the signal level within the rated operating range. The ADC module digitizes the received signal and provides the output to the FPGA demodulator and base-band processor module. Before configuring the FPGA for the digital demodulation, the symbol rate estimation is carried out at the host controller using a snapshot of the digitized samples. Based on the estimated symbol rate, the I-Q demodulation is carried out by the FPGA demodulator. The host controller uses a snapshot of the digital I-Q samples to classify the modulation scheme. The FPGA demodulator is finally configured for the estimated modulation and the symbol de-mapping is carried out to deliver the bitstream to the subsequent processing servers.

The implementation of the MC module is carried out in the COMINT platform shown in Figure 7.1. In the platform, a maximum of 4000 samples of the intermediate frequency

signal at 70 MHz are extracted for the estimation of the symbol rate. The sample size for the MC stage has been pre-fixed at 1000. The implementation has been carried out in a PXI-e platform using Labview development tool. After the symbol rate detection

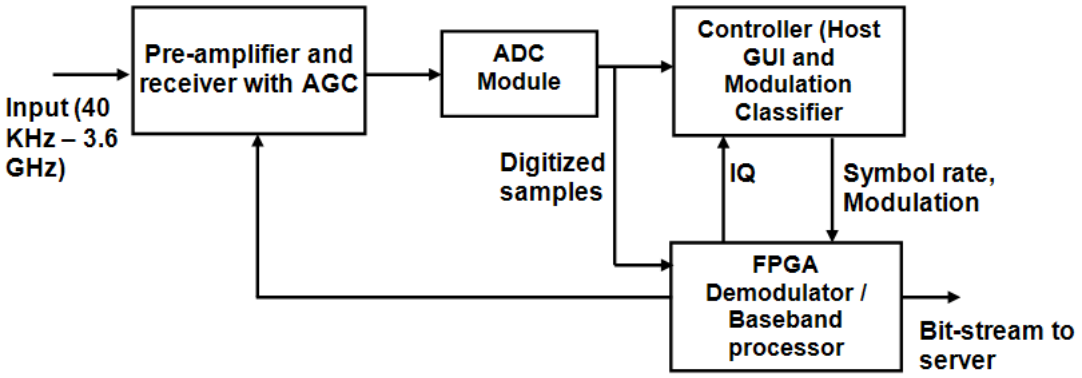

FIGURE 7.1: Broad architecture of the blind demodulator

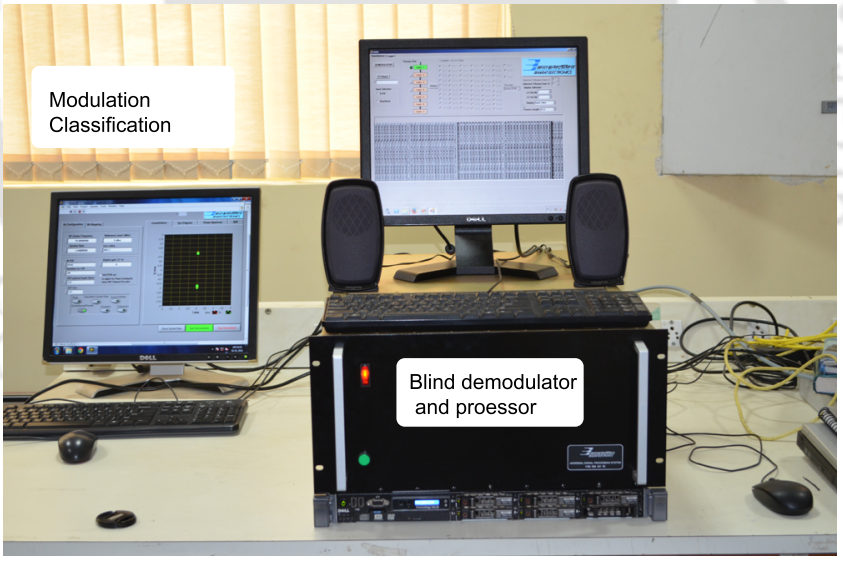

FIGURE 7.2: COMINT platform under implementation

using the method proposed in Chapter 3 at the host processor (Intel i7, 2.88 GHz, 4 GB RAM), the received signal is I-Q demodulated. Subsequently, the estimation of the signal gain, the phase offset and the noise power is carried out using the estimation methods proposed in Chapter 5 at the host processor of the PXI-e platform. The subsequent stage of QHLRT MC is implemented in the host processor. After the MC stage, the

blind demodulator, implemented in the PXI-e FPGA is configured as per the estimated modulation and the symbol rate. The demodulated signal is further processed in a server platform (quad core, 3 GHz, 64 GB RAM) for the extraction of intelligence.

7.4 Trial Deployment

Trials have been conducted for validating the COMINT system. This includes the laboratory tests and field trials in target deployment conditions. The laboratory testing primarily includes injection mode performance verification using various levels of SNRs. The summary of the injection mode tests is shown in Table 7.3. The results of the injection mode tests are found to be very close to the theoretical figures. During the field trials, the system was tested using an interception system onboard a light transport aircraft (Figure 7.3). In challenging deployment scenarios, the COMINT encounter signals with very short exposure to the receiver. This may be caused by the mobility of the target, mobility of the COMINT system, terrain conditions and the signal transmission protocol itself (e.g. burst, FH etc.). The trial platform is chosen to simulate the short duration exposures to the signal of interest. The scenario was further worsened by interception from a long distance. The received signal, after gain normalization, is shown in Figure 7.4 for various conditions of reception. The corresponding performances of the MC are summarized in Table 7.4. It is interesting to note that, the classification performance in a practical scenario may have deviations from the values established theoretically. The results suggest that, the achieved MC performance may be influenced by various nuisance parameters like the Doppler shift, fast fading etc. This may degrade the MC performance as compared to the theoretical values. However, the susceptibility to the nuisance parameters may be specific to the platform of deployment. The best performance may be expected for static deployments, while the same tends to deteriorate due to the mobility of the platform and the terrain uncertainty.

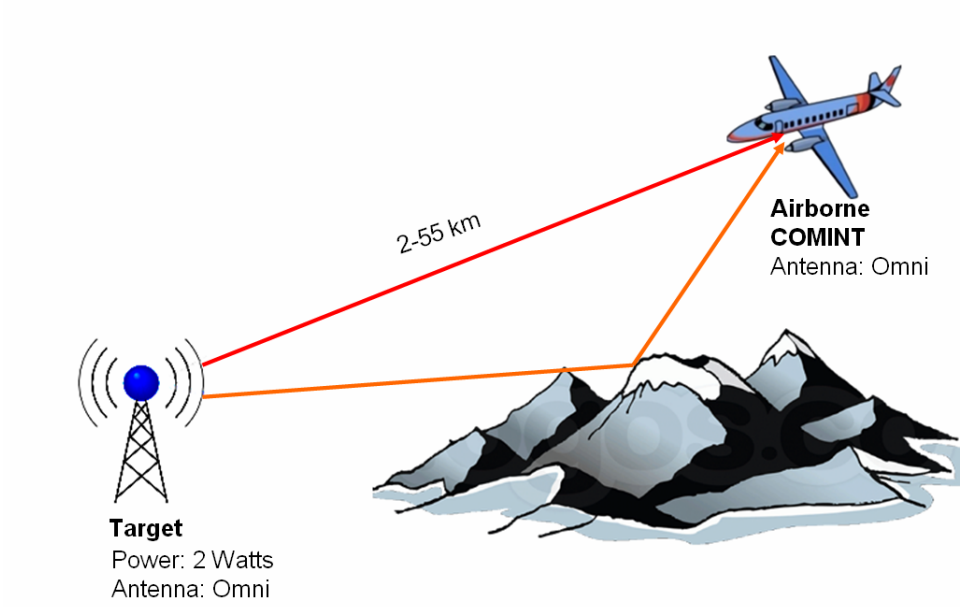

FIGURE 7.3: Deployment scenario of the proposed MC in airborne COMINT

SNR	BPSK	QPSK	8PSK	8QAM	16APSK	16QAM	32QAM	64QAM
10 dB	1.00	1.00	1.00	1.00	1.00	1.00	0.90	0.92
5 dB	1.00	1.00	1.00	1.00	0.95	0.97	0.84	0.86
0 dB	1.00	1.00	0.84	0.90	0.83	0.89	0.70	0.55
-5 dB	1.00	0.64	0.00	0.66	0.53	0.64	0.00	0.24

TABLE 7.3: Summary of laboratory tests: P_{cc} at various SNRs

7.5 Summary

In this Chapter, a case study of the MC deployment in a practical application is presented to correlate the expected and the achievable MC performance. For practical deployment, the observation interval is of significant importance, since it is governed by the number of samples required to achieve the desired parameter estimation accuracy and the MC performance. There is a possibility to fine tune the MC performance by considering the specific nuisance factors like Doppler shift, carrier frequency offset etc during the formulation of the algorithms. However, these aspects are more appropriate to be considered specific to the target conditions of deployment.

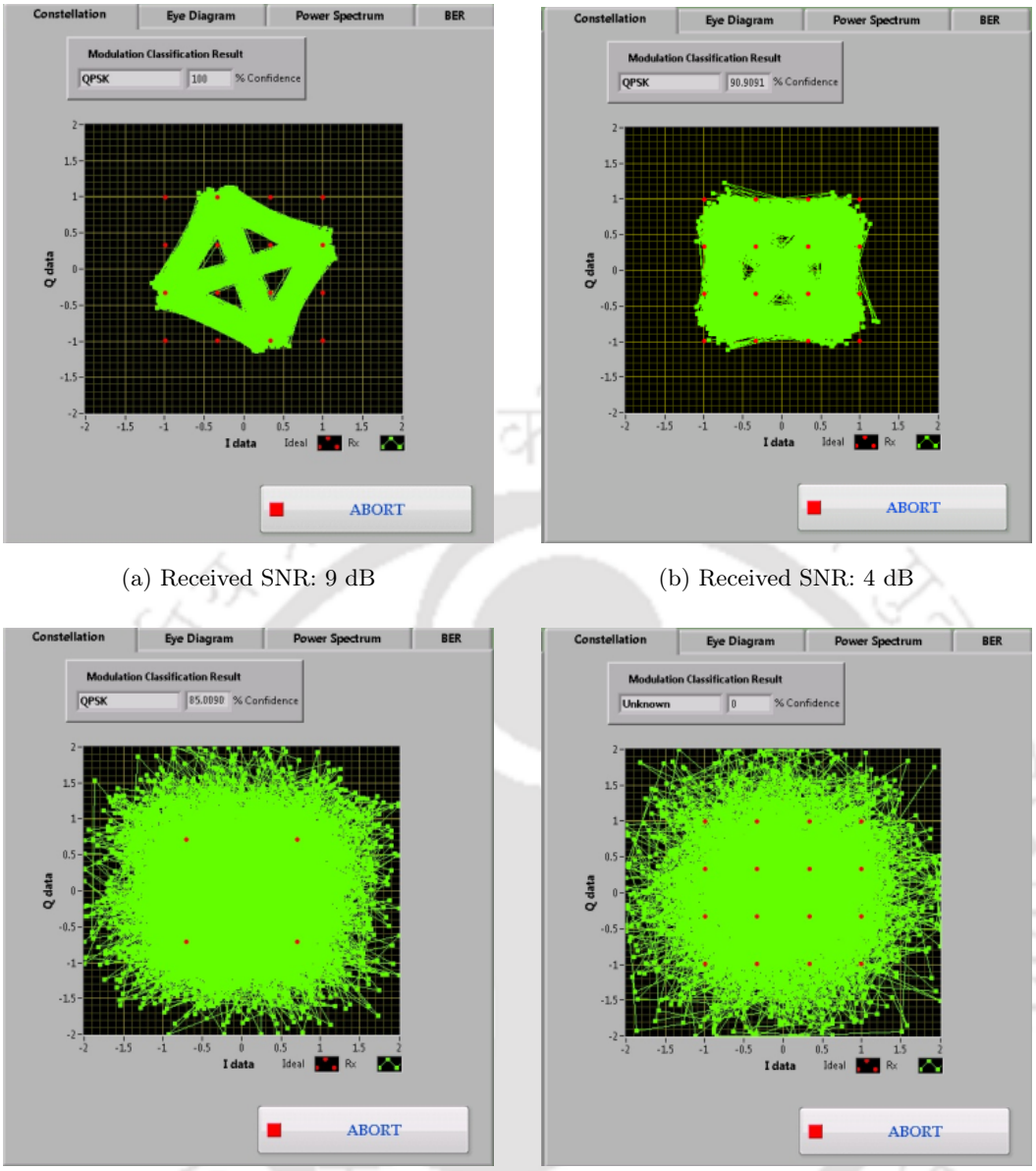

(a) Received SNR: 9 dB

(b) Received SNR: 4 dB

(c) Received SNR: 0 dB

(d) Received SNR: -5 dB

FIGURE 7.4: Reception of the SOI at various SNR cases

SNR	Measured Pcc	Theoretical Pcc	Nuisance factors
9 dB	1.00	1.00	Doppler shift
4 dB	0.90	1.00	Doppler shift
0 dB	0.85	1.00	Doppler shift, fast fading
-5 dB	0.00	0.75	Doppler shift, fast fading, timing offset

TABLE 7.4: Summary of field trials

8

Conclusions

The work carried out in this thesis primarily addresses the blind MC problem with a special focus on the performance improvement of the QHLRT classifiers in a wide range of practical scenarios. Although this challenging problem has been addressed extensively, there has been a requirement of achieving high classification performance in adverse channel conditions. The blind LB algorithms proposed so far use various parameter estimation methods in an unknown channel. As the importance of practical implementations increased, the complexity of the LB approach has been reduced by adopting near optimal classifiers. However, the performance rely mostly of the parameter estimation algorithms used as the pre-processing stages. The FB classification being relatively simpler from the implementation point of view, is also a popular method for MC. However, as illustrated in Chapter 2, LB is the preferred choice for designing practical MC, requiring high classification performance in a wide variety of operating conditions.

The focus of this work has been primarily towards the COMINT scenario, where intelligence from the received signal needs to be gathered under very poor reception scenarios. In many cases, the signal of interest (SOI) is almost hidden under the noise floor. At the same time the fading related distortions make the processing further challenging. However, the AWGN noise model is applicable in general for the practical scenarios. The contribution of the thesis is summarized below.

8.1 Summary of Contribution

The work proposed in this thesis assumes a high performance COMINT receiver with insignificant frequency and phase offsets. The MC problem has been addressed after the receiver has been locked onto the signal of interest. After introducing the concepts of blind MC and formulating the problems in Chapter 1, the thesis presents a state-of the art literature survey in Chapter 2.

In Chapter 3, a novel algorithm is proposed to estimate the symbol rate of the received signal. Based on second order cyclostationarity of the modulated signals, the new measure CDPP has been employed as a robust feature to estimate the symbol rate in a low SNR amidst fading related distortions. By the use of this proposal, the timing offset issues for the LB classification have been minimized, especially under adverse channel conditions.

In Chapter 4, the issue of gain uncertainty has been addressed by a novel algorithm for estimation of the signal gain employing FKM clustering algorithm. By using the estimates of the cluster centers of the received constellation, the channel gain is estimated by using geometric transformation. The proposed method formulates a generic approach for signal gain for a generic pool of digital modulations. The proposed method has laid the foundation for more accurate parameter estimators for the LB MC.

A comprehensive blind parameter estimation method is formulated in Chapter 5 under fading scenarios. New estimation methods have been proposed for the signal gain, the phase offset and the noise power, considering the practical implementation aspects. Exploiting the fact that the received base-band of the digitally modulated signal can be

considered as a Gaussian mixture model, this novel approach for the parameter estimation ensures better performances at low SNR conditions. Applying the EM algorithm, the cluster centers in the I-Q plane is estimated. As a pre-processing stage, the number of clusters in the received constellation is estimated by checking the Gaussianity of the estimated clusters. The signal gain and the phase offset are derived from the estimated cluster centers using geometric transformations. The noise power is estimated from the EM clustering algorithm and the estimated signal gain. The QHLRT classification employed with the estimated parameters showed improved performance in a variety of channel conditions especially simulating the COMINT scenarios.

In Chapter 6, the issue of the frequency selective fading has been addressed by proposing a blind equalization algorithm as a pre-processing stage. A hybrid equalization scheme has been formulated with the M-CMA as the first stage, while a modulation specific DDLMS and the second stage of equalization. The proposed scheme has achieved improved performance as compared to the individual performances of these methods in a blind scenario. Apart from the use in the blind MC, the algorithm may be suitable for other applications like cognitive radios and SDRs.

In Chapter 7, an example of the practical implementation of the blind MC is illustrated with analysis of the trial results. The design considerations and the achievable performance of the MC are brought out to highlight the constraints specific to the application area.

8.2 Scope for future work

The proposed methods for blind MC using QHLRT classifier are verified for the robust performance in adverse channel conditions. The research work in the thesis points to several extensions. A few of them are mentioned below.

1. **Computational complexity**: The computational complexity was prominent in classical scenarios. We considered the facts that with the current advancement of

processing resources, the significance of this issue has reduced in COMINT scenarios. For commercial scenarios like cognitive radios, the computational complexity of the proposed method still remains a prime factor to be addressed.

2. **Mitigation of fast fading**: Fast fading causes signal variations within the observation interval, posing a challenge on the blind estimation of parameters. Unlike conventional communication systems where certain known signal characteristics are employed for blind channel estimation, the same is not straightforward in blind MC. Research can be carried out to address this issue.

3. **Estimation of carrier frequency offset**: Carrier frequency offset is a result of imperfect receiver. This can causes severe model mismatch and thereby significantly degrading the MC performance. Estimation of Δf may be taken up as part of the preprocessing in blind MC.

4. **Generic signal classifier**: A generic classifier to address a wide variety of signals including conventional communication signals, the OFDM and MIMO signals, the pulsed RADAR signals etc may form the main focus for the future work on MC and signal classification as a whole. This type of signal classier will be relevant for the spectrum monitoring applications. A subset of the problem may be the case of a candidate pool containing both linear and non-linear digital modulations. This is a very challenging problem in the LB framework. A more practical approach may be to add an additional pre-processing stage to identify the linear and the non-linear classes using the FB method. There after, the linear modulations can be classified using LB method, while the other branch containing the non-linear pool may be addressed by FB methods. This approach of MC will ensure classification accuracy for the wider class of linear modulations and conserve computational resources by processing the non-linear class using the FB framework. The FB and LB classification branches in the decision tree may be further augmented with appropriate candidates to move closer towards the generic signal classifier.

Bibliography

[1] O. A. Dobre, A. Abdi, Y. Bar-Ness, and W. Su, "A Survey of Automatic Modulation Classification Techniques:Classical Approaches and New Trends," *IET Communication*, vol. 1, no. 2, pp. 137–156, 2007.

[2] O. A. Dobre, "Signal Identification for Emerging Intelligent Radios: Classical Problems and New Challenges," *IEEE Instrumentation and Measurement Magazine*, pp. 11–18, 2015.

[3] C. Y. Huang and A. Polydoros, "Likelihood Methods For MPSK Modulation Classification," *IEEE transaction on communicatios*, vol. 43, no. 2/3/4, pp. 1493–1503, February/March/April 1995.

[4] J. Sills, "Maximum-Likelihood Modulation Classification for PSK/QAM," in *Proc.IEEE Communication Conf.*, vol. 5, 1999.

[5] P. Panagiotou, A. Anastasopoulos, and A. Polydoros, "Likelihood Ratio Tests for Modulation Classification," in *Proc.IEEE Veh. Technol. Conf.*, vol. 2, Los Angeles, CA, October 2000, pp. 670–674.

[6] L. Hong and K. C. Ho, "An antenna array likelihood modulation classifier for BPSK and QPSK signals," in *IEEE MILCOM*, April 2002, pp. 647–651.

[7] O. A. Dobre, J. Zarzoso, Y. Bar-Ness, and W. Su, "On the Classification of Linearly Modulated Signals in Fading Channel," in *CISS Conf., Princeton University*, April 2004.

[8] E.E.Azzouz and A.K.Nandi, "Automatic Identification of Digital Modulation Types," *Elsevier Signal Processing*, vol. 47, pp. 55–69, 1995.

[9] A. Swami, S. Barbarossa, and B. Sadler, "Blind Source Separation and Signal Classification," in *proceedings of ASILOMAR*, October 2000, pp. 1187–1191.

[10] O. A. Dobre, A. Abidi, and Y. Bar-Ness, "Cyclostationarity-Based Modulation Classification of Liniear Digital Modulation in Flat Fading Channels," *Springer Wireless Personal Communication*, vol. 54, no. 4, pp. 699–717, September 2010.

[11] Z. Zhu, *Automatic Classification of Digital Communication Signal Modulations*. PhD thesis at Brunel University London, UK, 2014.

[12] J. M. III and J. Gerald Q. Maguire, "Cognitive Radio: Making Software Radios More Personal," *IEEE Personal Communications*, August 1999.

[13] M. Souryal, M. Ranganathan, J. Mink, and N. E. Ouni, "Real-time centralized spectrum monitoring: Feasibility, architecture, and latency," in *IEEE International Symposium on Dynamic Spectrum Access Networks (DySPAN)*, September 2015.

[14] Y. Wanxue and W. Keren, "A New Method to Symbol Rate Estimation of MPSK Signals," in *Proceedings of Congress on Image and Signal Processing 2008*, vol. 5, 2008, pp. 394–398.

[15] F. Hameed and O. A. Dobre, "On the Likelihood-Based Approach to Modulation Classification," *IEEE transaction on communicatios*, vol. 8, no. 12, February 2009.

[16] S.M.Kay, *Fundamentals of Statistical Signal Processing Volume-II, Detection Theory.* Prentice Hall, 1998.

[17] W. Wei and J. M. Mandel, "Maximum-likelihood classification for digital amplitude-phse modulations," *IEEE transaction on communicatios*, vol. 48, pp. 189–193, February 2000.

[18] A. Abidi, O. A. Dobre, and R. Choudhury, "Modulation Classification in Fading Channels Using Antenna Arrays," in *IEEE MILCOM*, 2004, pp. 211–228.

[19] O. A. Dobre, A. Abdi, Y. Bar-Ness, and W. Su, "Blind Modulation Classification: A Concept Whose Time Has Come," in *IEEE Sarnoff Symposium on Advances in Wired and Wireless Communications, Princeton*, April 2005.

[20] M. D. Wong and A. K. Nandi, "Semi-blind Algorithms for Automatic Classification of Digital Modulation Schemes," *Elsevier Signal Processing*, vol. 18, pp. 209–227, 2008.

[21] A. Puengnim, N. Thomas, J. Y. Tourneret, and JosepVidal, "Classification of Linear and Non-linear Modulations Using the Baum Welch Algorithm and MCMC Methods," *Elsevier Signal Processing*, vol. 90, pp. 3242–3255, 2010.

[22] V. G. Chavali and C. R. C. M. da Silva, "Classification of Digital Amplitude-phase Modulated Signals in Time-correlated Non-Gaussian Channels," *IEEE transaction on communicatios*, vol. 59, no. 8, pp. 2051–2056, June 2011.

[23] M. Derakhtian, A. A. Tadaion, and S. Gazor, "Modulation Classification of Linearly Modulated Signals in Slow Flat Fading Channels," *IET Signal Processing*, vol. 5, no. 5, pp. 443–450, 2011.

[24] W. C. Headley and C. R. C. M. da Silva, "Asynchronous Classification of Digital Amplitude-Phase Modulated Signals in Flat-Fading Channels," *IEEE Transactions on Communication*, vol. 59, no. 1, pp. 7–12, January 2011.

[25] V. G. Chavali and C. R. C. M. da Silva, "Classification of Digital Amplitude-Phase Modulated Signals in Time-Correlated Non-Gaussian Channels," *IEEE transaction on communicatios*, vol. 61, no. 6, pp. 2408–2419, June 2013.

[26] Z. Zhu and A. K. Nandi, "Blind Digital Modulation Classification using Minimum Distance Centroid Estimator and Non-parametric Likelihood Function," *IEEE transaction on Wireless Communicatios*, vol. 13, no. 8, pp. 4483–4494, April 2014.

[27] M. Mohanty, U. Satija, B. Ramkumar, and M. S. Manikandan, "Digital modulation classification under non-gaussian noise using sparse signal decomposition and maximum likelihood," in *Proceedings of NCC*, 2015.

[28] C. Schreyogg and J. Reichert, "Modulation Classification of QAM Schemes Using the DFT of Phase Histogram Combined With Modulus Information," in *IEEE MILCOM,*, November 1997, pp. 1372–1376.

[29] Y. Yang and C. H. Liu, "An Asymptotic Optimal Algorithm for Modulation Classification," *IIEEE Comm. Letters*, vol. 2, no. 4, pp. 117–119, 1998.

[30] K. C. Ho, W. Prokopiw, and Y. T. Chan, "Modulation Identification of Digital Signals by the Wavelet Transform," *IEE Proc. Radar, Sonar and Navig.*, vol. 147, no. 4, pp. 169–176, August 2000.

[31] L. Lichun, "Comments on Signal Classification Using Statistical Moments,," *IEEE Trans. Commun.*, vol. 50, no. 2, pp. 195–200, August 2002.

[32] M. W. Aslam, Z. Zhu, and A. K. Nandi, "Automatic Digital Modulation Classification Using Genetic Programming with K-Nearest Neighbor," in *proceedings of MICOM 2010*, November 2010, pp. 1731–1736.

[33] M. Zaerin and B. Seyfe, "Multiuser Modulation Classification Based on Cumulants in Additive White Gaussian Noise Channel," *IET Signal Processing*, vol. 6, no. 9, 2012.

[34] L. Pei-Hua, Z. Hong-Xin, W. Xu-Ying, X. Nan, and X. Yuan-Yuan, "Modulation Recognition of Communication Signals Based on High Order Cumulants and Support Vector Machine," *Elsevier*, vol. 19, pp. 61–65, June 2012.

[35] A. Swami, "Hierarchical Digital Modulation Classification Using Cumulants," *IEEE TRANSACTIONS ON COMMUNICATIONS*, vol. 48, no. 3, pp. 416–429, March 2000.

[36] C. M. Spooner, "On the Utility of Sixth-Order Cyclic Cumulants for RF Signal Classification," in *proceedings of ASILOMAR*, vol. 1, November 2001, pp. 890–897.

[37] O. A. Dobre, A. Abidi, Y. Bar-Ness, and W. Su, "Selection Combining for Modulation Recognition in Fading Channels," in *IEEE MILCOM*, vol. 4, October 2005, pp. 2499–2505.

[38] A. Fehske, J. Geaddert, and J. H. Reed, "A New Approach to Signal Classifcation Using Spectral Correlation and Neural Networks," in *Proc.IEEE International Symposium on New Frontiers in DySpan*, Nov 2005, pp. 212–215.

[39] NegarAhmadi, "Using Fuzzy Clustering and TTSAS Algorithm for Modulation Classification Based on Constellation Diagram," *ELSEVIER Artifical Intelligence*, vol. 23, pp. 357–370, 2010.

[40] V. Orlic and M. Dukic, "Multipath Channel Estimation Algorithm for Automatic Modulation Classification Using Sixth-order Cumulants," *Electronic Letters*, vol. 46, no. 19, September 2010.

[41] Y. Liu, A. Haimovich, W. Su, J. Dabin, and E. Kanterakis, "Modulation Classification of MIMO-OFDM Signals by Independent Component Analysis and Support Vector Machines," in *ASILOMAR 2011*, November 2011, pp. 1903–1907.

[42] B. Ramkumar, *Automatic Modulation Classifcation and Blind Equalization for Cognitive Radios.* PhD Dissertation,Virginia Polytechnic Institute and State University, 2011.

[43] J. Kuriakose, A. Rajesh, and P. K. Bora, "Improved PSK classification using spectral correlation functions," in *National Conference on Communication*, Feb 2014.

[44] G. Markovic and M. Dukic, "Cooperative Modulation Classification With Data Fusion for Multipath Fading Channels," *Electronic Letters*, vol. 49, no. 23, pp. 1494–1496, November 2013.

[45] M. S. Muhlhaus, M. Oner, O. A. Dobre, and F. K. Jondral, "A Low Complexity Modulation Classification Algorithm for MIMO Systems," *IEEE Commun. Lett.*, vol. 17, pp. 1881–1884, 2013.

[46] M. Marey and O. A. Dobre, "Blind Modulation Classification Algorithm for Single and Multiple-antenna Systems Over Frequency-selective Channels," *IEEE Signal Process. Lett.*, vol. 9, pp. 1098–1102, 2014.

[47] M. R. Bahloul, M. Z. Yusoff, and M. N. M. Saad, "Efficient and Low Complexity Modulation Classification Algorithm for MIMO Systems," *Res. J. Appl. Sci. Eng. Technol.*, vol. 9, no. 1, pp. 58–64, 2015.

[48] W. A. Gardner, *Cyclostationarity in Communication and Signal Processing.* IEEE press, 1994.

[49] L. Yan-ling, L. Bing-bing, and Y. Chang-yi, "Modulation Classification of MQAM Signals Using Particle Swarm Optimization and Subtractive Clustering," in *ICSP*, 2010.

[50] C. Yin, B. Li, and Y. Li, "Modulation Classification of MQAM Signals from Their Constellation Using Clustering," in *Second International Conference on Communication Software and Networks*, 2010.

[51] Y. Yang, C. H. Liu, and T. W. Soong, "A Log-likelihood Function-based Algorithm for QAM Signal Classification," *Elsevier Signal Processing*, vol. 70, pp. 61–71, 1998.

[52] H. C. Wu, M. Saquib, and Z. Yun, "Novel Automatic Modulation Classification Using Cumulant Features for Communications Via Multipath Channels," *IEEE Trans. on Wireless Communication*, vol. 7, no. 8, pp. 3098–3105, August 2008.

[53] O. A. Dobre, Y. B. Ness, and W. Su, "Higher-oder Cyclic Cumulants for High Order Modulation Classification," in *IEEE MILCOM 2003*, vol. 1, 2003, pp. 112–117.

[54] L. Pei-Hua, Z. Hong-Xin, W. Xu-Ying, X. Nan, and X. Yuan-Yuan, "Modulation Recognition of Communication Signals Based on High Order Cumulants and Support Vector Machine," *Elsevier Signal Processing*, vol. 19, pp. 61–65, June 2012.

[55] Z. Yu and W. Su, "A blind carrier frequency estimation algorithm for digitally modulated signals," in *IEEE MILCOM*, vol. 1, Nov 2004, pp. 48–53.

[56] Z. Yu and J. Bai, "Carrier frequency estimation in automatic modulation recognition environment," in *IEEE Int. Conf. on Information and Automation*, June 2010, pp. 1877–1882.

[57] M. Morelli and U. Mengali, "Carrier-frequency estimation for transmission over frequency selective channels," *IEEE Trans. Commun.*, vol. 48, no. 9, pp. 1580–1589, September 2000.

[58] Q. Wang, X. Yang, X. Yan, and K. Qin, "High-efficiency carrier frequency estimation algorithm for real-time multi-domain communication signal analysis," *Meterology and Measurement Systems*, vol. XXI, no. 2, pp. 281–292, 2014.

[59] Y.T.Chan, J.W.Plews, and K.C.Ho, "Symbol Rate Estimation by the Wavelet Transform, Circuits and Systems," in *Proceeding IEEE International Symposium ISCAS97*, vol. 1, 1997, pp. 177–180.

[60] C. Mosquera, S. Scalise, and R. Lopez-Valcarce, "Non-Data-Aided Symbol Rate Estimation of Linearly Modulated Signals," *IEEE Transaction on Signal processing*, vol. 56, pp. 664–674, Feb 2008.

[61] H. Wymeersch and M. Moeneclaey, "Blind Symbol Rate Detection for Low-complexity Multi-rate Receivers," in *Vehicular Technology Conference, VTC-2005*, 2005, pp. 1437–1440.

[62] W. Gardner, "Signal Interception, a Unifying Theoritical Framework for Feature Detection," *IEEE Transactions on Communication*, vol. 36, no. 8, August 1988.

[63] P. Ciblat, E. P. Loubaton, and G. B. Giannakis, "Asymptotic Analysis of Blind Cyclic Correlation-based Symbol-rate Estimators," *IEEE Transaction on Information Theory*, vol. 48, no. 7, pp. 1922–1934, July 2002.

[64] L. Mazet and P. Loubaton, "Cyclic Correlation Based Symbol Rate Estimation," in *Proceedings 33rd Asilomar Conf. on Signals, Systems, and Computers*, vol. 2, 1999, pp. 1009–1012.

[65] Z. Yu, Y. Shi, and W. Su, "Symbol-rate Estimation Based on Filter Bank," in *IEEE International Symposium on Circuits and Systems, 2005*, vol. 5, 2005, pp. 1437–1440.

[66] R. S. Roberts, W. A. Brown, and H. H. Loomis, "Computationally Efficient Algorithms for Clyclic Spectral Analysis," *IEEE Signal Processing Magazine*, pp. 38–49, April 1991.

[67] V. Choqueuse, S. Azou, K. Yao, L. Collin, and G. Burel, "Blind Modulation Recognition for MIMO Systems," in *Proceedings of Military Technical Academy Review*, vol. XIX, June 2009, pp. 183–196.

[68] A. Polydors and K. Kim, "On the Detection and Classification of Quadrature Digital Modulations in Broad-Band Noise," *IEEE Trans. on Comm.*, vol. 38, no. 8, pp. 1199–1211, August 1990.

[69] J. Lopez-Salcedo and G. Vazquez, "Asymptotic Equivalence Between the Unconditional Maximum Likelihood and the Square-law Nonlinearity Symbol Timing Estimation," in *IEEE Transactions on Signal Processing*, vol. 54, January 2006, pp. 244–257.

[70] P. Ciblat and M. Ghogho, "Blind NLLS Carrier-frequency Offset Estimation for QAM, PSK and PAM Modulations: Performance At low SNR," in *IEEE Transactions on Communications*, vol. 54, Oct 2006, pp. 1725–1730.

[71] F. Gini and G. B. Giannakis, "Frequency Offset and Symbol Timing Recovery in Flat-fading Channels: A Cyclostationary Approach," in *IEEE Transactions on Communications*, vol. 46, March 1998, pp. 400–411.

[72] Y. Yang, C. H. Liu, and C. Liu, "Algorithm for QAM Signal Classification Using Maximum Likelihood Approach Based on Joint Probability Densities of Phase and Amplitude," *CCITT*, vol. 32, no. 1, 2003.

[73] M. Moeneclaey and G. de Jonghe, "ML-Oriented NDA Carrier Synchronization for General Rotationally Symmetric Signal Constellations," *IEEE transaction on communicatios*, vol. 42, no. 8, pp. 2531–2533, August 1994.

[74] D. R. Pauluzzi and N. C. Beauliew, "A Comparison of SNR Estimation Techniques for AWGN Channel," *IEEE transaction on communicatios*, vol. 48, pp. 1681–1691, 2000.

[75] R. M. R. Giraldo, *QAM microwave Signal Transmission Over a Radio-over-fibre Link Using Semiconductor Optical Amplifiers.* Master degree thesis at University of Limerick, Ireland, 2008.

[76] H. Wijanto, Sugihartono, S. Tjondronegoro, and Kuspriyanto, "The Performance Improvement of Automatic Modulation Recognition Using Simple Feature Manipulation, Analysis of the HOS, and Voted Decision," in *Proceedings of World Academy of Science, Engineering and Technology*, vol. 58, June 2009.

[77] S. Chiu, "Fuzzy Model Identification Based on Cluster Estimation," *Journal of Intelligent and Fuzzy Systems*, vol. 2, no. 3, Sep 1994.

[78] S.M.Kay, *Fundamentals of Statistical Signal Processing Volume-I, Estimation Theory.* Prentice Hall, 1998.

[79] M. K. Pakhira, "A Linear Time-Complexity K-means Algorithm Using Cluster Shifting," in *Sixth International Conf. on Computational Intelligence and Comm. Networks*, 2014, pp. 647–651.

[80] R. J. Almecida and J. M. C. Sousa, "Comparison of Fuzzy Clustering Algorithms for Classification," in *International Sysmposium of Evolving Fuzzy Systems*, Sep 2006, pp. 112–117.

[81] J. F. Kolen and T. Hutcheson, "Reducing the Time Complexity of the Fuzzy C-means Algorithm," *IEEE transaction on fuzzy systems*, vol. 10, no. 2, April 2002.

[82] V. S. Moertini, "Introduction to Five Data Clustering Algorithms," *INTEGRAL*, vol. 7, no. 2, pp. 87–96, 2002.

[83] Z. Yao and B. Choi, "Bidirectional Hierarchical Clustering for Web Mining," in *IEEE international conf. on web intelligence*, Oct 2003, pp. 620–624.

[84] M. Hoffman, N. de Freitar, and A. Doucet, "An Expectation Maximization Algorithm for Continuous Markov Decision Process with Arbitrary Rewards," in *12th international conf. on artificial intelligence and statitics*, vol. 5, 2009.

[85] C. Liu and D. B. Rubin, "ML Estimation of the t Distribution Using EM and its extensions, ECM and ECME," *Statistica Sinica*, vol. 5, pp. 19–39, 1995.

[86] J. J. Shynk, *Probability, Random Variables and Random Processes: Theory and Signal Processing Applications.* Wiley, 2012.

[87] S. J. Nowlan and J. E. Hinton, "A Soft Decision Directed LMS Algorithm for Blind Equalization," *IEEE Transaction on Communications*, vol. 41, no. 2, pp. 275–279, February 1993.

[88] T. Saikumar, R. N. Devi, and K. K. Rao, "Adaptive MMSE Equalizer for Blind Fractional Spaced CMA Channel Equalization through LMS Algorithm," *International Journal of Ad hoc Sensor and Ubiquitous Computing*, vol. 3, no. 1, pp. 37–44, February 2012.

[89] J. M. Filho, M. D. Miranda, and M. T. Silva, "A Regional Multimodulus Algorithm for Blind Equalization of QAM Signals: Introduction and Steady-state Analysis," *Elsevier Signal Processing*, vol. 92, no. 11, April 2012.

[90] D. Godard, "Self-recovering equalization and carrier tracking in two-dimensional data communication systems," *IEEE Trans. on Comm.*, vol. 28, no. 11, pp. 1867–1875, 1980.

[91] K. N. Oh and Y. Chin, "Modified constant modulus algorithm: blind equalization and carrier phase recovery algorithm," in *IEEE Int. Conf. on Comm.*, 1995, pp. 498–502.

[92] J. Zhu, X.-R. Cao, , and R. wen Liu, "A Blind Fractionally Spaced Equalizer Using Higher Order Statistics," *IEEE TRANSACTIONS ON CIRCUITS AND SYSTEMSII: ANALOG AND DIGITAL SIGNAL PROCESSING,*, vol. 46, no. 6, pp. 755–763, June 1999.

[93] Z. Ding, *Adaptive Filters for Blind Equalization.* CRC Press LLC, 2000.

[94] A. Ikhlef and D. L. Guennec, "A Simplified Constant Modulus Algorithm for Blind Recovery of MIMO QAM and PSK Signals: A Criterion with Convergence Analysis," *EURASIP Journal onWireless Communications and Networking*, 2007.

[95] S. Abrar and A. K. Nandi, "Normalized Constant Modulus Algorithm for Blind Channel Equalization," *EUSIPCO.*, 2008.

[96] A. Goldsmith, *Wireless Comunications* . Cambridge University Press, 2005.

[97] "Digital modulations in communication systems- an introduction," White Paper, Agilent Technologies. [Online]. Available: http://cp.literature.agilent.com/litweb/pdf/5965-7160E.pdf

List of Publications

National and International Conferences

- **Gaurav Jyoti Phukan**, Prabin Kumar Bora, Rajesh A and Chavelli Ramesh, "**Amplitude Normalization in Blind Modulation Classification**," National Conference on Communication, IIT Kharagpur, Feb 2012.
- **Gaurav Jyoti Phukan** and Prabin Kumar Bora, "**An Algorithm to Mitigate Channel Distortion in Blind Modulation Classification**," National Conference on Communication, IIT Delhi, Feb 2013.
- **Gaurav Jyoti Phukan** and Prabin Kumar Bora, "**An Algorithm for Blind Symbol Rate Estimation Using Second Order Cyclostationarity**," International Conference on Signal Processing and Communication, IISc Bangalore, July 2014.

International Journals

- **Gaurav Jyoti Phukan** and Prabin Kumar Bora, "**Parameter Estimation for Blind Classification of Digital Modulations**," IET Signal Processing, April 2016.